Back Scatter Interferometric Sensor for Label-Free Medical Diagnostic Assays

Jepsen, Søren Terpager

Publication date:
2016

Document Version
Publisher's PDF, also known as Version of record

BACK SCATTER INTERFEROMETRIC SENSOR FOR LABEL-FREE MEDICAL DIAGNOSTIC ASSAYS

BY
SØREN T. JEPSEN

DISSERTATION SUBMITTED 2016

AALBORG UNIVERSITY
DENMARK

Back Scatter Interferometric Sensor for Label-Free Medical Diagnostic Assays

Søren T. Jepsen

2015

Dissertation submitted: January 2016

PhD supervisor: Clinical Professor Søren Risom Kristensen
Aalborg University

PhD committee: Professor, dr.med. Aase Handberg (chairman)
Aalborg University Hospital

Docent, PhD, Henrik Karstoft
Aarhus University School of Engineering – Signal

Research Assistant Professor Dmitri Markov
Vanderbilt University

PhD Series: Faculty of Medicine, Aalborg University

ISSN (online): 2246-1302
ISBN (online): 978-87-7112-468-2

Published by:
Aalborg University Press
Skjernvej 4A, 2nd floor
DK – 9220 Aalborg Ø
Phone: +45 99407140
aauf@forlag.aau.dk
forlag.aau.dk

Printed in Denmark by Rosendahls, 2016

Abstract

Back scatter interferometry is an optical method for detecting small changes in the refractive index of a fluid, claimed in the literature to have an exceptional detection limit and sensitivity due to a unique optical principle. Most importantly it has been used to detect biomolecular biding events such as protein-ligand binding in free solution without the use of label technology, which makes it an interesting candidate for use within the field of medical diagnostic assays. This thesis seeks to investigate the use of back scatter interferometry in clinical biochemistry, specifically addressing three areas of clinically relevant areas: immunoassays, protein binding studies and enzymatic assays. Initial findings of this study, suggested that the practical use of back scatter interferometry is severely limited by temperature variations and diffusion phenomena, but most importantly the sensitivity was found to scale with the optical path length of the sample in contrast to the acclaimed optical unique multi-pass principle, whereby light supposedly passes through the sample material multiple times. To demystify the optical principles of back scatter interferometry ray-tracing and wave based simulations were preformed and compared with experimental results. The findings decisively showed that the sensitivity of back scatter interferometry is given by the path length of the sample, disproving former suggestions on multi-pass phenomena. Experimental measurements using back scatter interferometry were preformed to detect the binding between: protein A - immunoglobulin G, trypsin - aminobenzamidine, trypsin - antitrypsin and antithrombin - heparin, but in all cases back scatter interferometry did not detect changes in refractive index that could be related to binding events. More promising results were found in the study of enzymatic reactions as the phosphorylation of glucose to glucose-6-phosphate by hexokinase was detected in a manner that could be used to quantitate the concentration of glucose in solution. Futhermore, the real time data was used to determine the Michaelis-Menten constant. Similarly the hydrolysis of adenosine triphosphate by the enzyme apyrase was also detected using back scatter interferometry. The physical interpretation of the signal in this system could be partly ascribed to the differences in refractivity between substrate and products, with possible contribution from the release of ions into solution. The measurements were confirmed using a commercial deflection type refractometer, thereby proving that the observations are not uniquely detected by BSI but can be measured using any sort of refractive index detector sufficing the sensitivity of the instrument is adequate. It must be concluded that the failure to detect various protein-ligand binding events studied in this work, not only makes it inapplicable for medical diagnostic immunoassays, but entirely questions the validity of measuring biomolecular binding events with BSI.

Resumé

Back scatter interferometry er en optisk måle metode der kan detektere små ændringer i en væskes brydningsindeks. Back scatter interferometry beskrives i literaturen til at fungere på baggrund af et unikt optisk princip der giver metoden en ekseptionæl god følsomhed og lav detektionsgrænse. Metoden har været anvendt til at detektere biomolekylære interaktioner mellem proteiner og ligander i fri opløsning uden brug af labels, hvilket gør metoden specielt relevant som en mulig metode inden for klinisk biokemiske analyser. Formålet med denne afhandling var at undersøge om BSI kan anvendes til klinisk biokemiske analyser, med særligt henblik på immunokemiske analyser samt studier af proteinbinding og enzymatiske analyser. De umiddelbare resultater indikerede imidlertid at den praktiske brug af back scatter interferometry begrænses af temperatur påvirkninger og diffusions fænomener. Endvidere findes det at metodens sensitivitet er afhængig af den optiske vejlængde, hvilket modsiger det der i literaturen beskrives som et "multi-pass" princip hvorved lyset gentagne gange paserer prøvematerialet. Sammenligning af optiske modeller baseret på ray-tracing og bølge-modeller med eksperimentielle resultater viste utvetydeligt at sensitiviteten i back scatter interferometry er direkte proportionel med den optiske vejlængde igennem prøvematerialet, hvilket modsiger "multi-pass" teorien. Eksperimentelle målinger med back scatter interferometry af proteinbinding for henholdsvis: protein A - immunoglobulin G, trypsin - aminobenzamidin, trypsin - antitrypsin og antithrombin - heparin, gav ikke ændringer i brydningsindekset som kunne relateres til proteinernes bindingstilstand. Målinger på enzymatiske reaktioner gav derimod tydelige ændringer i brydningsindekset. Den enzymatiske phosphorylering af glukose til glukose-6-phosphat af enzymet hexokinase blev detekteret hvilket muligør kvantificering af glukose koncentrationen i en ukendt opløsning. Endvidere blev Michaelismenten konstanten bestemt ud fra direkte kontinuerlige målinger. Tilsvarende blev enzymatisk hydrolyse af adenosintriphosphat af enzymet apyrase også detekteret ved brug af back scatter interferometry. Den fysiske årsag til signalet i disse reaktioner tilskrives dels forskellen i den specifikke refraktivitet mellem substrater og produkter men frigørelse af ioner til opløsningen under reaktionen bidrager også til ændringen af brydningsindekset. Målingerne blev verificeret ved brug af et kommercielt "refraktions" refraktometer, hvilket bekræfter at disse reaktioner ikke kun kan observeres ved brug af back scatter interferometry men generelt af brydningsindeks detektorer med tilstrækkelig sensitivitet. Idet back scatter interferometry ikke kunne detektere en binding af de ovennævnte protein-ligand systemer, må det konkluderes at back scatter interferometry er uegnet som detektor af immunkemiske reaktioner. Endvidere giver disse resultater grund til generelt at betvivle hvorvidt back scatter interferometry kan detektere biomolekylære bindinger i fri opløsning.

Preface

As scientists we set up hypothesis and seek to confirm or reject them through experimental verification. Although such experiments should of course not be biased one often hopes for positive confirmation rather than negative or uncertain results, as positive results are much more agreeable with a strict time schedule and an editors approval. However, when one engages in experimental work there is always a chance that the outcome and results will not be as expected. It is of course possible that the experiment has failed or is crippled by large uncertainties and the results should not be cause to reject a sound hypothesis. Therefore, when suddenly faced with results that defy previous dogma and contradict the claims of prestigious literature one certainly feels doubt and at some point self criticism becomes second nature. I would therefore like to thank those of my colleagues at Aalborg University Hospital who have taught me that results obtained on a methodical firm basis and common sense are second to none.

Furthermore, I would like to especially acknowledge firstly my supervisor professor Søren Risom Kristensen, whom despite multiple setbacks and departures from time-schedules has consisted with endless support. Professor Kristensen has an extraordinary talent for dissecting the complex and sometimes rambling ideas that he has been presented with during the course of this project. Secondly, I would like to acknowledge Henrik Shciøtt Sørensen, PhD, for having and keeping a creative open mind even against all odds and for inviting me to participate in this project in the first place. Torleif Trydal, MD, has served as assistant supervisor for a great part of this project and provided both moral support, but most importantly dared to ask the questions that were seemingly obvious but ultimately turned out to be of paramount importance. Lastly but not least, Thomas Martini Jørgensen, PhD, for a relentless devotion above and beyond reasonable expectations.

Søren T. Jepsen, December 2015

Contents

Thesis details

Thesis Title:
Back Scatter Interferometric Sensor for label-free medical diagnostic assays

Ph.D, Student:
Søren T. Jepsen

Supervisors:
Professor Søren Risom Kristensen, MD, DMSc, Aalborg University Hospital
Henrik Schiøtt Sørensen, PhD, formerly Danish Technical University
Thomas Martini Jørgensen, PhD, Danish Technical University
Torleif Trydal, MD, formerly Aalborg University Hospital

This thesis has been submitted for assessment in partial fulfillment of the PhD degree. The thesis is based on the following published scientific papers

I Jepsen ST, Jørgensen TM, Zong W, Trydal T, Kristensen SR, Sørensen HS (2014) Evaluation of back scatter interferometry, a method for detecting protein binding in solution. Analyst 00:1–7. doi: 10.1039/c4an01129e

II Jørgensen TM, Jepsen ST, Sørensen HS, di Gennaro AK, Kristensen SR (2015) Back scattering interferometry revisited – A theoretical and experimental investigation. Sensors Actuators B Chem 220:1328–1337. doi: 10.1016/j.snb.2015.06.121

(III) Unpublished work: Jepsen ST, Jørgensen TM, Sørensen HS, Kristensen SR. Real-time detection of enzymatic reactions using back scatter interferometry and conventional deflection refractometry

A poster presentation was given at IFCC WorldLab Istanbul 2014

Jepsen ST, Jørgensen TM, Trydal T, Sørensen HS, Kristensen SR (2014) Demystifying Back Scatter Interferometry - A Sensitive Refractive Index Detector. Abstract published in: Clin Chem Lab Med 2014; 52, Special Suppl, pp S1 – S1760, June 2014

Chapter 1

Introduction

In 2007 a technique called Back Scatter Interferometry (BSI) was presented in the renowned journal Science, demonstrating how biomolecular interactions could be studied in real-time without the use of labels and in a homogenous format.[1] Because biomolecular interactions are the hearth of many modern diagnostic assays, BSI presents an extraordinary possibility for not just an improved assay format but an entirely new way of performing such assays.

BSI is an interferometric differential refractive index detector and was first described by professor D.J. Bornhop in 1995.[2] In BSI, a small diameter capillary is illuminated by a laser and the reflected light forms an interference pattern that is sensitive to the change in refractive index of the sample within the capillary. Early investigations demonstrated that BSI could detect changes as low as 10^{-7} Refractive Index Units (RIU) on small picoliter probe volumes but further advances in signal processing and system configuration has improved the claimed limit of detection to $10^{-}9$ RIU.[2,3,4,5] The techniques intended use was as a column detector for capillary electrophoresis and liquid chromatography,[6] but in 1997 Bornhop et al.[7] demonstrated that BSI could detect the heat induced unfolding of an enzyme, which suggested that the technique was more than a mass detector. In 2000[8] the capillary was replaced with a semi circular channel etched in glass which introduced BSI as a method usable in the emerging market for miniturazed systems and since then BSI has been used as a chip-based biosensor to study a wide range of biomolecular interactions, including; ion-, small molecule- and protein-protein binding.[9,10,1,11,12,13,14,15,16,17,18,19,20] The technique is currently being commercialized for the drug-discovery market by Molecular Sensing, Inc. a US based company.

From the perspective of clinical biochemistry, BSI's ability to measure a distinct type of proteins namely antibodies and their specific binding to target proteins, is of special interest. Kussrow and Enders have investigated the use of BSI as a

potential diagnostic tool and found that syphilis antibody–antigen interactions could be detected in human serum samples.[21,22,23] Immunoassays constitute the majority of assays for detecting proteins in blood and urine and function by using specific antibodies to recognize and bind the target protein of interest. Traditionally, in order to quantify this binding event the antibody-protein complex must first be separated which can be achieved through binding the complex to a solid surface (i.e. a heterogeneous format) and then extensively washing to remove unbound antibodies. Secondly the bound antibody-protein complexes can only be detected by the use of some kind of label such as a fluorescent or radioactive marker. Although there are many variations on this type of assay format, the principles of separation and detection are fundamental in most immunoassays spanning the common pregnancy tests to the critically diagnostic assays of HIV and cancer-biomarkers. By removing the need for labels and separation BSI relies on the ability to detect and quantify the binding event between antibodies and target itself, thus promoting a glimmer of hope that such methods can be simplified, possibly reducing cost and turnover time for the benefit of patients.

1.1 Aim and hypothesis

This dissertation seeks to investigate the potential of BSI for use in clinical biochemistry, specifically addressing three areas of clinically relevant areas: immunoassays, protein binding studies and enzymatic assays.

Hypothesis I: Back Scatter Interferometry can be used as a quantitative label-free homegenous antithrombin immunoassay.

The high sensitivity of BSI, with detection limits in nanomolar ranges (e.g. IgG - Protein A),[1] suggests that BSI can be used as a quantitative immunoassay. This would allow for measurements to be done in label-free manner, without the use of a solid phase, on nanoliter volumes. Until now, BSI has been a valuable tool for research on protein binding. However, if BSI is to be used as a quantitative in vitro routine diagnostic assay, thorough validation of its performance in terms of preanalytical conditions, sensitivity, reproducibility and robustness is needed. The possible applications for BSI immunoassays are theoretically endless assuming antibodies are available for the specific analyte. In this project we will choose antithrombin as a useful model for validating BSI in the development of the immunoassay platform. Antithrombin is a protein responsible for regulating blood coagulation and is present in relatively high concentrations 4 µM to 6 µM in normal blood plasma, and so should be comfortably within the range BSI's detection capabilities.

Hypothesis II: The binding affinity of antithrombin to thrombin can be characterized in solution, in a label-free manner, with Back Scatter Interferometry

Theoretically, BSI is well suited for binding studies on antithrombin as it has been shown to undergo large conformational changes when binding to thrombin,[24,25] thus theoretically providing a proportional large shift in refractive index and therefore being detectable with BSI. From a clinical point of view binding studies could also be used to diagnose patients expressing protein mutations. An example is antithrombin mutants that displays altered binding affinity to heparin. Current methods for binding studies include Isothermal Titration Caliometry (ITC) and Surface Plasmon Resonance (SPR), which have provided detailed information on antithrombin kinetics.[26] ITC however requires relatively large amounts of samples and SPR requires proteins to be bound to a solid phase. BSI will allow label-free binding studies on antithrombin in a very low volume without the use of a solid phase.

Hypothesis III: Back Scatter Interferometry can be used to quantify enzymatic reactions, hereby expanding the possible applications of BSI for in vitro diagnostics.

Enzymes are important within clinical biochemistry, either as a target analyte or as reagent incorporated in assays to determine the amount of substrate and if enzymatic reactions are detectable by BSI it would expand the possible area of usage for the sensor. Previously SPR studies have shown that the binding between an enzyme and substrate can be detected and quantified,[27,28,29] however as SPR is sensitive to the changes in local mass on the sensor surface this type of detection is different from bulk refractive index sensing as performed by BSI. The earliest attempts of using BSI to study enzymatic reaction kinetics was performed by Swinney and Bornhop (2000) using β-hydroxybutyrate dehydrogenase, however, they used BSI as a polarimeter utilizing the fact that β-hydroxybutyrate is optically active.[30]

1.1.1 Thesis outline

The work presented in this thesis is based three papers (two published) that covers a wide range of topics from microfluidics to molecular kinetics and the thesis is therefore structed in chapters by topic.

Chapter 2 Background introduces the physics of interferometry and the refractive index as brief as possible for those unfamiliar with the concepts. Furthermore a discussion on the refractive index in relation to molecular interactions based on published literature is presented.

Chapter 3 Experimental setup and its limitations describes the experimental setup used in detail as well as discussing the consequences of inadequate microfluidc mixing and temperature control.

Chapter 4 Initial findings presents and discusses initial findings of paper I that questions and contradicts some of the fundamental claims and results found in the existing literature regarding BSI.

Chapter 5 Demystifying back scatter interferometry presents the results of the thorough investigation on the optical principles of BSI based on optical modelling and experimental results published in paper II.

Chapter 6 Protein binding studies and enzymatic reactions summarizes and presents the experimental results of protein binding and enzymatic reactions from paper II and III.

Chapter 7 Final discussion and conclusion contains a summary discussion and final conclusion on BSI as a possible method for use in clinical biochemistry

Chapter 2

Background

This chapter serves as an introduction to the physical principles of interferometry and the refractive index and also includes the theoretical basis for determining biomolecular binding and kinetics. Lastly, this chapter presents some theoretical considerations on the origin of the refractive index signal measured by BSI in relation to molecular interactions.

2.1 Back Scatter Interferometry

Interferometry is a method of measuring distance or refractive index based on the physical phenomenon of interference between waves, usually electromagnetic waves i.e. light. Back scatter interferometry is a technique that measures the refractive index of a fluid contained within a sample capillary or microfluidic channel. The technique is based on an interferometric sensing principle in which light from a laser source is directed at the capillary/channel and as the light gets reflected at the different interfaces between the sample fluid and walls of the capillary/channel it produces an observable fringe pattern consisting of bright and dark spots. The spatial position of these 'fringes' is proportional to the refractive index of the sample fluid and can be measured using a camera and signal processing equipment. The fringe pattern does not convey information on the absolute value of the sample refractive index and as such BSI cannot directly quantify the absolute refractive index, but is only sensitive to relative changes of refractive index of the sample fluid or the difference in refractive index between two subsequent samples. BSI therefore belongs to the type of so-called differential refractometers. For example the refractive index of water is 1.334 in absolute terms, but a differential refractometer can only measure the difference in refractive index between two samples, say the difference between water and saline water.

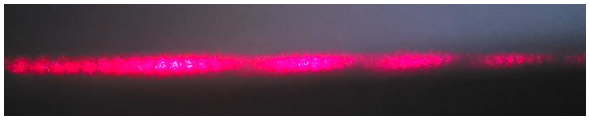

(a) Image of a fringe pattern projected onto a piece of black cardboard. The fringes are seen as periodic small bright spots occurring on a background of larger intensity variations.

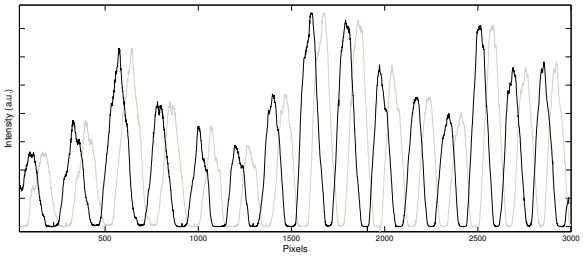

(b) Intensity plot of fringe patterns from two samples with different refractive index (black and grey lines) recorded using a 1x3000 pixel linear CCD array. The grey fringe pattern can be expressed as a spatially shifted form of the black fringe pattern, with the shift being proportional to the difference in refractive index.

Back scattered or back reflected?

The use of the term *scatter* in back scatter interferometry implies, at least to people within optics, elastic light scattering of light by small particles and molecules. This type of scattering formally known as Rayleigh scattering is very dependent on the particle size and wavelength of the light and a classic example is the strong scattering of blue light by the air which makes the sky blue for observes looking up at it. Light scattering can be used to characterize the size and shape of proteins and methods such as static- and dynamic light scattering are widely used within biochemistry. Although particle scattering is not involved in BSI some of the early investigations[3] have referenced the work of H.C van de Hulst, whom in his textbook "'Light Scattering by Small Particles"'[31] uses the term scattering in its most broadest sense for both particles and thin cylinders. A more correct word for BSI would therefore be back reflected, but because the technique has already been established in the literature using the term *back scatter* it has been adopted for use in this work as well.

2.2 Light as an electromagnetic wave

The duality of light means that it can be described as being both a particle and a wave but for the purpose of this work light will be represented as being an electromagnetic wave. Mostly we think of light as that visible to the eye, however, electromagnetic radiation is much more than just visible light. Radio waves, X-rays and micro waves, to name a few, are also electromagnetic waves that can be sorted in a spectrum according to the energy distribution of the different waves. The name spectrum refers to a wavelength, and the energy of a wave is related to its wavelength. The wavelength of visible light spans from 380 nm to 770 nm. The wavelength λ and frequency ν are related by the speed or velocity v of the wave. In empty space the velocity of light is $c \approx 3 \times 10^8 m/s$ and the relation is written as

$$c = \lambda\nu \tag{2.1}$$

ν has units of Hertz (Hz) which means cycles per second. Note the distinction between the symbols v for velocity and ν for frequency.

2.2.1 Refractive index, refraction and reflection

The speed of light depends on the refractive index n of the media that light is propagating. Traveling in a medium reduces the velocity of the propagating light by

$$v = c/n \tag{2.2}$$

The refractive index of water is often given as $n = 1.33$, thus light propagates slower through water than through empty space.

When light is incident on an interface of two media with different refractive index, light will be partially transmitted and partially reflected. The transmitted light will propagate at an angle given by Snell's law and the intensity of the reflected and transmitted light is given by the Fresnel equations. The refractive index is dependent on the wavelength and the angle of refraction is therefore also dependent on wavelength. This wavelength dependence is called dispersion and can be observed when sunlight entering a prism or raindrop is refracted at different angles according to wavelength, the latter giving rise to the rainbow observable on the sky when conditions are right.

2.2.2 Propagation of EM fields

As the name 'electromagnetic' (EM) implies, light consists of both an electronic field and a magnetic field. The Maxwell equations describe the relation between the electronic field (E) and magnetic fields (B) and are named after James Clerk Maxwell. The derivation of the Maxwell equations and the self propagating nature of electromagnetic radiation has been omitted here for sake of simplicity and the reader is referred to the numerous textbooks on the subject. What should be mentioned though is that the E and B fields are always perpendicular to each other and to the direction of propagation. Thus they travel in the same direction, with the same frequency, speed and wavelength. For many types of media the magnetic field properties are negligible and one only needs to characterize the E-field to describe the propagation of light through a media.

Mathematical representation

The E-field can be described as a plane harmonic wave, with an amplitude E_0 that when propagating in the z direction with velocity v as a function of time t can be written as:

$$E(z,t) = E_0 \cos\left(\frac{2\pi}{\lambda}(z - vt)\right) \tag{2.3}$$

If the wave instead propagates through a media with refractive index n, the velocity changes accordingly

$$E(z,t) = E_0 \cos\left(\frac{2\pi}{\lambda}(z - \frac{c}{n}t)\right) \tag{2.4}$$

The frequency ν is constant across boundaries of different media because the electromagnetic field must remain continuous and as a consequence hereof a change in wavelength occurs in accordance with equation 2.1.

The E-field described by equation 2.4 is often written using the terms angular frequency ω and the wavenumber (for vacuum) k_0

$$E(z,t) = E_0 \cos(k_0 z - \omega t) \tag{2.5}$$

where

$$\omega = \frac{2\pi c}{\lambda} = 2\pi\nu \tag{2.6}$$

$$k_0 = \frac{\omega}{c} = \frac{2\pi}{\lambda} \tag{2.7}$$

Using Euler's formula equation 2.5 can be written using a complex and exponential notation

$$\tilde{E}(z,t) = E_0 e^{i(kz-\omega t)} \tag{2.8}$$

The E-field is always considered as a complex value, but the physical representation of light is only given by the real part of the complex.

Refractive index causes a phase shift of the EM-wave

The entire argument $(kz - \omega t) = \phi$ is called *the phase* and is a function of both z and t and has units of radians ($1rad = 1/2\pi$). The phase change as a function of distance z only is referred to as the phase shift $(kz) = \varphi$. The phase shift represents the initial position of the waveforms maxima and an initial displacement of the entire wave in the direction +z or -z can be handled by adding or subtracting a value to the phase shift. The wave number was introduced as the vacuum wave number (k_0) but as stated above when light enters a media the wavelength changes according to the refractive index, hence the wave number also changes. The resultant wave number can be written as $k = k_0 + (n-1)k_0$ and inserting this expression into equation 2.8 gives:

$$\tilde{E}(z,t) = E_0 e^{i(k_0 z + (n-1)K_0 z - \omega t)} \tag{2.9}$$

which states that the refractive index is nothing but an added phase shift proportional to the distance traveled.

2.2.3 Interference of light from the principle of superposition

Two waves that intersect at a point in space can interfere with each other to produce a single combined wave. Using what is known as the principle of superposition it can be shown that the resultant superimposed intensity from two waves with the same frequency is a function of the phase difference between the two waves $\Delta\phi$. The intensity of two waves from the principle of superposition, using the simplified relationship $I = E^2$ is given as

$$I = (E_1 + E_2)^2 = E_{0,1}^2 + E_{0,2}^2 + 2E_{0,1}E_{0,2}\cos(\Delta\phi) \tag{2.10}$$

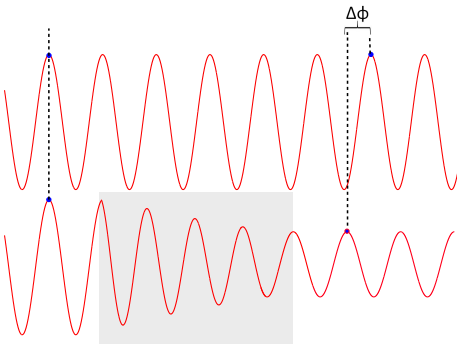

Figure 2.2: Light propagating a medium defined by the gray box with a refractive index $n > 1$ experiences a phase shift ($\Delta\phi$) relative to light traveling in vacuum ($n = 1$). Attenuation of the amplitude as shown occurs if the material is also absorbing.

When light interferes the result is said to be constructive when the resultant intensity is increased or destructive when an decrease in intensity occurs. Inspection of 2.10 reveals that maximum constructive interference occurs when the waves are in phase $\Delta\phi = 0$ and maximum destructive interference occurs when the phases are displaced by half a wavelength $\Delta\phi = \pm\pi$.

Two waves that start out in-phase may acquire a phase shift relative to each other by either traveling different physical path lengths ($z_1 \neq z_2$) or by traveling through two different media ($n_1 \neq n_2$), the difference is expressed as the optical path difference (OPD) and the resultant phase difference is

$$\Delta\phi = k_0(z_1 n_1 - z_2 n_2) = \frac{2\pi}{\lambda} OPD \tag{2.11}$$

Phase shift upon reflection

An additional 180° (π radians) phase shift of the reflected light occurs when light is reflected from a surface with a higher refractive index. No phase shift occurs upon reflection of a surface with a lower refractive index.

2.2.4 Interference pattern from light reflected by a capillary

The principles outline above are enough to explain how an interference pattern as that produced by BSI can be formed. In BSI, light from a coherent light source is reflected at the different air/glass and glass/fluid boundaries of a capillary or similar microfluidic channel, forming a number of separate reflected and refracted beams (see figure 5.2). When the beams coincide at a plane distant from the capillary they will interfere as stated above and an interference

pattern of bright and dark spots is formed. This interference pattern will be stationary if the optical path lengths i.e. the diameters and thickness of the glass and refractive indicies remain constant. However, a change in the refractive index of the sample fluid will change the optical path length for the light traversing the fluid with a resultant phase shift ultimately affecting the interference pattern accordingly.

2.3 The refractive index

2.3.1 Interaction of light with matter - explaining the refractive index

The detection and quantification of biomolecular interactions with BSI is a result of changes in the refractive index of the sample. It is therefore worthwhile to examine the nature behind the refractive index of proteins and molecules. To understand the physical origin of the refractive index one must first consider how light interacts with matter in the simplest form, namely the atom and its surrounding electrons.

The Lorentz oscillator

If a force such as an EM-field is applied to an atom the electrons will, in accordance with Newton's second law be displaced in proportion to the force applied. Atomic forces then act to bring the negatively charged electrons back towards the positively charged nucleus and the electrons will begin oscillating around the nucleus in response to the frequency of the field. This effectively produces an oscillating dipole that by itself radiates electromagnetic energy, a phenomenon known as Rayleigh scattering. The light produced by the oscillating electrons will interfere with the incident light resulting in amplitude and phase changes of the transmitted light. In the Lorentz model the electrons are tied to the nucleus with springs that act as a restoring force, balancing the electrons around the nucleus. Using Hooke's law for springs the following expression can be derived that relates the motion $x(t)$ of an electron around the nucleus to the incident E-field as

$$x(t) = x_0 e^{i\omega t} \tag{2.12}$$

where the amplitude is

$$x_0 = \frac{\mathbf{e}}{m(\omega_0^2 - \omega^2 - i\Gamma\omega)} E_{in} \tag{2.13}$$

m is the mass of the electron, $\mathbf{e}$ is the electrons charge and ω_0 is the intrinsic or resonance frequency, its physical meaning is that of the natural vibrations

frequency for the oscillator. As the frequency of the E-field approaches the resonance frequency ($\omega \to \omega_0$) the displacement is at its maximum. Included is also a term for dampening Γ that represents energy dissipation ensuring that the electrons do not oscillate for eternity. Most importantly this dissipation factor is complex valued and equation 3.11 has both a real and imaginary solution. The real part is related to dispersion (what we normally consider the refractive index) and the imaginary part to attenuation of light as shown in figure 2.3.

Polarizability

The displacement of the negatively charged electron creates a local dipole moment (p) that is equal to the product of the electron charge e and the distance x between the nucleus and the displaced electron.

$$p = ex \tag{2.14}$$

This displacement of electrons is called *polarization* and the relation between the field strength E_{in} and polarization is called the *polarizability* (α).

$$p = \alpha E_{in} \tag{2.15}$$

the polarizability is a measure of the nucleus' ability to exert control of the electrons and is often given as a volume (in cgs units) of cubic angstrom $10 \times 10^{-24}\,\mathrm{cm}$. Generally, the polarizability increases with the atomic number and radius. The macroscopic polarization (capital P) for a linear isotropic medium includes multiple atoms or valence electrons per unit volume denoted by the term N and using equations 3.13, 3.14 and 2.15 the macroscopic polarizability is written as

$$P = N\alpha E_{in} = \frac{Ne^2}{m}\frac{1}{\omega_0^2 - \omega^2 + i\Gamma\omega}E_{in} \tag{2.16}$$

The complex permittivity

A medium that can be polarized is said to be a dielectric medium, and the constitutive equations for a dielectric medium describe the response of medium to the electromagnetic field.

$$P = \varepsilon_0(\varepsilon - 1)E \tag{2.17}$$

The constitutive equations shall not be explained in further detail here except to introduce the terms permittivity ε also known as the dielectric constant that describes the constant relation between the electric displacement and the electric field intensity. In a non-magnetic material the refractive index is the square root of the relative permittivity ε_r

$$n = \sqrt{\varepsilon_r} = \sqrt{\varepsilon/\varepsilon_0} \tag{2.18}$$

where (ε_0) denotes the permittivity of vacuum.

Combing with equation 2.16 that was the expression obtained from the Lorentz model and using the constitutive material equations one finds that

$$\varepsilon = 1 + \frac{4\pi N e^2}{m} \frac{1}{\omega_0^2 - \omega^2 + i\Gamma\omega} E \tag{2.19}$$

Thus the permittivity has been defined using the Lorentz model and is found to be both a complex and frequency dependent function. A medium where the permittivity varies with frequency is said to be dispersive. From Maxwell's equations describing the relationship between the velocity of light and the permittivity, the real and imaginary parts of the complex index of refraction ($n = n' - in''$) can be related to the complex permittivity ($\varepsilon_r = \varepsilon_r^{'} - i\varepsilon_r^{''}$) and from 2.24 the following relations can be derived

$$n' = \sqrt{\frac{1}{2}\left(\varepsilon_r' + \sqrt{\varepsilon_r^{'\,2} + \varepsilon_r^{''2}}\right)} \tag{2.20}$$

$$n'' = \sqrt{\frac{1}{2}\left(-\varepsilon_r' + \sqrt{\varepsilon_r^{'\,2} + \varepsilon_r^{''2}}\right)} \tag{2.21}$$

As the refractive index is a complex number it follows that the wave number k is also complex and 2.48 can be written with the real and imaginary wave numbers separated

$$\tilde{E}(z,t) = Ae^{i(kz-\omega t)} = Ae^{(-k''z)}e^{i(k'z-\omega t)} \tag{2.22}$$

From this equation one finds that the imaginary part (k'') produces an exponential attenuation of the amplitude as light propagates the media as shown in figure 2.2. This attenuation as first discovered by Bougher, is known as absorption and described by the well known Lambert-Beer law. An example of the real and imaginary index of refraction using 2.21 and 2.22 is plotted in 2.3. The peaks are resonance phenomena with a width characterized by Γ and centered around the natural frequency ω_0. Likewise it explains the phenomena of dispersion and shows that the refractive index increases when approaching a resonance peak from a lower frequency, which is called normal dispersion and its counterpart anomalous dispersion when approaching a resonance peak from higher frequencies. Atoms with multiple resonant electrons will display multiple Lorentzian shaped peaks as seen when observing an absorption spectrum for many real substances. Another important notion is that the real and the imaginary part of the refractive index are related and the so-called Kramers-Kronig relationship presents a mathematical method for deriving the real part of the refractive index from the imaginary part and vice versa.

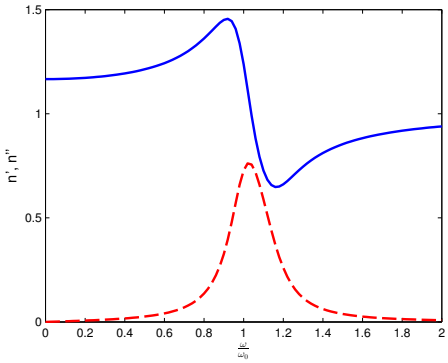

Figure 2.3: Real (solid line) and imaginary (dashed line) parts of the refractive index from a single Lorentzian oscillator. The angular frequency (ω)is normalized to the resonance freqency (ω_0)

Electronic, vibrational and orientation polarization

As shown above the permittivity and therefore also the refractive index are frequency dependent. The Lorentz model explains how polarization gives rise to dispersion, but one must also consider that there are different forms of polarization mechanics. Many molecules are polar or have charged groups that adds a static dipole moment to the molecule that will try and align against an applied EM-field. However, these effects known as ionic- and orientation-polarization are slow compared to the frequency of UV-visible light. The polar molecules and ions simply do not have time to reorient and the effects of ionic- and orientation-polarization effects vanish at optical frequencies. Therefore the only polarization in the UV-visible frequencies (THz) is the electronic polarization caused by the distortion of electrons around the nucleus which is fast enough to follow the oscillating field.

2.3.2 Polarization in a dense media

The harmonic oscillator has been used in both the explanation of the polarization of atoms as well as for a dielectric medium. As such it may be tempting to use the microscopic polarizability (α) to explain the refractive index of a media. However, the equations presented above are based on the assumption that N is sparsely populated i.e. the number of molecules per volume is very small, which is the case for gasses but not for denser mediums such as water. The difference lies in the fact that the applied field E will not be the same in the two cases. Following the explanation given by Richard Feynman in his lectures, the local atoms in a dense medium will feel the effect of nearby atoms being polarized as an additional local E field E_{loc}. Thus the applied field E and the effective field E_{eff} are not the same, but as long as the wavelength is

much longer than the spacing between atoms the following relation known as the Lorentz-Lorenz formula is valid

$$\frac{n^2-1}{n^2+2} = \frac{4\pi N e^2}{3m}\frac{1}{\omega_0^2-\omega^2} \tag{2.23}$$

The Lorentz-Lorenz formula holds for non-absorbing materials and can also be applied to polar liquids such as water at optical frequencies (UV-visible). It has taken its name after the two scientists Lorentz of Copenhagen and Lorenz of Leyden whom independently derived an identical expression for the relation between the refractive index and density of a liquid.

Refractivity

The polarizablity can also be expressed in a term called the molar refractivity (R) that expresses the polariziability of a mole of substance

$$R = 4/3\pi N_A \alpha \tag{2.24}$$

where N_A is the Avogadro number Setting $N \approx \rho$ in equation 2.23 the relationship between the molar refractivity, refractive index and density of a medium can be expressed using the Lorentz-Lorenz formula

$$R = \frac{n^2-1}{n^2+2}\frac{Mw}{\rho} \tag{2.25}$$

where Mw is the molecular weight and ρ is the density of the substance and $Mw/\rho = V_M$ where V_M is the molar volume which is used interchangeably in equation 2.25. Note that R has units of volume ($\mathrm{cm}^3\,\mathrm{mol}^{-1}$) whereas the refractive index (n) is without units. The term specific refrativity (r) is sometimes used and this simply expresses the refractivity in units of mass. Of particular importance is that the relation between the refractive index and the density is such that R is nearly constant. For instance the molar refractivity of water in vapor form is $3.72\,\mathrm{cm}^3\,\mathrm{mol}^{-1}$ and only changes to $3.72\,\mathrm{cm}^3\,\mathrm{mol}^{-1}$ when in condensed liquid form.[32] Thus if one measures the refractive index and the density with adequate precision then it is possible to determine the refractivity of a substance.

2.4 Biomolecular binding and kinetics

Determination of biomolecular affinity and rate constants are useful parameters for investigating a specific protein-ligand binding or enzymatic reactions, however the vast majority of assays withing the area clinical biochemistry are quantitative assays with a simple purpose of quantifying the amount of analyte present in a sample. Although biomolecular binding kinetics are essential preconditions for design and development of such assays, these underlying mechanisms are hidden from the users view and kinetic rate constants are rarely of any concern in the daily routines of a clinical biochemist. Affinity and rate constants are specific for each and every biomolecular interaction and the reason for determining affinity and rate constants with BSI within this work should be seen as evidence that the system measures binding events that are truly related to the specific binding or reaction of interest.

2.4.1 Determining affinity constants of biomolecular interactions

Biomolecular binding is governed by the the law of mass action and a simple binding between two species A and B can be described by the equilibrium equation:

$$A + B \underset{k_2}{\overset{k_1}{\rightleftharpoons}} AB \tag{2.26}$$

The rate at which the reaction proceeds towards AB is called association and is given by the rate constant k_1. Likewise the rate at which the reaction proceeds towards A+B is called dissociation and is given by the rate constant k_{-1}. Relating the rate constants one gets the affinity constants:

$$\text{Dissociation constant: } K_D = \frac{k_{-1}}{k_1} \tag{2.27}$$

$$\text{Binding constant: } K_B = \frac{k_1}{k_{-1}} \tag{2.28}$$

When the reaction is at equilibrium the affinity constants tells the amount of free and bound species present and the reaction scheme is arranged as follows, with square brackets usually indicating molar concentrations

$$K_D = \frac{[A][B]}{[AB]} \qquad Units : M \tag{2.29}$$

$$K_B = \frac{[AB]}{[A][B]} \qquad Units : M^{-1} \tag{2.30}$$

In order to determine the affinity constants one must determine from the total amount of $[A]_{Total}$; how much is bound in the form of $[AB]$ and how much is

free $[A]$. From equation 2.27 the following expression is generated, where the left side is usually referred to as the bound fraction of A

$$\frac{[AB]}{[A]_{Total}} = \frac{[B]}{[B] + k_D} \tag{2.31}$$

Thus if the concentration of A is kept constant a titration with varying amounts of B the bound fraction is a hyperbolic function of $[B]$. For a method such as BSI that directly measures [AB] the following equation can be used

$$AB = AB_{max} \frac{[B]}{[B] + k_D} \tag{2.32}$$

Here, AB and AB_{max} do not represent concentrations but are reported in the units of method used e.g. fluorescence, scintillation counts or radians in the case of BSI. AB_{max} is the signal measured if the maximum amount of A was bound and is used to normalize the curve. Therefore if AB is measured and plotted against a range of solutions where [B] is known, then K_D may be derived by the use of a nonlinear curve fitting algorithm. Historically other parameter estimation methods have been used such as the Scatchard plot.

2.5 Using BSI to measure [AB]

Irregardless of theoretical speculations into the physical origins of the signal measured by BSI, the ability to detect the formation of [AB] and derive the affinity constants relies on the assumption that the refractive index of the dissociated state (on the left side of the equilibrium equation 2.26) is different than the that of the system in the associated state (right side).

$$n_A + n_B \neq n_{AB} \tag{2.33}$$

2.5.1 End-point measurements

Measurement of [AB] by end-point measurements assumes that the reaction has obtained equilibrium, which means that although association and dissociation continues to occur there is no net change in free or bound [B] and the maximum amount of [AB] has been formed. To achieve a state of equilibrium it is necessary to incubate the solutions for a period of time that depends on K_D, sometimes several hours. Usually the concentration of A is held constant but B is titrated in a concentration range spanning from below K_D to several orders of magnitude above K_D, and the signal must be therefore corrected for the amount of unbound B. This is done by making a reference measurement on solutions that does not contain A and subtracting the reference value from the sample. Thus

$$\Delta n = n_{sample} - n_{reference} \tag{2.34}$$

Under such circumstances a plot of Δn vs. [B] should show a hyperbolic relationship that can be fitted to equation 2.47 to obtain K_D.

Subtraction of reference measurements is a standard procedure in various techniques used for studying biomolecular interactions and is considered good laboratory practice. The reason for using reference measurements is to take into account any deviation from linearity between [B] and the measured signal. Depending on the assay format, such deviations may appear from unspecific binding of B to matrix components, or from non-linear detector response. However, by introducing a second set of measurements one also introduces an additional source of error. From a practical point of view the sample and reference solutions must be exactly identical in terms of ligand concentrations but also buffer composition as both will affect RI and errors from manual pipetting should be carefully considered. Secondly, the measurements must also be performed in such a way that any changes in the system performance, such as baseline drift, is kept at a minimum between measurements. Due to the time it takes to inject and obtain a stable signal, the total collection time (not including any repetitions) is at minimum half an hour over which baseline drift can be significant. There are basically two approaches for performing end-point measurement:

1. Measure all the reference solutions first and then subsequently measure all the sample solutions.
2. Measure solutions interchangeably in pairs starting at the lowest concentration i.e. reference 1, sample 1, reference 2, sample 2 etc.

Both methods have disadvantages as method 1 is particularly sensitive to signal drift over time whereas method 2 is likely to be biased from sample contamination between each subsequent measurement, also known as carry-over. Both approaches were initially investigated for the measuremnt of protein A - IgG (see chapter 4) without any significant differences observed (data not shown), but method 2 was chosen as the method of choice and used for protein binding studies in chapter 6.

2.5.2 Real-time measurements

A second approach is to measure the formation of or dissipation of either product or reactant over time and derive the rate constants k_1 or k_{-1}. Apart from providing a real time image of the process there is also no use for reference measurements. However for many biochemical reactions or binding events the association rates are quite fast and measurements must be performed within a time span of seconds after mixing the reagents. Returning to the simple association process showed in equation 2.26 this reaction can be expressed in the form of an ordinary differential equation

$$\frac{d[AB]}{dt} = k_1[A][B] - k_{-1}[AB] \tag{2.35}$$

Usually it is not possible to measure k_1 directly as dissociation (k_{-1}) will occur as well. However, a practical form called the observed rate constant k_{obs} can be obtained and a solution to the differential equation can be derived in the form

$$AB_{(t)} = AB_{max}(1 - e^{-k_{obs}t}) \tag{2.36}$$

where $AB(t)$ is the signal from the amount of AB complexes present at the time t and AB_{max} is the maximum (plateau) value obtained for a given amount of B. Fitting a curve to the measured real-time data using nonlinear curve fitting algorithm k_{obs} can be estimated and by performing several real-time measurements with varying amounts of B a plot of K_{obs} vs [B] yields a straight line where the slope is equal to K_1 and the Y-intercept equals k_{-1}.

$$k_{obs} = k_1[B] + k_{-1} \tag{2.37}$$

K_D can now be found using equation 2.27. Both real-time [1,12] and end-point [13,11,19] determinations of K_D have been determined using BSI, although in the more resent papers end-point measurements seem to be preferred.

2.6 Determining kinetic constants for enzymatic reactions

The kinetics of enzymes binding to their substrate is another form of biomolecular binding as described above, with the notable exception that the enzyme is not consumed but instead catalyzes an existing chemical reaction. One of the particular features of enzymatic reactions is that reaction-order changes with the amount of substrate present. So for high amounts of substrate the reaction will be zero order whereas at low amounts it will proceed as a first order reaction. In the case of a single substrate enzyme-catalyzed reaction the product formation can be described as follows

$$S + E \underset{k_{-1}}{\overset{k_1}{\rightleftharpoons}} ES \xrightarrow{k_2} P + E \tag{2.38}$$

Here S denotes the substrate catalyzed by the enzyme E into the product P. The first step is the formation of a enzyme-substrate complex ES, which is governed by rate constants k_1 and k_{-1}. The second step is the release of product from the intact enzyme given by k_2. Under steady state assumptions it is normally assumed that the following holds:

$$[S] >> [E] + [ES] \qquad \frac{d(ES)}{dt} = 0 \qquad \frac{d(E)}{dt} = 0 \qquad [P] = 0 \tag{2.39}$$

and the formation of product over time, also called reaction velocity v, is given by the Michaelis-Menten equation

$$v = \frac{dP}{dt} = \frac{v_{max}[S]}{[S] + K_M} \tag{2.40}$$

where, v_{max} is the maximum velocity $v_{max} = k_2[E]$ and $K_M = (k_{-1} + k_2)/k_1$ is the Michaelis-Menten constant. Determining K_M from equation 2.40 requires the measurement of the reaction velocity (v) and therefore cannot be done by end-point measurements as for affinity constants (K_D). The velocity must be measured at steady state conditions which means that notably [ES] must be constant. The last condition $[P] = 0$ is often disregarded under the assumption that inhibition by the end product is negligible. At steady state conditions

$$v = [ES]k_2 \tag{2.41}$$

I.e. the product formation is linear over time and by measuring v for solutions with varying amount of substrates K_M and v_{max} may be derived, either by methods of nonlinear least-square fitting where v is plotted directly against [S] or using graphical interpretations such as the Lineveawer-Burk plot. To obtain the best estimation of the kinetic parameters the substrate concentration must span from well below K_M to amounts high enough to ensure that v_{max} is reached. In practical terms the challenge of satisfying steady state assumptions means that at low substrate concentrations the consumption of the small amount of substrate proceeds quickly and [ES] will not remain constant and ultimately the reaction will not be linear over a very long period of time. Of course this can be prevented if [E] is very low, but in return the velocity is reduced and measurement of such low product formation rates can be practical challenging. In terms of BSI there must be a difference in refractive index between substrate and product that is large enough to be detectable at concentrations lower than K_M, which can be well below micromolar ranges. Theoretically, one should also take into account a possible refractive index difference between substrate-bound and free enzyme, i.e. $n_E \neq n_{ES}$. However, typically the enzyme concentration will be in nanomolar concentrations and any contribution thereof would be quite small relative to the substrate concentrations that are often in micromolar ranges.

2.7 On the relation between refractive index and biomolecular interactions

Detection of molecular interactions in solution between substance A and B being; proteins, small ligand molecules, ions or any other substance, using BSI is based on the assumption that the resultant refractive index is non-additive (see eq.2.33) i.e. the refractive index of the solution containing bound complex AB is different than that of the solution with A and B in unbound states. According to the Lorentz-Lorenz formula (eq.2.23) such non additive properties would have to be a result of non additive properties of either density and/or the polarizability.

2.7.1 Refractive index and molecular interactions in mixtures of binary fluids

The non-additive properties of fluid mixtures have been extensively studied using refractive index in the literature, see for instance references:[33,34,35,36,37,38,39] and although such studies are often done on small molecules and at much higher concentrations than what is typically used in biomolecular protein binding studies, the underlying mechanism could provide valuable clues to discern the origin of the BSI-signal.

Molecular interactions e.g. dipole-dipole, ion-dipole, hydrogen bonding between solute and solvents can alter the thermodynamic properties of a mixed fluid including; volume, density, refractive index, viscosity and temperature. A typical example is how mixing parts of alcohol and water results in a volume that is less than the sum of the parts, humorously referred to as the bartenders conundrum.

Ideal mixtures

For an ideal mixture of two fluids the volume, density, specific and molar refractivity are additive properties. A number of so-called mixing rules have been developed that allows one to more or less accurately determine the refractive indices of solute, solvent or the total solution from refractive index and density of pure substances. Some of the rules are derived on a theoretical basis; Lorentz-Lorenz, Wiener and Heller, whereas others are derived empirically; Gladstone-Dale and Arago-Biot and circumstances under which these mixing-rules are best applied and used was first discussed by Heller in 1964.[40]

The Lorentz-Lorenz mixing rule:

$$\frac{n^2-1}{n^2+2} = \phi_1 \frac{n^2-1}{n^2+2} + \phi_1 \frac{n^2-1}{n^2+2} \tag{2.42}$$

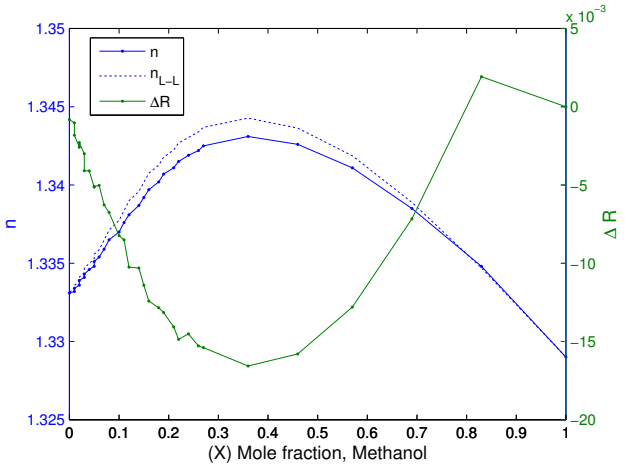

Figure 2.4: Refractive index of water-methanol mixture as a function of mole fraction. Measured values of n (solid blue line), predicted values of n using Lorentz-Lorentz mixing rule (solid blue line) and deviation of molar refractivity ΔR (solid green line, right axis)

where ϕ is the volume fraction determined from the pre-mixing volumes of the components. Volume fractions may be determined on a pure volume basis, molar volume or on a weight-fraction basis.[41] Similarly the molar refractivity of an ideal mixture based on the mole fraction X is

$$R_{12} = X_1 R_1 + X_2 R_2 \tag{2.43}$$

Non-ideal mixtures

It is customary to describe deviations from ideality as the difference between the observed and ideal values.

$$\Delta n_{12} = n_{obs} - \phi_1 n_1 + \phi_2 n_2 \tag{2.44}$$

$$\Delta R_{12} = R_{obs} - (X_1 R_1 + X_2 R_2) \tag{2.45}$$

One example of a simple binary mixture that displays volume contraction is that of water and methanol mixture. Figure 2.4 shows the refractive index of of water and methanol mixtures using data from *David R. Lide, ed., CRC Handbook of Chemistry and Physics, Internet Version 2005, www.hbcpnetbase.com, CRC Press, Boca.* Additionally the refractive index has been estimated using the Lorentz-Lorentz mixing rule[40,37] and ΔR is calculated from equation 2.46. The obtained values are in agreement with those found by Herráez and Belda (2006)[34] and Fucaloro (2002)[42]. As can be seen in figure 2.4 the predicted values of n are in good agreement with the measured values and the small differences are attributed to volume contraction. The figure also shows a non-linear deviation in ΔR and because the molar refractivity R is related to the

polarizability, ΔR is viewed as a measure of the overall change of polarizability due to the disruption and creation of contacts during mixing.[41]

The deviations in refractivity (polarizability) and volume changes from ideality were first related to molecular interactions by Aminabhavi and Munk (1979) using a contact term derived from the Flory-Huggins theory that represents the solvent-solute interaction. The authors have applied these interaction terms on both binary mixtures and polystyrene particles in a binary mixture of various solvents,[43,44,45] and they find that densities and refractive index of mixtures are better predicted when these terms are included. They note, however, that the effect of change in polarizability from interaction on the refractive index is small.

In summary the studies and use of various mixing-rules for binary fluids prove that in case of molecular interaction, the mixture density and polarizability can change and as a result the refractive index will deviate from ideal additive behavior.

2.7.2 Ab initio calculations on polarizability and molecular interactions

From the earliest work the polarizability of molecules has been described as being additive, meaning that the polarizability can be calculated by a sum of atomic and bond contributions.[46,47] With the advent of powerful computers it has been possible to make ab inito (quantum mechanical) calculations on the polarizability of larger molecules and clusters of molecules including amino acids at optical frequencies, although ab initio calculations on entire proteins are still limited.

An ab initio study by Millefiori, Alparone, Millefiori and Vanella (2008)[48] found that the polarizability of individual amino acids are not much dependent on molecular structure and conformation but that the polarizability deviated significantly from simple additivity. Hansen, Jensen, Åstrand and Mikkelsen (2005)[49] have adopted a classic interaction model (in contrast to quantum mechanical) that takes into account the induced dipole from neighboring polarized atoms. Their model has shown good agreement with ab initio calculations and has been applied to three proteins; ribonuclease inhibitor, lysozyme and green fluorescent protein demonstrating that the polarizability differed by around 10% from a simple additive model. This difference is attributed to the fact that the additive model does not take into account the peptide bonds between amino acids. They also studied the effect of intermolecular interaction on the polarizability between molecules and found that the effect of neighboring molecules on the isotropic polarizability is small.[50] It should be noted that the authors found a larger effect on the anisotropic polarizability, but as proteins and molecules in solution are randomly oriented only the isotropic polarizability

is of importance. Furthermore the classic interaction model was used by Jensen et al. (2002)[50] to show that the interaction effect in clusters of molecules is dependent on the distance between individual molecules as well the total distance. One of the molecules studied was urea which was also studied by Wu, Snijders and Lin (2002)[51] on an ab initio basis and both groups find that the deviation from additivity did not exceed 5%. Urea is interesting because it exhibits multiple hydrogen bond interactions that BSI is cited as being sensitive to,[52,20] in fact Pesciotta, Bornhop and Flowers (2011)[17] used BSI to detect hydrogen bond interaction with urea derivatives.

From these findings it must be concluded that there is a possible effect of intermolecular interactions on the electronic polarizability at optical frequencies, but that such an effect is small. As also noted by the authors a 30% change in polarizability will only result in an approximate 10% change in refractive index[53]. Although the available polarizability data on entire proteins is scarce and to the knowledge of this author there are no studies on the effects of protein interaction with ligands or other proteins, there seems to be little evidence to support the hypothesis of large changes in polarizability by intermolecular interaction or conformational changes of proteins.

2.7.3 The refractive index increment of proteins

The refractive index increment (dn/dc) is a constant that describes the increase in refractive index as a function of solute concentration. It is usually given in units of volume per mass $\mathrm{L\,g^{-1}}$. Thus in relation to protein complex formation the assumption of a change in refractive upon complex formation of two proteins (or protein-ligand) A and B requires that the dn/dc of the complex AB must be different than the sum of individual dn/dc values for A and B. It is also especially relevant in the case of BSI because differential refractometry is well suited for experimental determination of dn/dc values and when preforming end-point measurements (see sec2.5.1) one essentially measures the dn/dc of the solution. Theoretically the dn/dc can be derived by using an appropriate mixing-rule for dilute solutions as given by Heller[40,54].

$$dn/dc = \frac{3}{2}\bar{V}\left(\frac{n_2^2 - n_1^2}{n_2^2 + 2n_1^2}\right)n_1 \tag{2.46}$$

where $\bar{V}$ is the partial specific volume, n_1 and n_2 the refractive index of solvent and solute respectively. The dn/dc is clearly dependent on the refractive index of the solvent, and in the case $n_2 = n_1$ then $dn/dc = 0$. Ball and Ramsden (1998)[55] found that the dn/dc of proteins does depend on the refractive index of different buffer solutions, as one would expect from equation 2.46, but also found differences that did not seem to correlate to buffer RI and attributed these differences to ion-interactions between buffer and charged amino groups.

Partial volume of proteins and solute-solvent interaction

From equation 2.46 it is evident that dn/dc is dependent on the partial specific volume $\bar{V}$ of the solute and this relation is of interest because conformational changes of protein structure may induce a change in specific volume. Yang and Hajime (1963)used refractometry and dilatometry to measure the denaturation of a polypetide from a helix state to a coiled state (randomly ordered structure) and observed a volume increase and refractive index decrement associated with the transition.[56] In a similar study Bornhop et al. used BSI to study the unfolding of the protein T1 RNase.[7] Unfortunately, further published studies on the relation between protein structure and refractive index is lacking, except for the studies preformed using BSI. There has however, been extensive studies on the volume properties of proteins in relation to solvent-solute interaction and the partial volume $\bar{V}$ of proteins is generally conceived as consisting of the following contributions:[57,58]

$$\bar{\bar{V}} = V_W + V_T + V_I + \beta_{T0}RT \tag{2.47}$$

Where V_W is the intrinsic volume often approximated by its van der Waals volume and is inaccessible to solvent molecules, V_T is the thermal volume described as a void volume due to vibration and steric effects, the latter reflects the imperfect packing of solute and solvent molecules, V_I is the interaction volume which reflects the interaction between solvent and solute molecules, finally the last term is an effect of isothermal compressibility which is relatively small for proteins and often disregarded. The interaction volume (V_I) is viewed as the difference between the partial volumes of bulk solvent and solvent interacting with the solute. V_I is a negative term, thus the density of hydrating solvents (water) is higher then that of the bulk $\tilde{1}$0-15%[57] and this has lead to the proposal that measured changes in refractive index of protein interactions by BSI is the result of density changes in the hydration layer surrounding the molecule.[1,16] However, the volume change associated with protein folding/unfolding upon denaturation, which can be viewed as an extreme form of conformational change, or from binding to ligands or other proteins is generally found to be quite small ($< 1\%$).[59 60,61]

On the additivity of aminoacid dn/dc values

Early studies by McMeekin (1962) demonstrated that the refractive index of proteins n_p could be determined by a purely additive scheme of the amino acids.[62] Using the Lorentz-Lorentz equation the protein refractive index may be described by

$$n_p = \sqrt{\frac{2R_p + \bar{V}_p}{\bar{V}_p - R_p}} \tag{2.48}$$

where the specific refractivity r_p and the partial specific volume $\bar{V}_p$ of the protein are weighted averages of the contributions of all individual amino acids i.e an additive scheme

$$r_p = \frac{\sum r_a M w_a}{\sum M w_a} \tag{2.49}$$

where r_a is the refractivity of each amino acid and M_a its molecular mass. Similarly the protein partial specific volume is

$$\bar{V}_p = \frac{\sum \bar{V}_a M w_a}{\sum M w_a} \tag{2.50}$$

Expanding on the work of McMeekin[62], Zhao, Brown and Schuck (2011)[63] have made an extensive study on more than 62000 proteins from a genome database and determined their refractive index increment using the Wiener equation 2.46. They find that for all the proteins the dn/dc fits a gaussian distribution that narrows as protein size > 100kDa with a mean of $0.1902\,\mathrm{mL\,g^{-1}}$ for small proteins and $0.1899\,\mathrm{mL\,g^{-1}}$ for larger proteins. For human proteins the mean dn/dc is $0.1899\,\mathrm{mL\,g^{-1}}$ with a standard deviation of $0.0030\,\mathrm{mL\,g^{-1}}$. This range of dn/dc values is in good agreement with those obtained by various other authors[64] and it is not uncommon practice to simply use a constant of $0.19\,\mathrm{mL\,g^{-1}}$ for all proteins. When compared with the molar volume of the proteins Zhao et al. find an absence of cross correlation between volume and dn/dc, suggesting that overall the protein volume is not a predominant parameter for dn/dc, instead it is primarily given by the the composition of the different aminoacids.

Examples of calculated dn/dc values by Zhao et al.[63] for polypeptides consisting of a single type of amino acid predicted at 589 nm in water with 150 mM NaCl are shown in table 2.1. Experimental determination for two peptides was found to be in good agreement with theoretical predicted dn/dc values[63]. Although both the specific refractivities and volumes of amino acids used to calculate the dn/dc are experimentally determined, the additive approach only accounts for the intrinsic volume of the protein and the contributions from interaction and thermal volume is not included. By a rough estimate using equations 2.46 and 2.48 a 1% change in partial volume of a given protein, which as discussed above is the general volume change associated with denaturation, only produces a change on the third decimal place of the dn/dc which means

Amino acid	R cm^3/mol	$\bar{V_M}$ ml/g	r cm^3/g	dn/dc ml/g
Arginine	39.47	0.70	0.253	0.206
Histidine	34.62	0.67	0.253	0.219
Lysine	34.10	0.82	0.266	0.181
Alanine	17.15	0.74	0.242	0.167
Tryptophane	55.24	0.74	0.297	0.277
Tyrosine	44.34	0.71	0.272	0.240

Table 2.1: Molar refractivity (R), partial molar volume ($\bar{V_M}$) and refractivity (r) are from McMeekin[62] and dn/dc values for polypeptides of single amino acid types have been calculated by Zhao et al.[63] using those values.

that the protein concentration will have to be high (i.e. several milligrams per liter) for the refractive index to change 10^{-6} RIU.

Chapter 3

Experimental setup and its limitations

This chapter details the experimental setup of the back scatter interferometer as well as an investigation of the problems associated with microfluidic sample mixing and diffusion of solutes. The consequence of artificial binding signals caused by these problems is discussed and the use of BSI for real-time measurements is questioned.

3.1 Initial design plans

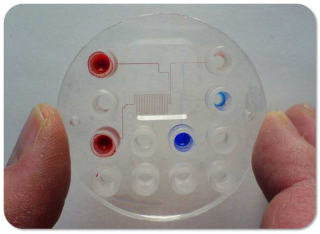

Figure 3.1: The DTU chip

A main component of the back scatter interferometer, or any interferometer for that matter, is the optical cavity where the laser beam interrogates the sample. The first BSI systems published used thin glass round microcapillaries with inner diameters around 250 µm and smaller, but the more recent experiments featured microfluidic chips made in either glass or PDMS with integrated square or semi-circular channel geometries.[2,3,8] A microfluidic polymer chip fabricated at the Danish Technical University with a semi-circular channel structure similar to that used in recent work by Bornhop et al.(2007)[1] was originally planned for use in this project. The chip also featured a microfluidic serpentine-mixer that allows for on-chip rapid mixing and merging of fluids from two inlets. However, due to technical difficulties not within control of this author, such a functional chip could not be fabricated. Instead, attempts were shifted to find a suitable alternative and various forms of glass and polymer capillaries were tested.

3.2 The capillary

The choice of using glass capillaries designed for blood collection was an arbitrary choice at first. Various polymer capillaries were tested, but the glass capillary produced a high contrast fringe pattern that was reproducible upon exchanging the capillary. The thick capillary wall (250 µm) means that the channel is less likely to deform from stress upon mounting the capillary with clamp springs and screws and although not fully realized at the time the large diameter also ensures a high sensitivity.

Capillary specifications

The capillary has a 1.40 and 1.90 mm (± 0.05 mm) inner and outer diameter respectively, the initial length is 125 mm but this is cut down to approximately 4-5 cm. According to the manufacturer (Vitrex medical A/S, Herlev, Denmark) the glass is soda glass, but the refractive index is not precisely known. The refractive index of was set to 1.515 but the excact calue will depend on the manufacturing process and ingredients of the glass.[65,66,67]

Changes to experimental setup

The setup has developed and evolved over time as the project progressed and both temperature control and signal processing has been updated on multiple occasions, but the core optical components; the capillary and the laser, have remained unchanged. As shall be rigorously explained later (see chapter 5), the sensitivity is largely dependent on the capillary geometry and since the same capillary dimensions has been used consistently, unless specifically stated otherwise, the sensitivity is identical across the various design alterations.

3.3 Optical components

All the optical components are mounted on an optical breadboard (50 cm x 40 cm) that reduces vibrations (Thorlabs, Göteborg, Sweden). An optical enclosure mounted on the breadboard blocks light and partially shields the setup from temperature and acoustic vibrations from the environment. A linear polarized HeNE laser (632.8 nm, 25LHP991-230, Melles Griot, Carlsbad, USA) is mounted on the breadboard but encased in an additional Styrofoam box with a fan that ventilates the laser to prevent overheating. The laser beam is passed through an optical density filter and directed perpendicular onto the capillary using a kinematic mirror (M1). The resulting fringepattern is directed with a second kinematic mirror (M2) towards the detector (CCD). The distance between capillary and CCD has been adjusted on multiple occasions. Initially the distance was 35 cm which projects approximately 15 fringes onto the CCD and provides a good spatial resolution of the fringepattern. This distance was later on reduced to 15 cm to improve frequency resolution as described in chapter 5.

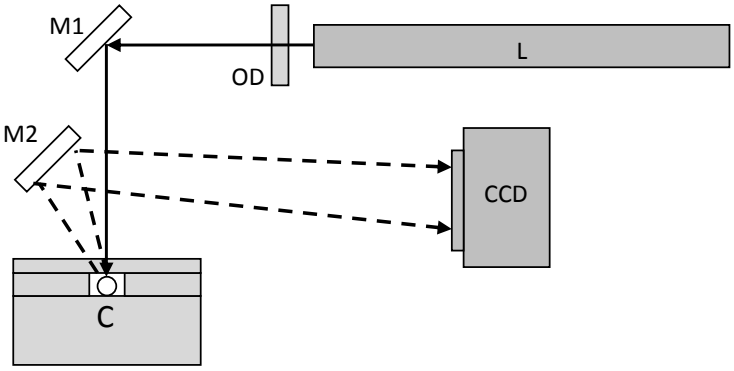

Figure 3.2: Schematic presentation of the BSI optical setup. The beam from the laser (L) passes an optical density filter (OD) and is directed using a mirror (M1) onto the capillary (C). A part of the resulting interference pattern (shown as dashed lines) is directed onto the CCD via a secondary mirror (M2).

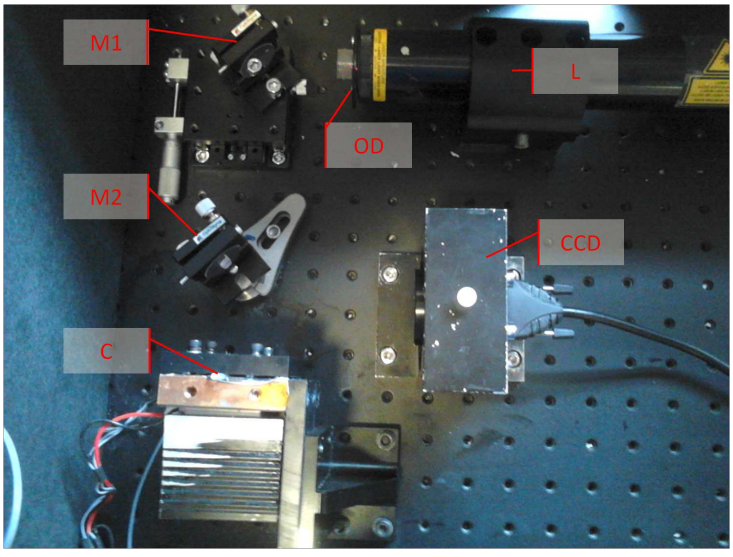

Figure 3.3: The experimental setup as photographed from above. Designations correspond to those given in figure 3.2

3.4 LabVIEW data acquisition and control interface

The LabVIEW program environment (LabVIEW 2011, National Instruments) was used for data acquisition and signal processing as well as pump and CCD control through a custom build general user interface. LabVIEW data acquisition and control points:

- CCD readout and control settings
- Temperature readout: Capillary
- Temperature readout: Optical enclosure
- Temperature readout: Laser
- Temperature readout: Peltier controller (Analog voltage)
- Pump control (on/off, pump rate)

All acquired data was stored as .txt files for later use in MATLAB (MathWorks(®)). Temperature data from the thermistors was acquired with a NI 9211 24-bit Thermocouple Differential Analog Input Module (National Instruments). Another data acquisition card (NI USB-6008, National Instruments) was used to control the pumps and monitor the temperature sensor from the TED 200 peltier temperature controller via an analog voltage output that is proportional to the actual value of the temperature.

3.5 Imaging and signal processing

When the laser impinges the capillary orthogonally the resultant fringe pattern spans a circle of 360° around the capillary, with a height corresponding to that of the laser beam and the fringe pattern intensity can be fully sampled using a one-dimensional array of pixels. As the fringe pattern is monochromatic there is also no need for color resolution. The chosen detector was a 3000 pixel linear CCD with a pixel width of 8 µm (Garry 3000 SD, Ames Photonics, Texas, USA). The small width of the pixels means that the entire array of 3000 pixels is only 22 mm wide, which ensures that minute fringe translations can be detected. The number of pixels per fringe (i.e. resolution) depends on the distance between the capillary and the CCD and similarly due to the circular nature of the fringe patter, moving the CCD further away from the capillary also increases the physical translation of the fringes across the CCD-array. The CCD image integration time can be set between 10 µs to 30 s and was set as high as possible without the image saturating to get a good fringe contrast (i.e. the

difference between dark and bright spots). A value of 250 µs was appropriate in most cases.

3.5.1 Fourier transform

Signal processing of the collected fringe pattern was performed in LabView with a Fourier transform algorithm chosen as the method for detecting fringe translation. The Fourier transform is based on an assumption that a function can be constructed (Fourier synthesis) or deconstructed (Fourier analysis) using a number of sinusoid waveform functions, representing a continuous wave that has an amplitude (A), frequency (ω) and phase (Φ). Note that this description of the fringe pattern is mathematically analog to the description of electromagnetic fields given in chapter 2 but to discern the two notations the fringe pattern phase is denoted with a capital phi.

The fringe pattern can be regarded as a continuous waveform that is a function of the angle $f(\theta)$ relative to the impinging laser beam, but when it is sampled by the CCD the signal becomes discrete, consisting of a finite integer number of points, one for each pixel. This discrete function is written as $f[n]$ where n known as the spatial variable is the pixel-number, thus $f[n] = x_0, x_1, x_2..., x_{N-1}$ with N=3000. (The use of square brackets denote a discrete function).

Observing the sampled fringe pattern one can see that it is composed of fringes with varying width and amplitude, thus it is composed of multiple waveforms with distinct frequencies. Fourier analysis transforms the sampled signal from the spatial domain (the image of the fringe pattern) into a frequency domain where the multiple waveforms are separated according to their frequency. Normally, the concept of frequency relates to time with unit commonly in Hz, but because the signal is a spatial image the frequency is related the spatial width in terms of pixels. Thus high frequency components describe narrow fringes and low frequency components describe the wide fringes. To make a Fourier transform of a discrete function the Discrete Fourier Transform (DFT) is used:

$$F[k] = \sum_{n=0}^{N-1} f[n] e^{-i(2\pi/N)kn} \tag{3.1}$$

$k = 0, 1, ..., N-1$ The result is a range of complex phasors $F_k = A_k e^{i\Phi_k}$ containing the amplitude and phase of the k'th frequency. A graphical representation of the frequency domain can be made by plotting the amplitude content of each frequency component against the frequency. Such a plot is called a *spectrum*. Traditionally in earlier works on BSI one has searched for a single dominating frequency that is thought to represent the fringes most sensitive to changes in sample refractive index.[4] Since the phase shift of a waveform describes its position relative to $x = 0$ then monitoring the phase shift of the dominant fre-

quency gives the translation of the fringe pattern. The phase can be calculated as $\Phi = tan^{-1}\frac{Re(X_k)}{Im(X_k}$) and is returned in units of radians.

Note on units The unit radians comes from using a Fourier transform. Using other algorithms can produce other units for instance in some of the work by Bornhnop et. al, they use pixels.

3.5.2 Phase unambiguity

Phase extraction of fringe patterns is imposed with a number of complications. Due to the cyclic nature of the sinosoid waveform a phase shift of 2π rad is equivalent to the wave maxima shifting a full period and cannot be discerned from the original position. The phase is said to be indeterminate by a factor of 2π and some effort must be put into detecting phase shifts that are larger then this. For example a shift of 2.5π is indeterminate from a negative shift of -1.5π. Therefore a high sampling rate must be used to ensure that the sign unambiguity of phase shifts can be resolved. A sampling rate of 120 Hz i.e. two times per second has been used for all CCD data collected. As a further practicality it is important to note the orientation of the CCD, otherwise the direction of the fringe translation can be misinterpreted.

3.5.3 Additional signal processing

LabVIEW has a range of signal processing tools available and one can spend a significant amount of time on improving the signal processing by using windowing functions, filters and elegant ways of unwrapping phase changes. For instance a Hanning window is used to improve the frequency resolution, although the significance of said filter settings or use of other window types has not been thoroughly investigated. Inevitably, improving the signal processing algorithms is of little value if the nature of the fringepattern is not fully understood. Chapter 5 takes a deeper look into the physical origin of the fringepattern and using that knowledge an appropriate signal algorithm has been developed.

3.6 Temperature control

The refractive index of water changes on the order 10^{-4}/ RIU $^{\circ}C^{-1}$ and temperature control is therefore by far the largest experimental concern. Due to thermal heat expansion of the optical components a stable temperature inside the optical enclosure is also required, which requires a significant warm up period of at least 4-hours.

3.6.1 Capillary mounting and heating

The capillary is mounted on a custom built copper block (8 x 8 x 1 cm) and is held into place by a front mounted plastic plate fastened with spring loaded screws. To improve thermal contact between the capillary and copper block, the capillary sits in a milled V-grove that is filled with heat conductive thermal paste, except for a small section where the laser hits the capillary. The heating is provided by a peltier element fitted to the copper block and regulated with a thermoelectric temperature controller (TED 200C, Thorlabs, Munich, Germany). The TED has a temperature sensor (thermistor) placed on the copper block to provide temperature feedback. An aluminium grating fitted to the 'cold' side of the peltier element provides amble thermal contact with the air which is required for a peltier element to function. A stable temperature is easiest achievable when the heat produced by the laser and peltier element is in equilibrium with the heat dissipation to the room atmosphere. Therefore the capillary temperature is usually at 25 °C, a few degrees higher than room temperature. Setting it lower than room temperature requires an active heat removal from the peltier element, which means the excess heat would have to be transported outside the optical enclosure, which is unpractical.

3.6.2 Miniature thermocouples

To fully investigate the influence of temperature variation on the signal additional temperature sensors were installed. The inner diameter of the capillary is large enough to allow small 0.25 mm diameter thermocouple temperature sensors (Omega Engineering Ltd.) to be placed inside the capillary very close to the actual sample volume. The sensors are K-type thermocouples with a sensitivity of $40\,\mu V\,°C^{-1}$. Furthermore additional temperature sensors were installed on the laser and in the optical enclosure as both the laser output and optical components such as mirror-mounts are sensitive to temperature variations. As can be seen on figure 3.4, switching the temperature controller (TED) off the temperature of the copper block drops and the signal changes accordingly. The change in sample temperature is quickly registered by the thermistor inside the capillary.

3.6.3 Sample preheating

Despite good attempts to ensure temperature control of the capillary, the system could not maintain a stable temperature when liquid was pumped through. As shown in figure 3.5 there is an abrupt change in signal after starting the pump and when flow is stopped the signal returns to the previous baseline. This disturbance in the signal is an effect of a temperature difference between the sample liquid and the capillary. Due to the relatively large bulk volume

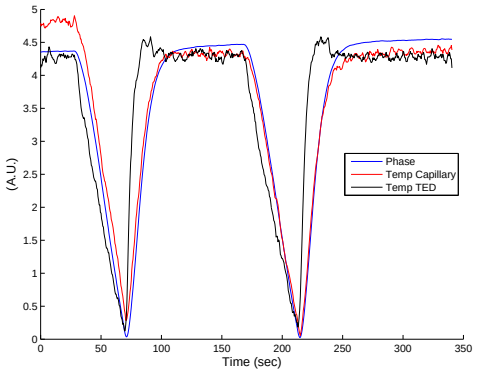

Figure 3.4: Switching the temperature control off (TED voltage output, black line) results in an immediate drop in sample temperature (red line) and change in BSI signal changes occurs (phase, blue line). For ease of comparison the values have been scaled to a common y-axis and phase values inverted because the drop in temperature actually produces an increase in RI.

of sample liquid the heat flux from the copper block through the capillary and into the sample is not high enough and the temperature equilibrium is offset. To solve this problem sample fluid was passed through a preheating section of stainless steel tubing; 40 cm in length and 250 µm inner diameter fit onto the copper block. The preheating improved the heat exchange as can be seen in figure 3.5, but for preheating to be effective the flowrate cannot exceed 1 mL/ min. Failure to effectively preheat the sample produces an exponential change in signal that can easily be mistaken for a binding signal.

3.6.4 Long term stability

Continuous measurements of the signal and temperature over a 22-hour period, revealed a significant drift of the signal which seemed to be correlated with observable temperature changes in both the capillary and inside the optical enclosure. There was also a clear correlation between the temperature changes of the capillary and the temperature in the optical enclosure. As a result, two improvements were made. Firstly, the laser was enclosed and insulated in a separate Styrofoam box with a small fan that actively ventilated excess heat out of the optical enclosure. Secondly, the TED's temperature sensor was repositioned on the copper block to be closer to the capillary and further away from the peltier element, enabling an improved response to changes in ambient temperature. As a result of these modifications the temperature stability and control was markedly improved. Results on long term stability are published in paper I but briefly restated; an average drift on the order $0.005\,\mathrm{rad\,h^{-1}} = 10^{-7}$ $\mathrm{RIU\,h^{-1}}$ is observable over a period of 18 hours.

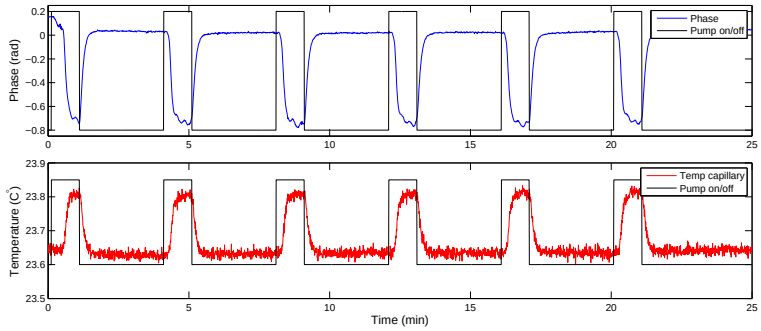

(a) No preheating installed

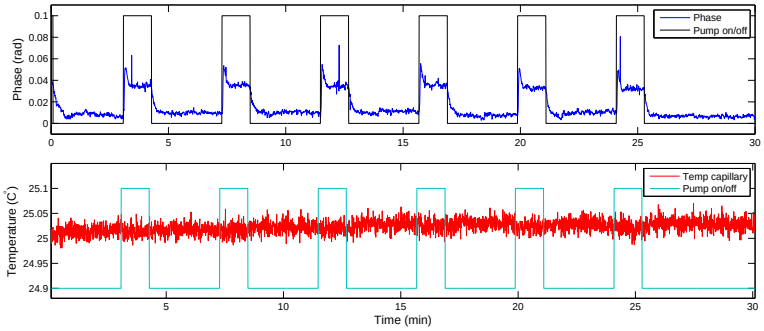

(b) After preheating has been installed

Figure 3.5: Without preheating the signal can be seen to decrease (blue line) by approximately 0.7 rad when flow is started (black line) and as flow is stopped the signal returns to the baseline level again. Simultaneous recordings of the temperature inside the capillary (red line) clearly correlates the signal change with a 0.15 °C change in temperature. When preheating is applied the signal only changes 0.04 rad when the pump is active and no change in capillary temperature is observable.

3.6.5 Comparison of temperature control with BSI systems used in other studies

The system used in this study was installed in a room that also houses other laboratory equipment and personnel. Although the room has climate control temperature variations are observed especially during hot summer days as well as during night time when laboratory equipment is idle. Consequently such room temperature variations affected the experimental system and the drop in temperature observed around the 21-hour mark in figure 3.6 (top figure) corresponds to 8 am, where staff turn up for work which affects the temperature as they open doors and turn on machinery. The difficulties related to temperature control are in contrast to the BSI systems used in many of the published stud-

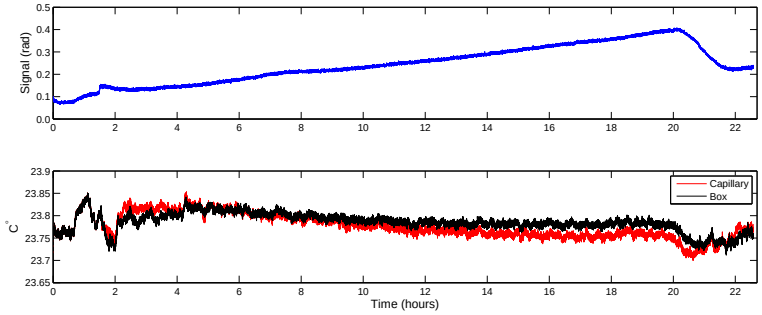

(a) Before improvements

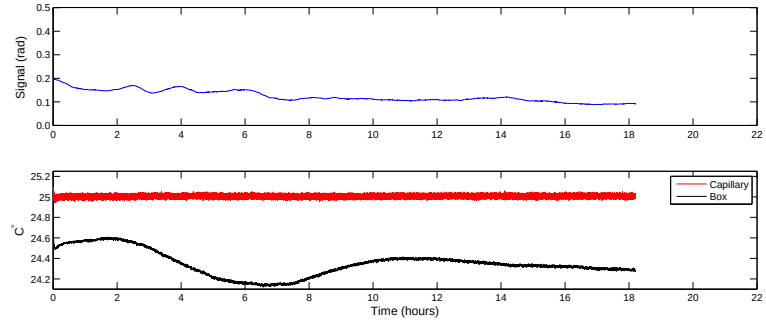

(b) After improvements

Figure 3.6: With improved preheating and insulated encasing of laser the long term temperature and signal stability was improved markedly. The figure displays the signal (blue) and temperature in capillary (red) and optical enclosure (black) prior to improvements (a) and after (b).

ies, in which temperature control is done by a peltier heating device similar to that used in this study, but apparently without the use of any form of optical or temperature enclosure.[12,68] Strict room temperature control is mentioned in the thesis by Latham (2007),[69] but none of the previous studies have embarked on monitoring the actual temperature. To the knowledge of this author prototype instruments from MSI, the company responsible for commercializing and producing BSI instruments, are encased in a protective housing but no data is available on the temperature stability of the equipment when operated in a normal laboratory environment.

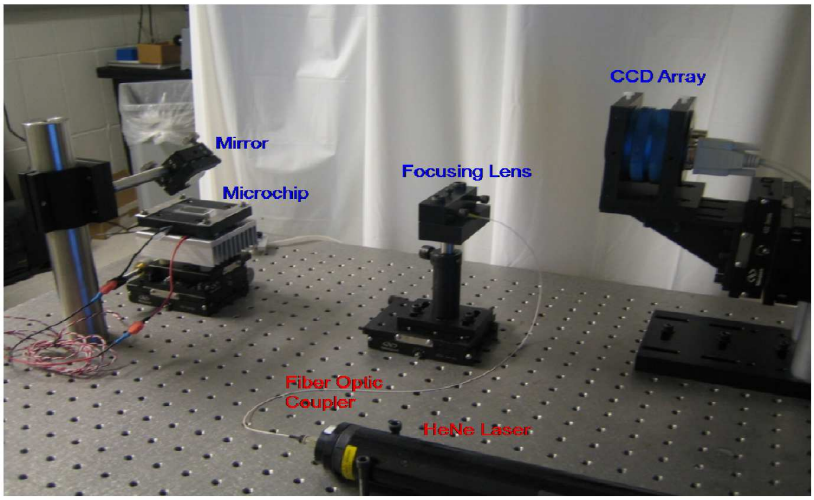

Figure 3.7: Many BSI studies have been done with open optical setups such as this experimental setup used in: *Latham JC, Stein R a., Bornhop DJ, Mchaourab HS (2009) Free-solution label-free detection of alpha-crystallin chaperone interactions by back-scattering interferometry. Anal Chem 81:1865–1871.* Picture is from supporting information

3.7 Microfludic flow and mixing

One of the most promising aspects of BSI is the real-time detection of biomolecular binding or enzymatic reactions. However, to perform real-time measurements, rapid mixing of reagents is required because reactions and binding events can occur on the timescale of seconds. Microfluidics offer appealing possibilities for miniaturized sample and reagent handling, but it also imposes a unique set of challenges when compared to our everyday macroscopic life and one of the more challenging aspects is mixing. In the previous section it was shown how temperature changes can produce a signal that mimics a binding signal and in this section it will be shown that similar artifact signals can be produced as a result of insufficient mixing and various diffusion phenomena.

3.7.1 Microfluidics

Mircofluidcs is the life at low Reynolds numbers, as so elegantly stated by Purcell[70] in a talk about how viscous forces dominates and inertia is irrelevant when the scale of things is really small. The Reynolds number (Re) is defined as a dimensionless ratio between the inertial forces and the viscous forces and for flow in a cylinder such as the capillary it is given as:

$$Re = \frac{UL}{v} = \frac{QD_H}{vA} \tag{3.2}$$

where U is the mean flow velocity, v is the kinematic viscosity of the fluid and L is the characteristic length over which the mass transport occurs, D_H is known as the hydrodynamic diameter in this case it is simply the diameter, Q denotes flowrate and A is the cross section area. For low Reynolds numbers ($Re < 2000$), which occurs with small diameters or low flowrates, flow is said to be laminar. In the laminar flow regime viscous forces dominate and flow evolves along a set of predictable streamlines with constant velocity. At really high Reynolds numbers these ordered streamlines break down and flow evolves in an unpredictable manner and is said to be turbulent. As the name implies the dimensions used in microfluidics are small and flow is laminar.

Microfluidc mixing

In general transport occurs either by *convection* resulting from the bulk motion of fluids, or by *diffusion* which is the random movement of molecules. Mixing fluids in a laminar flow regime poses a challenge, since transport across one streamline to another only occurs by diffusion. The velocity profile for laminar flow though a cylinder is a parabolic function of the radial position, with the highest velocity on the axial center line. The flow is unidirectional i.e. downstream and mass transport by convection only occurs in the direction of the

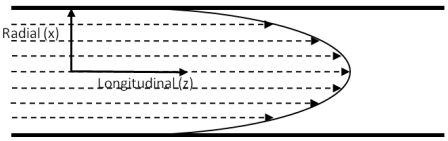

Figure 3.8: Flow into a cylinder develops a parabolic flow profile with maximum velocity at the center. If flow is laminar then mass transport occurs in the longitudinal z-direction by convection and transport in radial x-direction across streamlines (stippled lines) only occurs by diffusion

flow . Therefore any mass transport in the radial direction, across streamlines, only occurs by diffusion. Diffusion of particles in fluid is characterized by Brownian motion and the average distance (x) traveled by a particle or molecule in a given time interval (t) is

$$x = \sqrt{2Dt} \tag{3.3}$$

where D is the diffusion coefficient. Diffusion coefficients in water range from $10^{-9}\mathrm{m}^2/\,\mathrm{sec}$ for small molecules and ions and up to $10^{-11}\mathrm{m}^2/\,\mathrm{sec}$ for proteins. Since diffusion is a slow process a major problem within the area of microfluidics is therefore how to mix two flowstreams on a short timescale. Many microfluidic methods for mixing operate on a principle of reducing the distance between mixing layers (streamlines). In one method, called squeezing, the channel diameter is simply reduced which effectively reduces the diffusion distance. Another method relies on repeatedly splitting and merging flow streams, again the aim is to reduce the diffusion distance.

3.7.2 The micromixer and pumps

Without the planned BSI-chip the system lacked a means for mixing fluid. Instead, a commercial microfluid-mixer (thinXXS Microtechnology AG) shown in the image was purchased. The chip features a variety of so-called serpentine mixers that creates a Dean flow through a series of curved channels, whereby fluid is forced through a series of curvatures, thus creating a centripetal force and fluid from one side of the channel is forced outwards forming radial flow vortices that increases mixing efficiency.[71] This mixing scheme is identical to that used by Bornhop et al. for their real-time binding experiments, however, in their setup flow was produced by applying a vacuum to the outlet.[23,11] A vacuum source creates a pressure driven flow, however actual flow rates

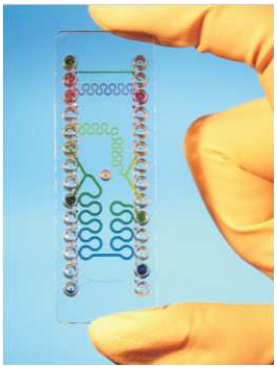

Figure 3.9: Commercial serpentine mixer.

are difficult to control with a vacuum source. In this project as an attempt to ensure reproducibility and increase the control of flow and volume the vacuum suction was replaced with pumps on the inlet side.

Pump control and calibration

The initial pumps selected were syringe pumps NE-50 from New Era Pump Systems Inc that were controlled using SyringePumpPro software. The pumps allows the user to insert and use a variety of different syringes. Motor power is transmitted via a screw spindle to the syringe plunger and the dispensing rate is controlled by the speed of the motor. Syringe pumps are regarded as being accurate in the volume dispensed, however the exact volumetric rate depends not only on the speed i.e. rounds per minute (RPM) but also on the inner diameter of the syringe and the software came with a list of pre-calibrated syringe diameters, thus desired flow rates can be entered directly into the program user interface in volumetric units ($\mathrm{ml\,min^{-1}}$). The later added peristaltic pump was controlled via LabVIEW. The flow of the peristaltic pump is set based on the rotations per minute of the pump wheel and actual flow rate depends on the internal diameter of the tubing installed. Using a precision scale weight the amount of fluid pumped at different rotation speeds was measured and a calibration curve was produced that was used to convert RPM to actual volumetric flow rates.

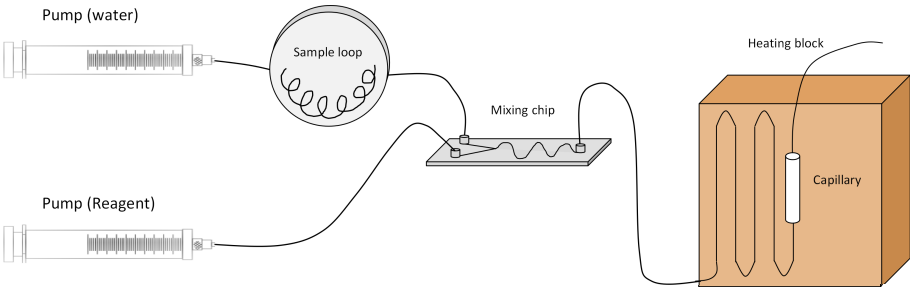

Figure 3.10: A schematic of the flow control setup. Two syringpumps generate the flow and a sample loop has been inserted for manual injection of small sample volumes. Flow is merged and mixed on a microfluidic mixing chip before it enters a preheating system and finally, the capillary.

3.8 Pulsatile pumps and problems associated with longitudinal diffusion

Unfortunately, as it turned out, syringe pumps are prone to delivering a slightly pulsating flow attributed to the spindle mechanism driving the syringe plunger, thus the flow rate will vary slightly over time in a sinusoidal pattern. When two pumps are used in conjunction with two different fluids these pulsatile variations in flow rate causes the concentration of the combined mixture to vary downstream. This can evidently be seen in figure 3.11 where pure water and a $0.009\,\mathrm{g\,ml^{-1}}$ NaCl solution are mixed 1:1 at various flow rates using two 5 ml syringes. It should be noted that the capillary used at this stage in the study was a 1 mm polymer capillary for which the sensitivity was found to be $4384\,\mathrm{rad\,g^{-1}\,ml^{-1}}$. The range of the variation (i.e. min-max amplitude) is $\approx$ 1 rad at 75+75 µl/ min, which corresponds to a concentration of 2.3×10^{-4} $\mathrm{g\,ml^{-1}}$ NaCl. The intended concentration of mixing NaCl and water 1:1 is $0.0045\,\mathrm{g\,ml^{-1}}$ and the variation expressed in percentage of the intended concentrations is $(2.3\times10^{-4}/0.0045)\times100 = 5\%$. In regards to mixing accuracy 5% constitutes a large and unsatisfying source of error.

The concentration gradient downstream can be seen to vary in a sinusoidal fashion with a characteristic time and time between the peaks seems to depend on the flowrate. Since the syringe diameter is a constant then flowrate is determined solely by the RPM and it is evident that increasing RPM reduces the time between adjacent concentration peaks. However, increasing flow Q in a pipe flow with diameter d increase the mean flow velocity $\bar{u}$:

$$\bar{u} = \frac{4Q}{\pi d^2} \tag{3.4}$$

By calculating the mean velocity, assuming 1 mm diameter and measuring the average time between concentration peaks, the distance in terms of length between the peaks is calculated as peak separation×velocity=peak distance and is found to be reasonably constant ≈130 mm see table 3.1.

Diameter (mm)	Peak separation (sec)	Total flowrate (µl/ min)	Velocity (mm/ sec)	Peak distance (mm)
1	6	1000	21.2	127
1	12.5	500	10.6	133
1	25	250	5.3	133
1	45	125	2.7	119

Table 3.1: Flowrate, velocity and and peak separation distance of data shown in figure 3.11

Now one might think that the mixer will even out this concentration variation, however, most microfluidc mixers are designed to mix in the radial direction

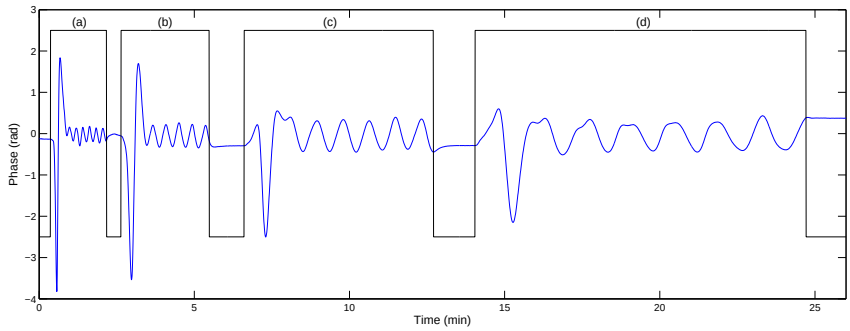

Figure 3.11: Water and NaCl solution is mixed in a 1:1 ratio with flowrates: (a) 500+500 µl/ min, (b) 250+250 µl/ min, (c) 125+125 µl/ min and (d) 75+75 µl/ min. The pulsatile flow delivered by the pumps cause the concentration to vary downstream in a sinusoidal pattern.

and not in the longitudinal direction. The worst case being when the distance between the concentration peaks are large compared to the length of the mixer. In the example calculated above, the inner diameter of the tubing was set to 1 mm, corresponding to the capillary used. A decrease in channel diameter increases the velocity according to equation 3.4 and therefore also increases the peak separation distance.

3.8.1 Longitudinal diffusion - peak decay time

When flow is stopped diffusion will act to even out the longitudinal concentration gradients caused by the pulsatile flow and solutes will diffuse from areas with high concentration towards lower concentrations. Such a flux of solutes be it protein or other reagent contents would change the refractive index and could therefore cause an unwanted contribution to the measured signal. A rough estimate of the time needed for these concentration peaks to decay can be found using Fick's second law for diffusion in an one-dimensional unsteady system i.e. one where concentration C is not constant.

$$\frac{dC}{dt} = D\frac{d^2C}{dz^2} \tag{3.5}$$

D is the diffusion coefficient for the solute and z denotes the longitudinal axis. In order to solve a diffusion problem for a system a solution to Fick's second law must be found. For the problem concerning longitudinal dispersion at hand, the sinusoidal concentration variation along z can be described as

$$C = \bar{C} + B_0 \sin\left(\frac{\pi z}{l}\right) \tag{3.6}$$

$\bar{C}$ is the average concentration and B_0 is the maximum concentration difference from $\bar{C}$ i.e. the amplitude of the sine wave. The characteristic peak distance is

l as described above. For such a system the solution of Fick's second law can be shown to take the form:[72]

$$C(t) = \bar{C} + B_0 \sin\left(\frac{\pi x}{l}\right) e^{-t/\tau} \tag{3.7}$$

Thus the sine wave decays exponentially with a characteristic relaxation time $\tau = (l^2)/(\pi^2 D)$ and the time it would take for diffusion to reduce the peak amplitude by 50% would be:

$$t_{1/2} = \frac{ln(2)}{\frac{\pi^2 D}{l^2}} \tag{3.8}$$

For a diffusion coefficient D=$10^{-9}\,\mathrm{m}^2/\,\mathrm{sec}$ and length l=130 mm, $t_{1/2}$ is more than 300 h. Considering that the separation between concentration peaks (l) will be much larger in sections of tubing with much smaller inner diameters, the longitudinal concentration variation will for all practical purposes not vanish by acts of diffusion. On the other hand since the half time is so large the local changes in concentration caused by longitudinal diffusion will also be quite small and even negligible within the smaller timescale of minutes.

3.9 Fluid displacement and problems associated with radial diffusion

Exchanging the fluid inside the capillary is termed fluid displacement and is a combined effect of both diffusion and convection. The interaction between convective and diffusive dispersion of a solute in a cylinder flow leads to a characteristic solute dispersion, known as Taylor dispersion. For an intruding front or pulse of a solute this dispersion phenomena results in the average cross sectional concentration profile becoming sigmoidal (or Gaussian in case of a pulse) as it travels downstream and has been well characterized in the analysis first laid out by Taylor (1953) and Aris (1956).[73,74] Taylor flow analysis has previously been used to determine diffusion coefficients of various proteins and macromolecules from RI measurements of fluid injections.[75] To determine the effect of radial diffusion on the BSI signal during injection of a fluid two dispersion models; one assuming pure convective flow and one assuming convective-diffusive flow (Taylor-flow), is fitted to the signal of a sodium chloride solution entering the capillary.

Convective flow: The mean concentration over a cross-section of the capillary a point z is a parabolic function of time t, mean velocity $\bar{u}$ and the mean concentration:

$$C(t, z) = C_0\ 1 - \left(\frac{z}{2\bar{u}t}\right) \tag{3.9}$$

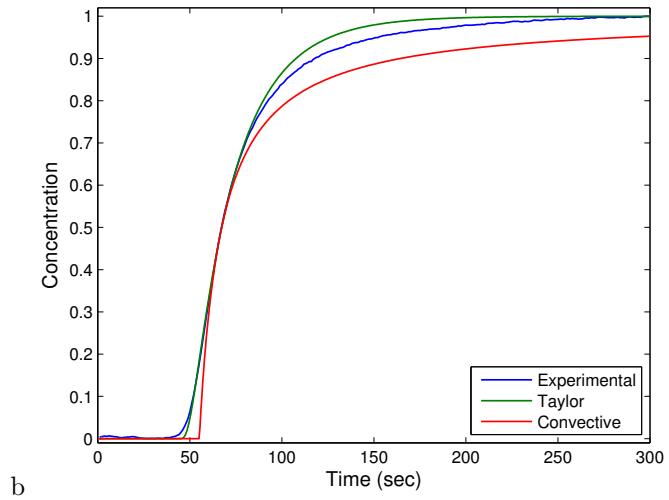

b

Figure 3.12: A NaCl solution is pumped into the capillary containing water at a flowrate of 192 µl/ min and fluid displacement is completed after 300 sec corresponding to a total volume of 1 ml. Experimental data (blue), Taylor (green), convective (red)

Taylor-flow: Following Quinn[75] the mean concentration for a convective-diffusive flow is given by:

$$C(t,z) = 0.5\ C_0 \left[1 - erf \frac{1 - t/\tau}{2\sqrt{\frac{k}{\bar{u}z}\frac{t}{\tau}}}\right] \tag{3.10}$$

where $\tau = z/\bar{u}$ is the mean residence time and C_0 the initial concentration and $k = (\bar{u}^2 d^2)/(192D)) + D$ is the Taylor-Aris dispersion coefficient.

The results are shown in figure 3.12 for a capillary with a diameter $d = 1.4\,\text{mm}$ and $z = 50\,\text{cm}$. The experimental configuration consists of various connective tubing and a pre-heating module with varying diameters and the fluid entering the capillary is subject to dispersion before entering the capillary and an exact model of the concentration profile is difficult to obtain. However, the convective-diffusive model (Taylor flow) fits the experimental data better than a model which only assumes convective flow, demonstrating that effects of radial diffusion cannot be neglected.

3.9.1 Carryover

The dominating process acting to exchange fluid near the capillary walls where the velocity approaches zero is diffusion. Therefore, if fluid injection into the capillary occurs over a time scale that is short compared with the diffusion

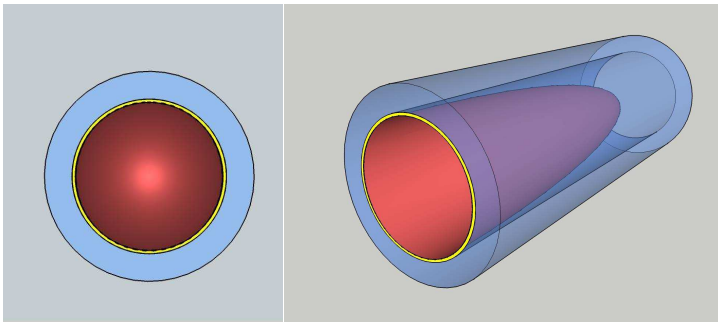

Figure 3.13: Laminar flow into the capillary produces a thin annulus of fluid near the capillary wall, shown as a yellow ring, where fluid displacement is incomplete.

coefficient of the solutes, there will remain a layer close to the capillary wall where fluid is not fully exchanged, resulting in a radial concentration gradient. If the invading fluid has a higher concentration of the solute then diffusion of solute will occur outwards towards the capillary walls and the final concentration of the entire volume will be lower than the invading fluid. Accordingly, if the invading fluid is of lesser concentration than the displaced fluid then the resulting mixed fluid will have a higher concentration than the invading fluid. Such dilution or contamination is often referred to as sample carryover and is a common cause of error in many types of assays. For assays that use labels such as fluorescent labeled proteins, the dilution factor from carryover is often negligible and only contamination with material containing fluorescent labeled material will affect the signal significantly. In the case of BSI the refractive index is affected by all the solutes and constituents in the carryover and should be considered a significant cause of error. Furthermore in a generic absorbance or fluorescent measurement the signal represents an average over the entire sample volume and local fluxes of solute does not affect the measured signal. In BSI, the sample beam path of the interrogating laser only samples a part of the cross sectional area of the capillary (this is verified in chapter 5.3) and could therefore be susceptible to local variations of solute diffusing radially across the beam path effectively mimicking a binding-signal in case of real-time measurements. It is therefore worthwhile to investigate how and on what timescale radial diffusion occurs.

3.9.2 Model for radial diffusion

The approach shall be a simplistic one, seeking to examine the timescale of the diffusion process, i.e. how long does it take for diffusion to complete? Here it is assumed that flow of liquid into a cylinder with incomplete mixing of the displacing fluid results in a thin annulus adjacent to the capillary walls with a thickness a, containing what is leftover of the displaced fluid, that is much

smaller than the capillary radius R. It is assumed that the radial concentration profile within bulk and annulus is uniformly distributed, eg. the concentration is 1 across the entire radial direction of the annulus and similarly 0 across the entire bulk radius. Secondly, for a fully developed laminar flow there will be a longitudinal concentration gradient dC/dz but as the flow profile stretches out over a length much larger than the capillary diameter this gradient will be small and is disregarded. Thirdly, the model is reverted to a simple one-dimensionel model, thus ignoring the radial aspects of the cylinder and the cross-sectional area increases with radius. However, the term radius is kept to describe the one-dimensional channel half-width.

Diffusion of solute from a thin layer adjacent to the walls

This first examination describes diffusion of solute from the thin annulus along the walls and into the bulk solution. Since the thickness of the layer along the wall is assumed to be very small ($a << R$) it is simplified into a point source. Diffusion from a finite point source into an infinite medium may be written as

$$C(x,t) = \frac{1}{2}\frac{C_0}{2\sqrt{\pi Dt}} exp(-\frac{x^2}{4Dt}) \tag{3.11}$$

By placing a single point source R' at $x = R$ and $x = -R$ the symmetry condition around $x = 0$, assures that the concentration gradient at the center is zero. However, half the solution from a point source will diffuse towards center of the capillary but the other half will diffuse out of the capillary. By following the solutions of superposition and reflection as given by Crank [76] the impermeable boundaries at $x = R$ and $x = -R$ can be modeled by positioning two point sources at each of the boundaries, thus in effect all the solute diffusing outside the radius will be reflected back into the cylinder. (This is done by cancellation of the first term in equation 3.11). Expanding to include two point sources at $x = -R$ and $x = R$ equation 3.11 becomes

$$C(x,t) = \frac{C_0}{\sqrt{\pi Dt}} \left[exp(-\frac{(x-R')^2}{4Dt}) + \frac{(x+R')^2}{4Dt}) \right] \tag{3.12}$$

As time increases and the sources widen, they will eventually expand and cross over the opposite boundary, which means that the solute is not contained within the boundaries. Applying the so-called method of *images* whereby a summation of additional point sources are applied in symmetry will result in zero net flux across the boundaries if an infinite amount of sources are used. For practical purposes only a couple additional sources are needed to secure a reasonable convergence ($n \approx 4$) The distribution of the point sources are shown in figure 3.14.

$$C(x,t) = \frac{C_0}{\sqrt{\pi Dt}} \sum_{m=-n}^{+n} \left[exp(-\frac{(x-2mR-R')^2}{4Dt}) + exp(-\frac{(x-2mR+R')^2}{4Dt}) \right] \tag{3.13}$$

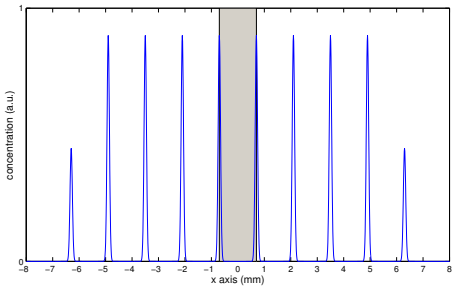

Figure 3.14: Method of images: Diffusion from capillary wall into bulk. The capillary shown by the shaded area with R=0.7 mm and point sources positioned symmetrically around the capillary center by the method of images. Time is advanced slightly ($t > 0$) to clearly show the initial spread of the initial point sources.

The results of the method is shown in figure 3.15 where the concentration at the capillary center ($x = 0$) is seen to increase as solute diffuses from the walls on a timescale that is significantly dependent on the diffusion coefficient and channel radius.

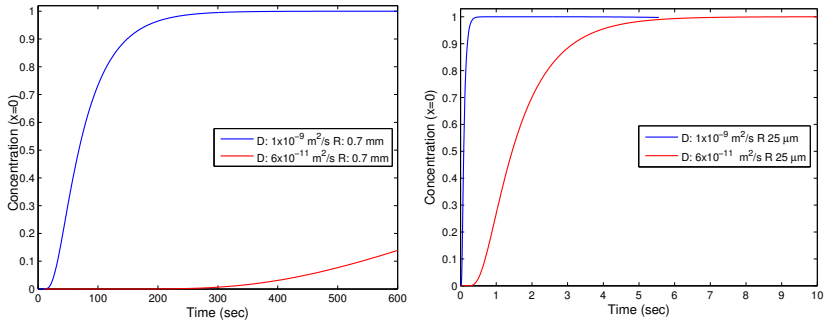

(a) Radius 0.7 mm **(b)** Radius 25 µm

Figure 3.15: Concentration at channel center (x=0) over time using eq. 3.13 for two molecules with different diffusion coefficients; $1 \times 10^{-9} m^2/sec$ and $6 \times 10^{-11} m^2/sec$ representing a small molecule and a protein.

Diffusion of solute from bulk towards the walls

This second examination describes diffusion of solute from the invading bulk fluid into the thin annulus. Again the model is simplified into a one dimension as above except that the annulus (a) cannot be infinitely thin and the initial bulk concentration is given the with W with $W = R - a$. The solution to this problem is well known and is solved by superposition of an infinite amount of point sources over the length which produces the so called error function.[77] Again the method of images is applied to ensure that solute stays within the capillary boundaries, see figure 3.16. Two channels with radius R=0.7 mm and R=25 µm are used to visualize the dramatic effect of channel dimensions and the width of the annulus is 0.1 mm and 5 µm respectively.

$$C(x,t) = \frac{1}{2}\frac{C_0}{\sqrt{\pi Dt}}\sum_{m=-n}^{+n}\left[erf(\frac{(W-2mR-x)^2}{4Dt}) + erf(-\frac{(W-2mR+x)^2}{4Dt})\right] \tag{3.14}$$

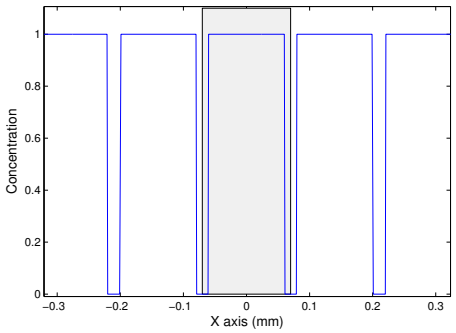

Figure 3.16: Initial conditions at t=0 with W=0.6 mm the gray shaded area marks the diameter of the capillary

The results of diffusion from bulk are shown in figure 3.17 and it is evident that time it takes to even out a radial concentration gradient is very dependent on the radius but also on the diffusion coefficient, as expected from eq 3.3. Thus for a large diameter channel the gradient will settle within minutes for small molecules (see figure 3.17a) but requires hours for larger macromolecules such as proteins (data not shown). Using a small 25 µm diameter channel equivalent to that used by Bornhop et. al[1] radial concentration gradients will settle within 1-2 seconds for small molecules (data not shown) and within 5 seconds for larger macromolecules (see figure 3.17b).

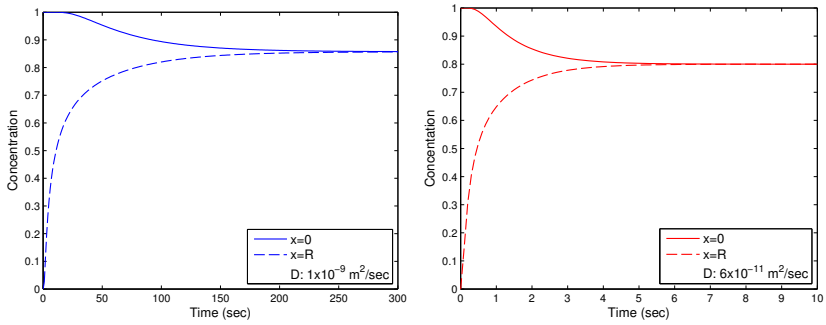

(a) Radius 0.7 mm, W 0.6 mm, Diffusion coef. $1 \times 10^{-9} m^2/sec$

(b) Radius 25 µm, W 20 µm, Diffusion coef. $6 \times 10^{-11} m^2/sec$

Figure 3.17: Concentration at channel center (x=0, solid line) and wall (x=R, stippled line) over time using eq.3.14

3.9.3 Radial diffusion an erroneous source of binding signal

As was shown initially in section 3.12 fluid displacement occurs via Taylor flow where diffusion at the channel walls is the dominating process of mass transport. The time it takes to fully displace a fluid is therefore not only a function of convective properties such as flow velocity alone, but also dependent on diffusion in the radial direction. This poses a limit on how fast fluid can be fully displaced by the time it takes for a radial concentration gradient to settle and simply increasing the flow velocity does not proportionally increase fluid displacement. Because fluid mixing and injection into the capillary must be realized within a rapid timescale, much less than the time for binding equilibrium to occur, experimental conditions have focused on rapid high velocity injections. However, such cases would favor the development of radial concentration gradients and carry over effects as described above. As can be seen from the examples on radial diffusion shown in figures 3.15 and 3.17 the shape of the plots very much resembles the a real-time binding signal (see section 2.6) and one must consider the possibility that diffusion could be a significant contribution to the observed real-time binding signals presented in much of the BSI literature. In his thesis on BSI H.S. Sørensen (2006) also notes that: *"Incomplete mixing result in binding curves with more than one binding event appearing."*[78] This suggests that diffusion phenomena were observed but misinterpreted as biomolecular binding events.

3.10 Abandoning the method for real-time protein binding measurement

In light of the combined difficulties arising from pulsatile pumps and carryover, the real-time binding experiments planned for this project were canceled and focus was put on performing end-point experiments instead.

Chapter 4

Initial findings

This chapter presents initial experimental findings as published in Paper I concerning the sensitivity and and minimum detectability. Long term stability and additional error contributions are also examined and discussed including the effects of dissolved gasses in the sample liquid. These findings indicate that the current BSI system is just as sensitive as those used to study free solution biomolecular interactions and an attempt is made to reproduce the experimental binding study of Protein A - Immunoglobulin G complex formation first demonstrated by Bornhop et al.

4.1 Limit of detection and sensitivity of BSI

In the literature BSI is advocated as having a very low *detection limit* or *limit of detection*, surpassing 10^{-8}RIU [5] and this is attributed to a multi-pass configuration that increases the effective optical pathlength to many times the channel's diameter. [68]

However, the methodology applied to determine the detection limit is not strictly according to standard practice. The International Union of Pure and Applied Chemistry (IUPAC) defines the limit of detection x_L as the concentration or quantity that can be detected with reasonable certainty and is given as: $x_L = \bar{x}_b + k\ sd_b$, where $\bar{x}_b$ is the mean of a number of blank measures, sd_b is the standard deviation of the means and k indicates the confidence factor usually 3. Despite quoting the detection limit in many of the published studies on BSI, the exact methodology is rarely described in detail, although on numerous occasions Bornhop et al. determine the limit of detection as the relationship between the sensitivity, determined from the slope of a calibration curve, and the short-term noise usually defined as standard deviation (σ) over a period of time on a blank sample such as buffer or water. [5,3]

$$\text{detection limit} = \frac{k \times \text{short-term noise}}{\text{sensitivity}} \tag{4.1}$$

This approach is more compatible with the term *minimum detectability* defined in the ASTM standard for Refractive Index Detectors Used in Liquid Chromatography. [79] The ASTM approach is best suited for a chromatographic setup where the signal is a peak that must be discerned from a continuous baseline signal and does not necessarily reflect the signal variation observed in upon repeated batch-injections used for end-point measurements. Furthermore this short-term signal noise is not defined or measured consistently throughout the various studies, for example Swinney, Markov and Bornhop defined a timescale of 25 seconds, [80] whereas Wang and Bornhop only used 5 seconds for short-term noise. [5] Even timescales as low as 400 ms has been used. [4]

It should be noted that these 'detection limits' are often determined using a single analyte such as glycerol and the signal is therefore related to the amount of analyte present, whereas the signal produced in a biomolecular binding event is of different nature and does not dependent on concentration in the same manner. The detection limits should therefore be used with caution as qualitative indicators of BSI's capabilities to detect biomolecular binding events.

4.1.1 Sensitivity

IUPAC defines sensitivity as the slope of a calibration curve, thus relating the observed signal to the amount of analyte present. For BSI the observed signal is

a translation of fringes on a screen that is measured in radians, thus giving units of rad/$\frac{\text{g}}{\text{L}}$. According to the ASTM standardthe sensitivity should be defined as the signal output per unit concentration of the test substance,[79] where the signal output is converted to refractive index units (RIU) by a calibration curve of known standards and the sensitivity would be in units of RIU/$\frac{\text{g}}{\text{L}}$. The ASTM approach requires a precise knowledge of the refractive index of the standards used - on the other hand the IUPAC sensitivity would be specific for the type of analyte used.

Definition and methods for determining minimum detectability and sensitivity in this work

Following the approach in the ASTM standard the minimum detectability is defined as two times the short-term noise divided by the sensitivity for aquas solutions of sodium chloride. The short-term noise is defined as 5σ over a period of 2 minutes, thus the minimum detectability corresponds to a 10σ detection limit when adopting the approach of Bornhop et al. In this work the term sensitivity is defined as the observed signal relative to the refractive index, in units $\text{rad}\,\text{RIU}^{-1}$, obtained from the slope of a sodium chloride calibration curve using dn/dc from literature. This approach allows one to convert any observed signal in radians to RIU by multiplication with the sensitivity, irregardless of the signal originating from an amount of analyte, temperature, or a binding signal.

4.1.2 Results on minimum detectability and sensitivity

The sensitivity was determined using sodium chloride standard solutions and was found to be $27\,011\,\text{rad}\,\text{RIU}^{-1}$. The minimum detectability for sodium chloride was found to be $4.04\,\mu\text{g}\,\text{ml}^{-1}$. Using the dn/dc for sodium chloride ($0.174\,\text{g}\,\text{ml}^{-1}$)the minimum detectability in RI units is 7.03×10^{-7} RIU.

4.1.3 The effect of degassing

Using an in-line degasser the difference between atmospheric equilibrated water and degassed water was examined and found to be 1.26×10^{-6} RIU. The amount of dissolved gasses depends on the temperature and the results found here indicate that attention to such effects should be considered when storing solvents or using freshly mixed or thawed reagents. Degassing of solvents should also be considered a source of error if the temperature of the introduced solvent is different to the temperature in the BSI capillary.

4.1.4 Long term stability

The long term stability was examined by monitoring the signal over a period of 18 hours, see figure 3.6. The signal was found exert an average negative drift of 2.0×10^{-7}RIU h^{-1}. The cause of this drift could not be attributed to changes in capillary temperature alone, but is most likely a combined effect including thermal expansion of the optical mounts from changes in ambient temperature. Long term stability should be considered a source of error when performing end-point measurements because the entire set of measurements are often collected over a prolonged period of time.

4.1.5 Discussion of the experimental sensitivity

Following the work of Becker, Köhler and Müller[81] the fringe displacement of an interferometer where the beam traverses the sample twice can be given by

$$\Delta\phi = \frac{2\pi}{\lambda} 2nd \tag{4.2}$$

where d is the geometric path length across the sample channel which for the capillary: $d = 1.4$ mm assuming the light is aimed at the center of the capillary. Using 6.3 the theoretical sensitivity is found to be 27 802 rad RIU^{-1} which is in good agreement with the theoretical sensitivity 27 011 rad RIU^{-1} which strongly suggests that light only traverses through the sample twice corresponding to a single reflection inside the capillary. The experimentally determined sensitivity is 6.6 times higher compared to the sensitivity reported by Markov et al.[4] using a capillary with with a 5.6 times smaller inner diameter (250 µm). This difference in sensitivity seems to correspond well with the difference in capillary diameters, which evidently contradicts the previous claims that BSI sensitivity is independent of capillary diameter.[3]

4.1.6 Comparison of sensitivity and 'detection limits' with BSI systems described in literature

As discussed initially a direct comparison between limits of detection would not be meaningful because of the methodical differences, but the current minimum detectability of 7.03×10^{-7}RIU does seem comparable with many of the previously published results of which some are listed in table 4.1. A better parameter for comparison is the sensitivity but this has only been reported in units of radians on a single occasion[4] and was found to be much lower than the current system which suggests that the reported detection limits are a result of very low short-term noise levels. The current system should therefore, in terms of sensitivity and 'detection limit', be capable of reproducing the biomolecular binding measurements that have been obtained using various BSI systems.

Reported		Channel	Ref.
Detection limit (3σ)	1.94×10^{-7} RIU	75 µm (i.d.)	[3]
	1.96×10^{-7} RIU	775 µm (i.d.)	
Detection limit (2σ)	2.78×10^{-6} RIU	250 µm (i.d.)	[7]
Detection limit (3σ)	9.67×10^{-6} RIU	50 µm radius†	[82]
Sensitivity	4082 rad/RIU‡		[4]
Detection limit (3σ)	7×10^{-8} RIU	250 µm (i.d.)	
Detection limit (3σ)	8.32×10^{-6} RIU	90×40 µm	[9]
Detection limit (3σ)	6.9×10^{-9} RIU	550 µm (i.d.)	[5]
Sensitivity	27011 rad/RIU		[83]This study
Min. detectability (10σ)	7.03×10^{-7} RIU	1400 µm (i.d.)	

Table 4.1: Reported detection limits and sensitivity for various BSI setups including the current. (†)semi-circular channel. (‡) calculated using dn/dc for glycerol (1.3032×10^{-5} RIU/mM)

4.2 Initial findings on protein A - immunoglobulin G binding

Because of the varying detection limits, channel diameters and geometries used in the previously published studies and the lack of presented data in RI units, it was decided to reproduce the previously published protein A - IgG experiment [1] on the current setup in order to gain precise knowledge of the signals magnitude. As shown in chapter 3 diffusion from incomplete mixing and inadequate preheating of the injected sample could produce signals that were both exponential in shape and on a time-scale of seconds to minutes and therefore resembled the real-time molecular binding signals and it was clear that real-time measurements would be difficult to produce. As a result of these findings it was decided to use end-point measurements instead.

4.2.1 Protein A - IgG binding stochiometry and affinity

Protein A is a protein located on the surface of the bacteria *Staphylococcus aureus*. It is widely used in immunoassays because it binds the Fc part of most Immunoglobulin G types (IgG). When coated onto a solid surface, it can be used to bind and immobilize immunoglobulin to the surface of a biosensor or multi-well plate for antibody-antigen capture. The protein is 42 kDa, about one third the size of IgG, and consist primarily of three α-helixes. Protein A has four binding sites for IgG and each IgG has two sites where protein A may bind. Thus complex formations beyond 1:1 stochiometry is possible and does occur at higher IgG concentrations. [84,85] Binding with immunoglobulin is not reported to be associated with any significant conformational changes in the structure of either protein. [86]

4.2.2 Materials and methods

The experiment was set up as differential end-point measurements in which the signal attributable to protein binding is the difference in signal between two sets of IgG solutions incubated with and without a fixed amount of protein A. The experiment was preformed using an early version of the current BSI setup which meant that the signal processing did not make full use of the de-chirping algorithm (see chapter 5) and although multiple frequencies were evident it was still unclear how these frequencies were related to different beam paths inside the capillary. The immunoglobulin purchased for this experiment (I4506, Sigma) is from pooled human serum, and purified using ion-exchange chromatography, which means it is polyclonal and contains a mix of IgG subtypes (IgG_{1-4}). Strictly speaking, one cannot determine a precise K_D for a population of proteins and the obtained affinity constant will be a combination

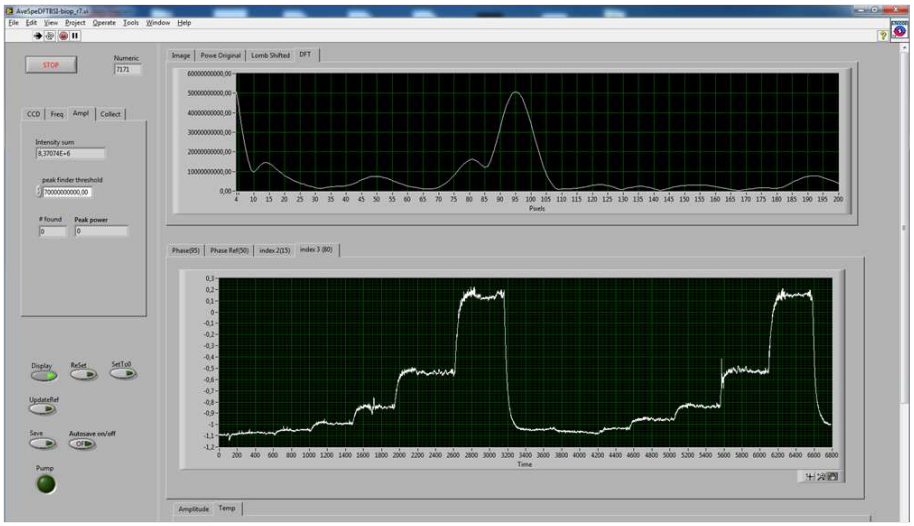

Figure 4.1: Screen-shot of the Labview program. The frequency spectrum is shown in the upper graph with a noticeable dominating frequency and several smaller frequencies. Lower graph shows a recording of the corresponding phase of two IgG standard curves.

of the various proteins. It is important to note that the binding to protein A occurs on the immunoglobulin heavy chain fragment, the so-called Fc part, that is usually termed the constant part in contrast to the two light chains that are variable parts responsible for antigen binding. However, there may be allotype variation in the heavy chain domains of IgG due to the usage of different alleles on the C gene used to produce immunoglobulin.[87] Despite these possibilities for variations in binding stochiometry and affinity, protein A is widely used and proven method for capturing immunoglobulins of all classes.

Determination of K_D in face of ligand depletion

To experimentally determine (K_D) the concentration of IgG should be titrated to cover a range from well below K_D up to a factor of 10 or higher. For protein A - IgG the reported K_D found in literature extends from 10^{-7} M to as low as 10^{-11} M and was reported by Bornhop et al. using BSI to be 6.05×10^{-9}M.[88,89,90,1] This wide range of affinity constants is attributed to complex formations of various stochiometry. As explained in chapter 2 K_D can be determined by nonlinear regression of equation 2.4.1. The equation is a simplification that approximates the unbound fraction of IgG as being equal to the total amount of IgG added. However, if the protein A concentration is much larger than K_D a significant amount of IgG will be bound in complex form, commonly known as ligand depletion and the assumption of equation 2.4.1 does not hold. Ideally, the protein A concentration should therefore be

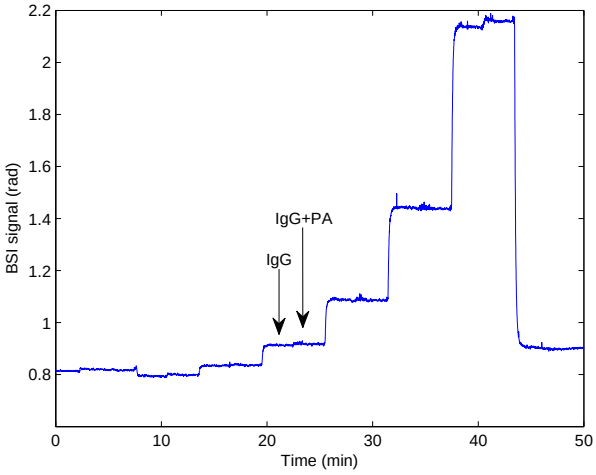

Figure 4.2: Example of raw phase data of paired IgG-protein A measurements starting with the lowest concentration. 2.5nM protein A and 59nM to 1852nM IgG were used.

kept well below K_D, however, as it is also assumed that the signal i.e. change in refractive index, is proportional to the total amount of protein complex formed, increasing the amount of protein A should therefore generate a larger signal which would be easier to detect. The experiment was therefore performed with two concentrations of protein A: 2.5 nM and 10 nM, the former being identical to the concentration used in the study by Bornhop et al.[1] In case of ligand depletion equation 2.4.1 can be replaced by a theoretical model in which the amount of complex $[AB]$ formed is calculated using the following equation where $[A]_T$ and $[B]_T$ are the total concentrations of protein A and IgG respectively.[91] A plot of theoretical binding curves using this equation is shown in figure 4.4.

$$[AB] = \frac{([A]_T + [B]_T + K_D) - \sqrt{([A]_T + [B]_T + K_D)^2 - 4[A]_T[B]_T}}{2} \tag{4.3}$$

4.2.3 Results

The data from a series of end-point measurements were not indicative of protein A - Immunoglobulin binding events. Noticeably the differential signals between IgG and IgG+protein A solutions, shown as bar plots in figs 4.3, were seemingly randomly distributed as both positive and negative differences. The dn/dc for IgG was found to be $0.183\,\mathrm{g\,mL^{-1}}$ from a calibration curve of IgG in Tris buffer, which is in good agreement with typical values for proteins.[63,55]

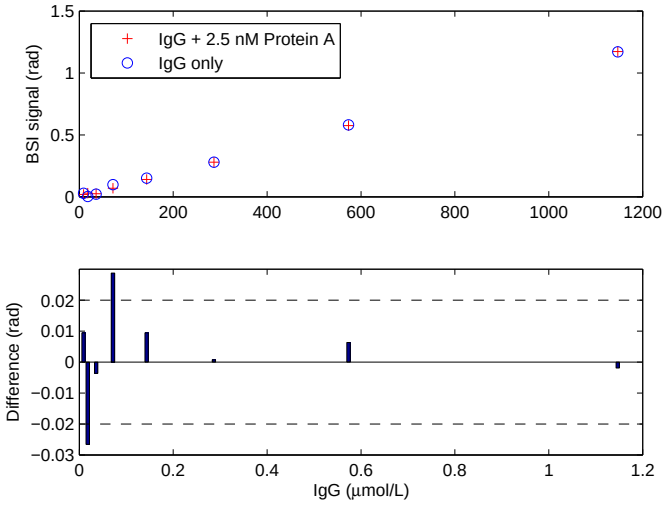

(a) End-point data of 17 nM to 1150 nM IgG incubated with 2.5 nM protein A

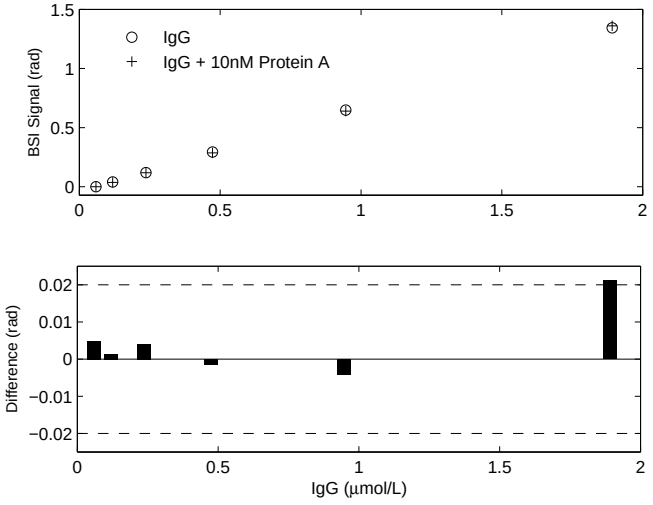

(b) End-point data of 59 nM to 1890 nM IgG incubated with 10 nM protein A

Figure 4.3: Results from two IgG - protein A binding experiments with different protein A concentrations are shown above. The scatter plots show the measured signal in units of radians for IgG incubated with(+) and without(o) protein A. The bar plots show the difference in signal with and without added protein A. Dotted lines mark the limit of the minimum detectability indicating that the measured difference is insignificant.

4.2.4 Discussion on protein concentrations used

In the experimental results published the concentration of IgG ranged from 17 nM up to 1.89 µM which is a notably larger range than what was used in the published study by Bornhop et al., where concentrations only ranged from 10 nM to 40 nM.[1] A plot of the theoretical fraction of protein A bound to IgG using equation 6.3 is shown in figure 4.4 for different K_D-values.

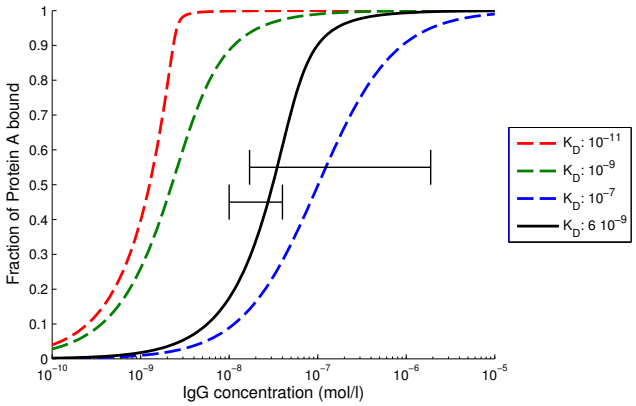

Figure 4.4: Theoretical fraction of protein A (2.5 nM) bound by IgG as a function of IgG concentration (log scale) for different values of K_D, including the value determined by Bornhop et al.(black solid line). The vertical bars indicate the concentration ranges of IgG used by Bornhop et al. (lower bar) and this study (upper bar).

As can be seen from the figure if the K_D lies in the picomolar range (10^{-11}) all protein A will be bound even at low concentrations of IgG, in which case no binding would be observed. To produce a binding curve for a picomolar K_D the IgG concentration would have to be lowered accordingly and IgG concentrations would fall well below the minimum detectability which would not produce reliable data. In fact even the protein A concentrations used in the current experiments is below the limit of minimum detectability as the addition of 10 nM protein A corresponds to a refractive index change of 7.6×10^{-8} RIU (using dn/dc: 0.18) and as can be seen on figure 4.3 the measured difference between solutions containing IgG and IgG+protein A is generally smaller than the minimum detectability (dotted lines). This is also the case for the IgG-protein A data shown by Bornhop et al., as they describe a detection limit of 10^{-6} RIU, yet they detect binding signals in the range of 1-1.5 rad.[1] Thus their detected binding signal is larger than the bulk RI contribution from the added protein itself.

Chapter 5

Demystifying back scatter interferometry

Back scatter interferometry has been claimed to have an extraordinary sensitivity and a unique principle of operation. However, experimental investigations of the sensitivity and stability, presented in paper I, raises numerous concerns about the fundamental optical principles governing BSI. Furthermore, the failure to reproduce a binding signal from protein A and Immunoglobulin G begged the question whether this was due to differences in the experimental setups used in the current study and that of Bornhop et al. In this chapter the fundamental optical workings are thoroughly re-investigated and a set of theoretical ray tracing and experimental findings that contradicts much of the existing literature on BSI is presented. These findings are also published in paper II. As a result of this insight an advanced signal processing algorithm is devised.

5.1 Methods for optical modeling

Two methods have been applied to model the current experimental setup: a ray-tracing and a wave-based model.

5.1.1 Ray tracing model

Optical ray tracing is based on tracking the direction of propagation of a discrete number of light rays within a coordinate system. At each interface between two media with different refractive index the angle of refracted and reflected beam is determined using Snell's law and the geometrical path length for each individual ray can be traced throughout the system. The optical path length is then obtained by multiplication with the refractive index of the media traversed. The amplitude of the reflected and refracted rays is calculated using the Fresnel equations. According to the Fresnel equations at small incident angles <15° the reflectivity of both polarization states is practically identical but for larger angles there is a difference in reflectivity for s- and p-polarised light and ray-tracing results must be obtained for each polarization state. In addition when light is reflected off a medium with a higher index of refraction, there is a 180° phase shift of the reflected wave. In terms of radians this is equivalent to subtracting or adding π to the phase. The phase of the transmitted wave always remains unaltered.

Total internal reflection must be accounted for if light is incident on a media with a lower refractive index and the incident angle is large. The criteria for total internal refelction is $\frac{n_i}{n_t} sin(\theta_i) > 1$ at which point all light is reflected. In the case of light going from glass to water the incident angle required for total internal reflection is approximately 60°, depending on the precise index of the glass and water. Thus, in case of BSI total internal reflectance is a possibility only when the light passes from glass to water or air and the angle of incidence is relatively large, which only occurs when light impinges the capillary (or microfluidic channel) near outer edges and not near the center where the light is incident close to normal on the glass. Thus for light reflected directly backwards as in most BSI setups, including the current, total internal reflection does not contribute significantly to formation of the fringe pattern.

The intensity of the fringe pattern at a plane of detection that symbolizes the CCD is calculated on basis of equation 2.10 (see also equation 1 in Paper II). Because a discrete number of rays are used, interpolation is used to produce a continuous fringe pattern.

5.1.2 Wave-based model

The interference pattern from light reflected and refracted in a cylindrical geometry has also been solved using Maxwells' equations.[31] Such wave based models have previously been used to characterize the fringe pattern produced by BSI[92] and substantial work has been done by H.S Sørensen in relation to his thesis on BSI.[78,10] Further work was done by H.S Sørensen as part of this project to adopt the model to the dimensions of the current setup and the results are also presented in paper II. The wave-based model is advantageous because it also describes the effects of diffraction, but requires extensive computing time and does not allow one to track individual rays propagating the system, the latter has proven much helpful in relating parts of the fringe pattern to specific ray-paths inside the capillary.

5.2 Results

Both ray-tracing and a wave-based method was used to model the current capillary setup and the results are presented and discussed in paper II. It was found that both ray-tracing and wave-based models were in very good agreement with each other, producing nearly identical fringe patterns shown in figure 5 in paper II. By visual comparison the modeled fringe patterns were also in good agreement with the experimentally observed fringes and differences are related to the experimental uncertainties of the diameters and refractive index, as well as an uncertainty of the angle of observation, which is difficult to measure in the experimental setup. From the modeling it was found that the frequency of the interference patterns is governed by the refraction of light through the media interfaces and noticeable changes in the frequency-peaks can be seen in the spectrum if the refractive index changes are > 0.02 RIU. As refraction of the beam entering the sample fluid also alters the geometrical path length through the sample, this consequently also alters the sensitivity. The sensitivity is therefore dependent on the absolute sample refractive index and for large changes in refractive index one cannot assume that the signal is linear with refractive index. However, for such small changes in sample refractive index that are measured in relation to protein binding and ezymatic measurements, the frequency can be treated as being constant and changes in fringe position can be measured by tracking the phase of a single constant frequency component. As can be seen in figure 5.2 the rays that are reflected directly backwards i.e. at an angle close to the incident beam ($\Theta \rightarrow 0°$), are all rays that are incident near the center of the capillary. Those rays incident near the edges of the capillary are refracted at a large angle and do not contribute to the interference pattern formed at observation angles approximately less than($20°$). To this extent the full geometry of the sample channel is of little importance for light reflected directly backwards and the channel could be round, square or semi-circular, for

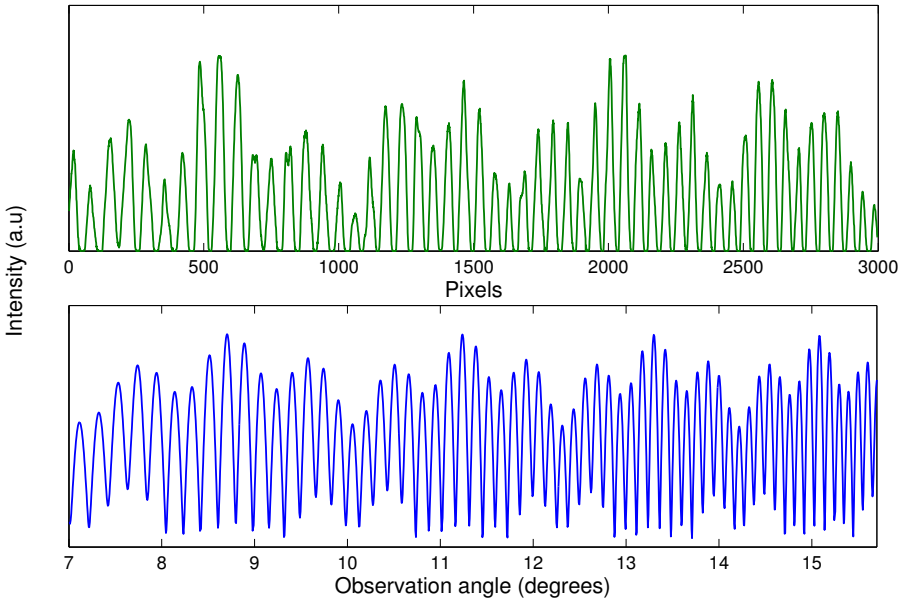

Figure 5.1: Top plot shows a typical fringepattern from experiments recorded by the CCD. Bottom plot is the fringepattern produced by ray-tracing in the observation angles that equivalent to the position of the CCD in the experimental setup.

small changes in refractive index where refraction is negligible, the sensitivity will be given by the distance across the channel center.

On the assumption of the simple two dimensional model used for characterizing diffusion

Ray tracing proves that the beam paths contributing to the observed fringe pattern are not distributed across the full cross-sectional area of the capillary, but are in fact confined within a limited trajectory that is near the center of the capillary. This validates the assumption that the fringe pattern will be sensitive to local radial variations in refractive index and the simplistic two dimensional model used in section 3.10 is therefore quite representative of the actual system.

5.2.1 De-chirping

The fringes are widest at small angles, however, the results of the ray tracing experiments suggested that the change in fringe width varies as a linear function of the observation angle for angles 0-20° as shown in figure 7 in paper II. This gradual change in fringe width represents a gradual change in frequency as

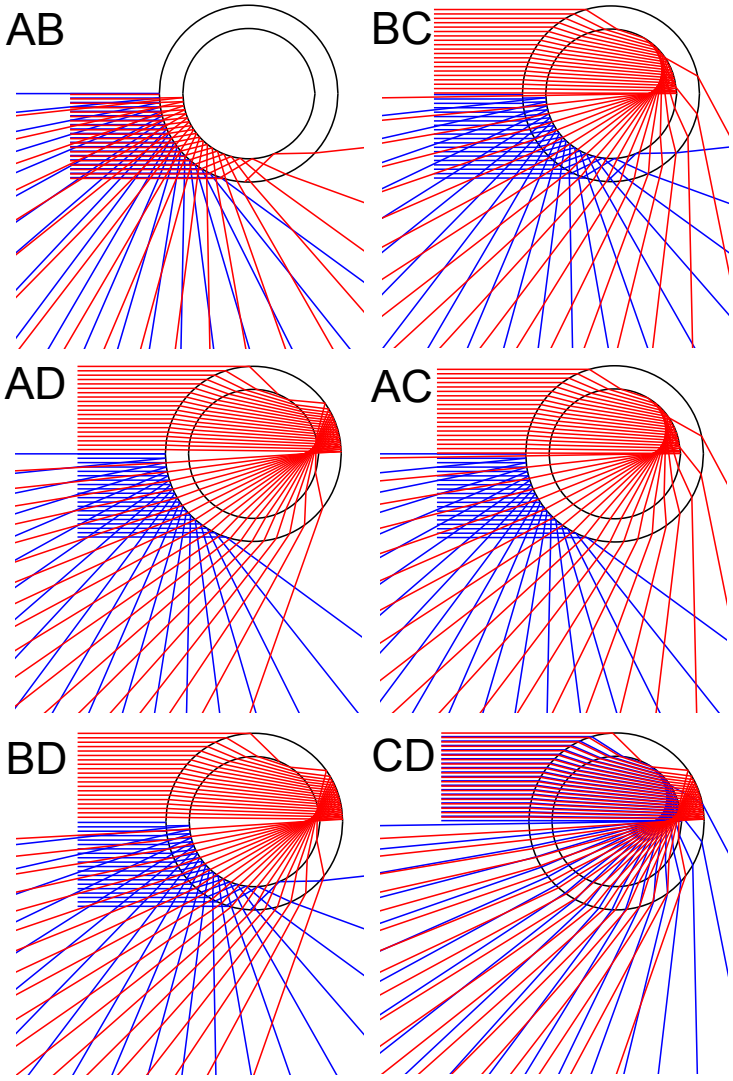

Figure 5.2: Cross sectional view of the capillary showing the light impinging from the left. Six possible combinations of the four beam paths (A, B, C D) each producing a distinct interference pattern. Notice that in the first combination (AB) none of the rays traverse the media contained within the capillary and should therefore not be sensitive to the medias refractive index. Upon closer inspection one also finds that the beams reflected directly backwards, which is where the detector is located, all have beam paths very close to the center (origo) of the capillary and that their incident angles are nearly orthogonal which minimizes the angle of refraction.

a function of observation angle and the spectrum peaks are broadened as a result. A signal with gradually increasing or decreasing frequency over the signal duration is often referred to as a chirped signal and by estimating this chirp function one can de-chirp the signal, producing a set of fringes that have identical width over the entire length of the signal and consequently a single sharp frequency component in the spectrum.

The de-chirping algorithm used is based on selecting a single frequency component corresponding to the interference pattern formed by a single set of rays e.g. BD. It is found that the intensity (I) of such a single fringe pattern can described by a quadratic chirp function with an empirically determined offset factor B:

$$I(x) = Acos(\omega(x + B)^2 + \phi) \tag{5.1}$$

Where x is the observation angle or pixel number, A, ω, B are constants and ϕ a phase shift. By making a coordinate transformation from $x \rightarrow X'$ where

$$X' = (x + B)^2 \tag{5.2}$$

and setting B to a correct size produces a fringe pattern that appears without a chirp

$$I(X') = Acos(\omega x' + \phi) \tag{5.3}$$

The spectrum representation of I(X') is then used to extract the phase values. The offset factor B is different for each interference pattern (AB, AC, AD, BC, BD, CD) and an ideal de-chirp algorithm should take this into consideration.

5.2.2 Improved spectrum

Applying the de-chip algorithm at first produced a spectrum containing four distinct peaks as can be seen on figure **??**, but by moving the CCD closer to the capillary more fringes are sampled and the frequency resolution is improved and a total of six frequency peaks can be distinguished (see figure 5.3). Because the fringes are de-chirped the frequency spectrum is also less dependent the angle of observation and the frequencies remain reasonably constant even if the CCD is moved outwards to higher observation angles.

5.3 Discussion

From a physical point of view, one cannot ignore the fact that beams will be reflected more than once but the resulting intensity of light from multiple reflections will be very small. From the Fresnel equations one finds that the intensity of light reflected from an air/glass or a glass/water interface is always $< 4\%$ and $< 0.4\%$ respectively and the intensity of multiple reflected beams will therefore be very small.

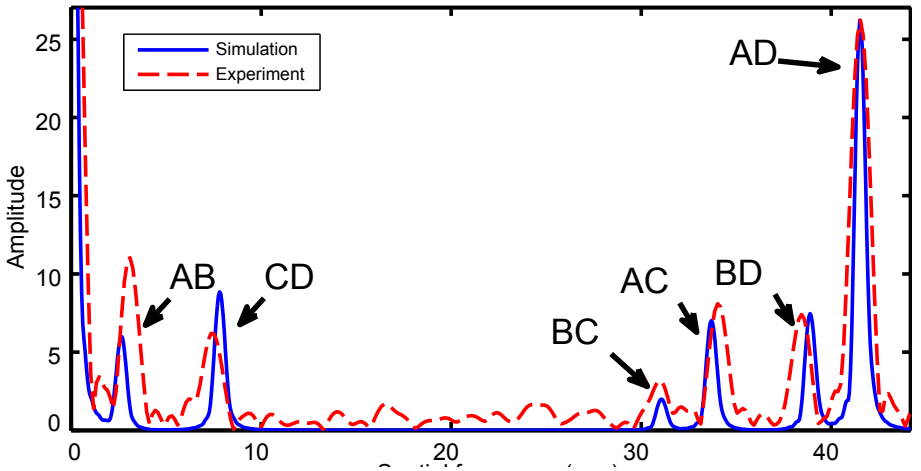

Figure 5.3: Frequency spectrum after de-chirping algorithm of fringe pattern as simulated by ray tracing (solid line and exeprimental setup (dahsed line). The experimental x-axis has been scaled to fit the ray tracing x-axis due to different scale of units.

Ray-tracing results proved to fully describe the fringe pattern with rays reflected at four instances (A, B C and D) which combines to produce six individual fringe patterns (AB, AC, AD, BC, BD, and CD). In case there was a significant contribution from beams reflected multiple times, one would expect to find additional frequencies besides the six in the experimentally observed frequency spectrum, which is not the case.

From the optical models the sensitivity is found to be directly proportional to the inner diameter of the capillary and as can be seen on figure 8 in paper II, the sensitivity is highest near the directly backwards reflected light. In fact for light reflected directly backwards at zero degrees the optical path difference corresponds to exactly twice the capillary inner diameter and the fringe shift can therefore be described by the simple expression used in section 4.1.5:

$$\Delta n \Delta\phi = \frac{2\pi}{\lambda} 2nd \tag{5.4}$$

I.e if the optical path difference ($OPD = 2nd$) between sample and reference beams (e.g A and D) changes exactly one wavelength 632.8 nm the optical phase shift ($\Delta\phi = \frac{2\pi}{\lambda}$) becomes exactly 2π radians. Correspondingly the the fringes reflected directly backwards will have moved a full cycle and the signal using the Fourier transformation is also $\Delta\Phi = 2\pi$. Thus for the directly backwards reflected light the signal in radians (Φ) is equal to the optical phase shift (ϕ) also in radians.

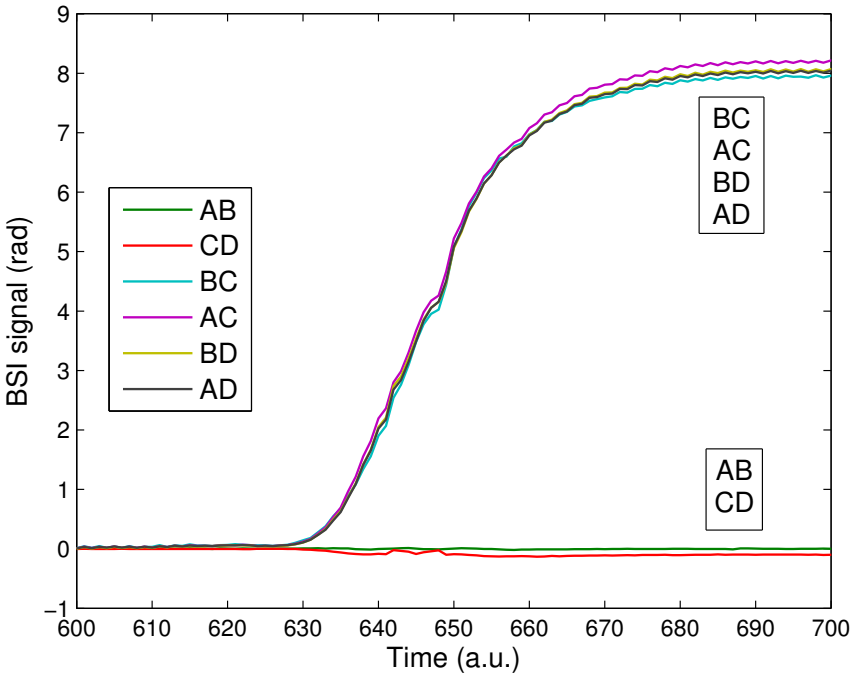

Figure 5.4: BSI signal (phase) for all six frequencies upon injection of a sodium chloride solution. Frequencies AB and CD show little or no sensitivity to the bulk RI, whereas frequencies BC,AC,BD,AD show equal sensitivity.

Chapter 6

Protein binding studies and enzymatic reactions

An essential claim of BSI is its utility to detect bio-molecular binding events. Although numerous articles have been published demonstrating the detection of various protein-ligand interactions the underlying physical theories on how such events alter the refractive index are still vague at best. Conformational changes in protein structure and exclusion of buried water molecules have been suggested as underlying mechanisms that responsible for changes in refractive index. In this chapter these claims are put to the test by using BSI to study three different types of protein binding events using fluorescence spectroscopy as a reference method. Finally BSI is used to study the enzymatic reactions of apyrase and hexokinase and results are verified using a commercial available refractometer.

6.1 Investigation of protein binding from exemplary experiments

A wide assortment of protein-ligand binding systems have previously been characterized with BSI including small molecule enzyme inhibitors,[20,17,18,15,13,21] as well as aptamers binding to human α-Thrombin.[16] The proposed mechanisms for the BSI signal are centered around mechanisms related to conformational changes in proteins structure and change in the so-called waters of hydration that accounts for the number of water molecules tied to the protein surface.[17,14,11,18]

> Several studies have shown that these shifts correlate well with ligand– receptor binding interactions and can result from conformational changes, solvation/desolvation, changes in dipole moments, and polarizability
> (Haddad, Young, Heindel, Bornhop and Flowers,2012)[18]

6.2 Methods

6.2.1 Fluorescence spectroscopy as a reference method

Currently only a few of the published free-solution binding studies using BSI have been verified with other experimental procedures and often verification has been given by comparing binding constants with literature values (See Latham, Stein, Bornhop, and Mchaourab[12] for an example where BSI is verified with iso thermal caliometry and fluorescence spectroscopy). In order to actually verify that a binding event has occurred fluorescence spectroscopy (FS) was chosen as a reference method. It is the method of choice because FS permits binding to be studied in free-solution and on identical samples i.e. same buffer systems and protein concentrations as those measured on BSI. The ligand of choice was the small molecule p-aminobenzadimine that is bound by trypsin and thrombin with an average K_D of 6.1 and 65 µM respectively. It is weakly flourescent in water but binding to trypsin-like proteins causes a shift in both absorption and emission peaks and increases fluorescence intensity.[93] FS can also detect changes in the intrinsic fluorescence of amino-acids; tryptophan, tyrosine and phenylalanine that are sensitive to the presence of nearby molecules including water[94] and many of the same mechanisms producing shifts in intrinsic fluorescence are also suggested to be responsible for the measured signal in BSI. Intrinsic fluorescence was used to detect the binding between antithrombin and heparin.

Despite initial plans to use BSI for immunoassays, antibodies are poor candidates for investigating the origin of the BSI signal. Firstly, antigen-antibody

binding is not normally associated with large conformational changes.[86] Secondly, most antibodies have a high affinity for their target and the concentrations needed to determine K_D experimentally would consequently be in the pico- and nano-molar range, which would be below the minimum detectability of the current system. Instead it was decided to investigate three different protein-ligand systems that were known to exhibit either large conformational changes and/or changes of hydration state upon binding. Furthermore the protein-ligand dissociation constant should be within the minimum detectability of BSI and perhaps most importantly should be easily verified by a reference method. The three chosen systems are:

- Trypsin - p-Aminobenzamidine
- Trypsin - Antitrypsin
- Antithrombin - Heparin

Trypsin - p-Aminobenzamidine

p-Aminobenzadimine is an enzyme inhibitor derived from benzamidine that binds most trypsin-like proteases and has been used as a fluorescent probe to characterize their binding sites.[93,95,96] Binding of benzamidine (and p-aminobenzamidine) to trypsin involves hydrophobic interactions and hydrogen bonds, but does not confer conformational changes.[97,98,99]

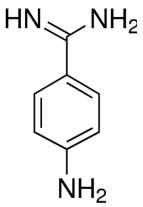

Figure 6.1: p-aminobenzamidine

Trypsin - Antitrypsin

The initial aim and objectives of this project proposed a study of antithrombin binding to thrombin because of the known conformational changes associated with the complex formation. Although antithrombin could be obtained locally as it is purified in an in-house procedure it was decided to use the similar proteins antitrypsin and trypsin instead due to cost and availability, however, the two systems share many similarities. Both antithrombin and antitrypsin are protease inhibitors belonging to the serpin superfamily and they are very similar in size and protein structure,[100] but most importantly, both proteins have a reactive site loop that covalently bind their respective target protease (thrombin or trypsin). Upon binding the serpin-protease complex undergoes a structural conformational change whereby a reactive site loop and target protease are moved to the opposite end of the serpin.[24,25] The conformational change results in a transfer of 73 ± 7 water molecules to bulk solution.[101] Because of the covalent binding dissociation rates are very slow and dissociation constants (K_D) are practically infinitely small. This does not imply that binding occurs instantly and rates of association and dissociation can be characterized by real-time measurements, but since the current BSI setup is limited to performing

end-point measurements an alternative approach is taken to measure the binding of trypsin-antitrypsin. Because antitrypsin binds to trypsin at the same active site as p-aminobenzadimine, trypsin and p-aminobenzamidine will compete for binding. Trypsin is therefore pre-incubated with p-aminobenzamidine and then titrated with increasing amounts of antitrypsin which will displace p-aminobenzamidine producing a detectable shift in the fluorescence spectra.

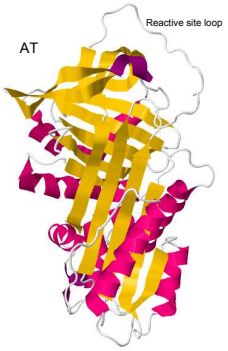

(a) Native antitrypsin

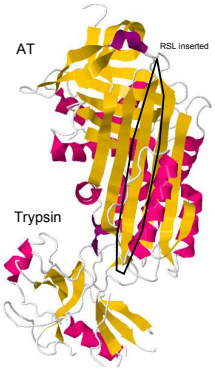

(b) Antitrypsin-Trypsin complex with reactive site loop inserted

Antithrombin - Heparin

Binding of heparin to antithrombin is well known to enhance the rate of association for antithrombin-thrombin complex formation. Heparin is a glycosaminoglycan consisting of a long chain of sulfated disaccharides that usually contain uronic acid giving the whole molecule a highly negative charge. Heparin binding to antithrombin causes a conformational change that is associated with release of 158 ± 11 water molecules from reactants to bulk.[102,103] The binding causes an increase in the intrinsic florescence of tryptophan residues in antithrombin and the binding can be measured using FS.[104] The commercial grade heparin used in the experiment was unfractionated and concentration was not indicated in mass units but in International standard Units (IU/mL) and quantitative determination of K_D was therefore not possible. However, since the purpose was only to confirm heparin binding a pseudo-binding curve was acceptable for this experiment.

6.2.2 Results

Results: p-aminobenzamidine - trypsin

For the p-aminobenzamidine-trypsin binding a clear binding curve was observed using FS and K_D determined to be 4.0 ± 1.6µM in agreement with literature.[93] The differential signal from BSI measurements performed in triplicate did not produce a significant binding curve. It is noteworthy that the refractive index contribution of p-aminobenzamidine itself is quite low and a standard curve with p-aminobenzadimine did not show a significant change in BSI signal over a concentration range of 2-100 µM. The observed average differential signal of 0.2 rad $\approx 7 \times 10^{-6}$ RIU is in agreement with the theoretical 9×10^{-6}RI increment from 2 µM trypsin (assuming MW: 24 kDa and dn/dc: 0.18 ml/g).

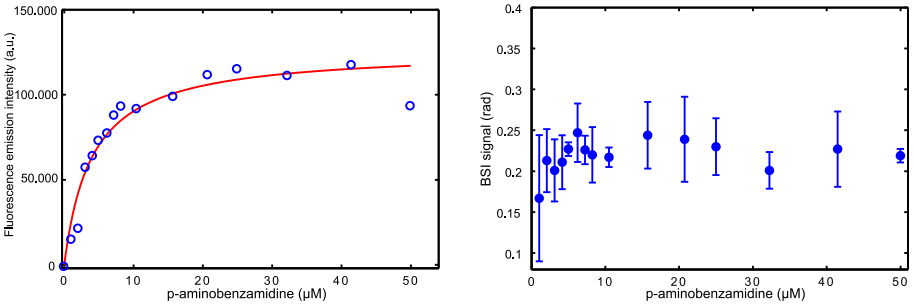

Figure 6.3: Binding between trypsin (2 µM) and increasing concentrations of the small molecule p-aminobenzamidine by FS (left) and BSI (right). Solid line shows non-linear fit used to determine K_D

Results: Trypsin - Antitrypsin

A linear decrease in fluorescence intensity is seen upon addition of antitrypsin as p-aminobenzadiamine is displaced from trypsin. As the antitrypsin concentration exceeds the concentration of trypsin no further drop in fluorescence intensity is observed indicating that all p-aminobenzadiamine has been displaced. In contrast the BSI signal was linear with increasing antitrypsin concentration over a wide range and no change in signal was observable as the antitrypsin concentration exceeded 4 µM. Thus the displacement of p-aminobenzamidine from trypsin could not be detected with BSI in this case either, in agreement with previous experiment, nor did the trypsin-antitrypsin binding produce a change in refractive index observable with BSI.

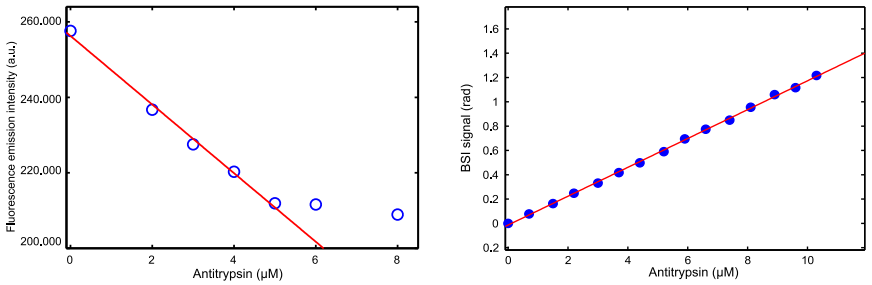

Figure 6.4: Binding between trypsin preincubated with p-aminobenzamidine (4 µM) and increasing concentrations of antitrypsin by FS (left) and BSI (right). Solid line shows linear fit to data (only first 5 data points fitted for FS).

Results: Antithrombin - Heparin

Binding between antithrombin and heparin produced a change in fluorescence intensity resembling a binding curve that saturated in signal as heparin concentration exceeded 10 IU/mL. In contrast the differential BSI signal did not show a binding-signal.

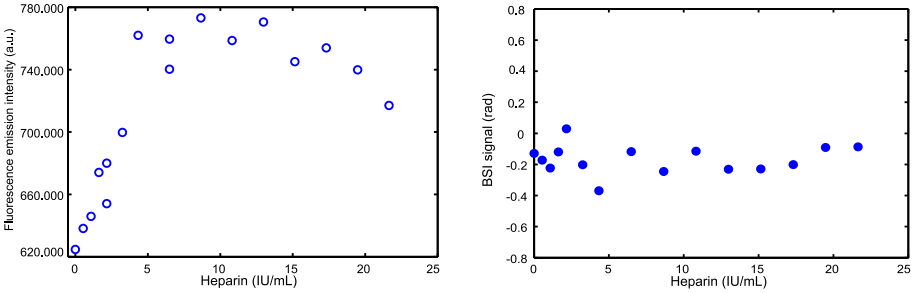

Figure 6.5: Binding between antithrombin (1.6 µM) and increasing concentrations of unfractionated heparin by FS; intrinsic fluorescence (left) and BSI (right).

6.2.3 Discussion

Three exemplary systems of protein-ligand or protein-protein binding were measured using BSI and FS as a reference method. Binding was verified in all three cases by FS but BSI failed to produce clear evidence of a binding signal.

In the small ligand case with the trypsin inhibitor p-aminobenzamidine the origin of the signal should come from the hydrogen bonds between ligand and amino acids in the protein. The binding is not associated with protein conformational changes or significant change in waters of hydration. These findings are in contrast to a similar study where Bornhop et al. used BSI to

detect interaction of the enzyme carbonic anhydrase and its inhibitors,[13] with carbonic anhydrase and its inhibitors present in nanomolar and micromolar ranges respectively. The inhibitor binding to carbonic anhydrase is also primarily through various hydrogen bonds but coordination to a single Zn(II) ion is also involved, which could be important considering that the polarizability of ions is dependent on their surrounding environment.[105,106,107] The binding between antitrypsin-trypsin and antithrombin-heparin is known to be associated with large conformational changes of protein structure as well as release of water from the protein structure to the bulk solution, which have been attributed as the responsible mechanisms for the BSI binding signal. If protein refractive index changes due to conformational changes in protein structure, then the observed signal should scale with the amount of protein present. For both experiments protein concentrations were in the micromolar range, which is high compared to the protein concentrations generally used in BSI literature and from these results it must therefore be concluded that conformational changes did not confer large changes in protein refractive index. Likewise the amount of water bound to or released from the protein did not have an effect on the refractive index of the solution large enough to be detected by BSI.

6.3 Enzymatic assays

The third and unpublished paper (paperIII: Real-time detection of enzymatic reactions using back scatter interferometry and conventional deflection refractometry) describes the measurement of two enzymatic reactions. Firstly; the phosphorylation of glucose by the enzyme hexokinase and secondly; the hydrolysis of adenosine triphosphate by the enzyme apyrase. The measurements were preformed as real-time measurements and the kinetic Michaelis-Menten constant (K_M) was determined for hexokinase from initial velocities.

6.3.1 Methods

With a firm knowledge of how BSI functions and having determined that the that the minimum detectability of the setup is closer to $10^{-7}RIU$ and not 10^{-9} or lower as proposed by Bornhop et al. it was reasonable to assume that high quality refractometers could also measure what BSI could. In the carnivorous department of such refractometers is the T-rEX, a differential refractometer marketed by Wyatt, with an extraordinary minimum detectability of $10^{-9}RIU$. The T-rEX is in principle an ordinary deflection refractometer that measures the angle of refraction from light entering a sample prism cell using light with a wavelength of 658 nm. The high sensitivity is attributed to an improved detection scheme that can detect very small angles of refraction. For the latter part of this project involving the enzymatic studies a T-rEX refractometer, kindly made available by the department of Chemistry and Bioscience at Aalborg University, was used as a reference instrument to verify the BSI results.

Figure 6.6: The T-rEX refractometer

6.3.2 Results

dn/dc:

The refractive index increment (dn/dc) for the substrates and products; glucose, glucose-6-phosphate, ATP and ADP was determined using the T-rEX. The dn/dc for glucose and glucose-6-phosphate was also determined using BSI and the results were in excellent agreement with those obtained using the T-rEX. The differences between dn/dc values of glucose and glucose-6-phosphate was 1.48×10^{-5} RIU mM^{-1} giving a predictive estimate of the the change in refractive index that one should expect from the enzymatic reaction.

Enzymatic reactions:

Real-time measurements of the enzymatic reactions produced signals that initially increased linearly over time and proceeded as a non-linear increase until plateauing at a maximal end-point signal. These observations are in good agreement with the kinetics of enzymatic reactions. The relationship between the observed end-point values and intial substrate concentrations was linear and the slope of end-point values vs. [substrate] yields the observed change in refractive index per mole of substrate. The observed values were; 0.96×10^{-5} RIU/mM for glucose→glucose-6-phosphate, 1.51×10^{-5} RIU/mM for ATP→AMP and 0.675×10^{-5} RIU/mM for ADP→AMP. The difference between these predicted and observed quantities were discussed and related to the release and transfer of free inorganic phosphate ions. Phosphate ions are negatively charged and will decrease the refractivity of the neighboring solvents, thus the binding and releasing of phosphate groups from adenosine triphosphate lowers the refractive index of a solution.[108]

Enzyme kinetics:

For hexokinase K_M for glucose was determined using the real-time BSI data and found to be 0.33 mM in good agreement with literature values.

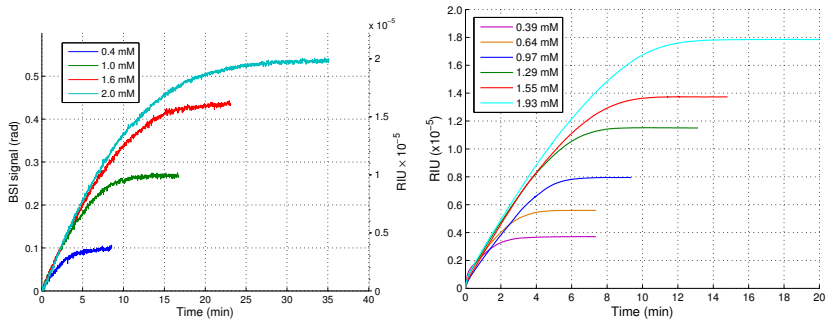

(a) BSI **(b)** T-rEX

Figure 6.7: Real-time enzymatic phosphorylation by hexokinase of various D-glucose substrate concentrations measured using BSI and the T-rEX. Data shown is collected immediately after completion the sample injection and all initial values have been adjusted to zero.

6.3.3 Discussion

Challenges for low K_M reactions

Initial attempts to measure the Apyrase reaciton on BSI proved difficult. Practically the low millimolar k_M means that the enzyme achieves maximum ve-

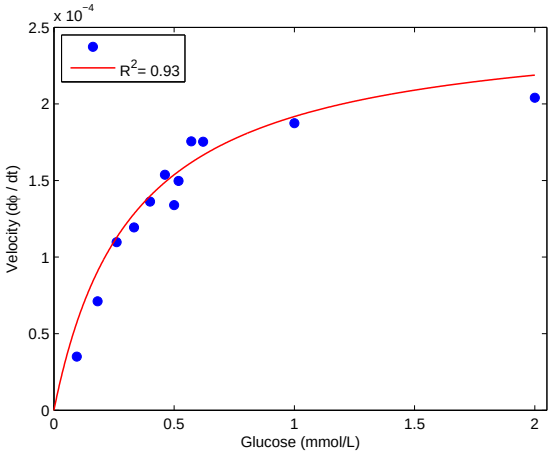

Figure 6.8: Hexokinase substrate saturation curve: Initial velocity measured as change in signal (radians) over time versus glucose concentrations reveal a hyperbolic dependency. K_M is 0.33 mMby non-linear regression (solid line, $R^2 = 0.93$)

locity even at low concentrations of substrate. With low concentrations of substrate, the reaction can be finished before the sample has been fully injected and low amount of substrate also produces a proportional low endpoint signal. An attempt to solve this issue was to use low concentrations of Apryase (1 nM) but this results in very long reaction times and signal drift then becomes significant. Thus attempts to determine K_M which requires the measurement of initial velocity were abandoned, although evidence and signs of enzymatic reactions was evident from the data collected (example shown in figure 6.9). As described in the section below, carryover effects also disturbed some of the BSI measurements causing further discrepancy between data sets.

Observed carryover in enzymatic reactions

The issue of contamination between subsequent sample injections as a result of diffusion and inadequate mixing was discussed on a theoretical basis in chapter 3. As enzymes are proteins adsorption to the the capillary surface is therefore a viable concern and during the experimental investigations of enzymatic reactions it became evident that there was a carryover of enzymatic activity between sample injections. This was clearly seen as blank injections containing only substrate and no enzyme produced the same signal as if enzyme was still present. This could only be observed in injections when the capillary had prior been exposed to enzyme and rigorous cleaning of the capillary with HCL and 2-propanol removed any signs of enzymatic carryover activity. In some experiments it was also observed that the enzymatic activity increased over time as multiple subsequent injections of enzyme solutions were introduced into the

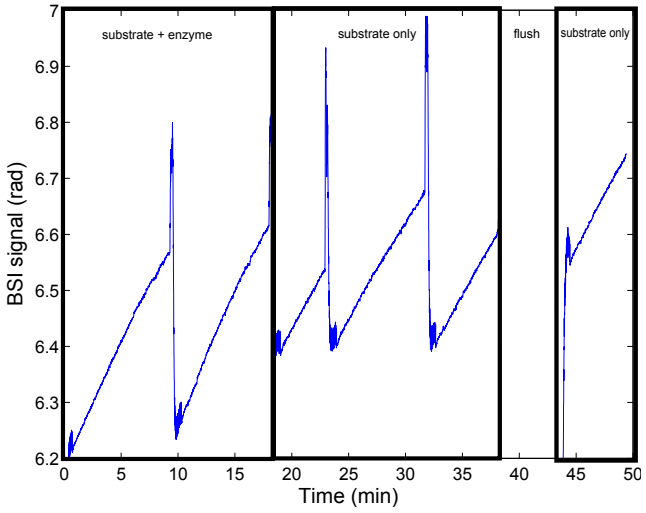

Figure 6.9: Carryover of enzyme activity: Two injections of apyrase and ATP followed by three injections of blanks (substrate only). Even after a flush with buffer the system still retains enzyme activity as evident in the last injection of blank.

system, suggesting an increasing build-up of enzyme in the system. It must therefore be concluded that this carryover of enzyme activity is evidence by proxy that proteins adsorb to the surface of the capillary.

Back Scatter Polarimetry?

The results presented in the here are a first, or are they? A publication by Swinney and Bornhop (2000) describes how a back scatter interferometer setup is utilized to measure in real-time the transition of the β-hydroxybutyrate to acetoacetate by the enzyme β-hydroxybutyrate dehydrogenase.[30] However, the authors claim that the instrument is setup to function as a polarimeter, which is obtained by observing a limited region of so-called high frequency fringes that are sensitive to the plane of polarization and not the refractive index of the sample.[109] Accordingly the measured signal is a result of a difference in optical activity between the substrate β-hydroxybutyrate $[\alpha]^{25} = -24.5°$ and the product acetoacetate $[\alpha]^{25} = 0°$.

From the results presented in chapter 5, it is indeed possible to produce high-frequency fringes that are insensitive to the refractive index and appear to vary between different polarization states of the laser. However, such fringes can only be reproduced using a wave based model, which suggests that they are a result of a diffraction phenomena. Although diffraction from a capillary is predominantly dependent on the size of the capillary and not the refractive index,[110] diffraction angles has been showed to vary when diffraction occurs in a chiral media.[111] It would thus appear that Swinney and Bornhop constructed

something akin to a diffraction polarimeter and accordingly the signal from the enzymatic reaction was a polarimetric signal produced by changes in the anisotropy of the media and not the refractive index.

Refractive index of chiral media

Despite just having made an effort to dissociate effects of polarization from the refractive index it must be stated that they are indeed related. First one must consider that linearly polarized light may be described as being composed of equal parts right handed- and left handed-circularly polarized light that are in phase with each other. The effects of a chiral media on linearly polarized light may now be understood by treating the chiral media as having two different refractive indexes; n_d and n_l. When light propagates the media a distance (z) the right- and left-circularly polarized parts experience two different refractive indexes causing a relative phase difference between the polarization states ($\Delta\Theta$) which also determines the total rotation angle of the combined linearly polarized light

$$\Delta\Theta = \frac{2\pi}{\lambda}\frac{n_d - d_l}{2}z \tag{6.1}$$

Thus the difference between n_d and n_l controls the optical rotation. At the same time the phase of the light experiences a phase delay that corresponds to the average refractive index $n_{avg} = \frac{n_l+n_d}{2}$. In terms of BSI it would therefore be reasonable to expect that a change in the specific optical rotation angle of a chiral molecule would cause a shift in refractive index of the sample fluid and consequently a fringe shift. However, one must also take into consideration that circularly polarized light changes its direction of rotation upon reflection from a surface. Thus right handed circularly polarized light becomes left handed and vice versa. Thus any rotation of the polarization vector will be annulled if the light travels an equidistant path before and after reflection. This will certainly be the case when observing the BSI pattern close to the centroid (i.e. 180° to the incident beam) and even far from the centroid the path difference is small. In the case of a semicircular geometry the path distance between incoming light and that reflected from the flat back side is more pronounced than for a circular geometry and in theory a chiral media would change the polarization of the light.

6.4 Protein adsorption to the capillary wall

Detection of protein binding to other surface immobilized proteins with BSI has been demonstrated using both round and square channels designs.[9,112,10] The effect of an adsorbed protein layer on the observed fringe pattern was also been studied by a wave-based model and it was found that the signal is proportional to the change in optical path length due to the adsorbed protein layer.[10] The signal from surface adsorption is in contrast to the signal from free-solution binding events. In the former, the adsorbed protein forms a specific protein layer that is, depending on the specific proteins, a few nanometers in thickness with a refractive index around 1.4,[113] in the latter free-solution event the signal arises as a a small refractive index of the bulk fluid. Any unspecific binding of proteins to the surface of the capillary during a free-solution binding measurement will therefore contribute with an erroneous signal. In the case of end-point measurements the a peotential increasing build-up of adsorption proteins from multiple sample injections would also also result in errorneous signal depending on how the end-point measurements are performed. The effect of protein adsorption in this study come from several observations made, especially during the protein A - IgG binding experiments and a few ad-hoc experiments have been permed as well. However, a thorough study requires a methods to accurately control the thickness and refractive index of the protein layer and the chemical modification and preparation of the capillary glass surface associated with such a process would require are beyond the scope of this study. Furthermore the methods normally used for verification of protein adsorped layers such as atomic force microscopy (AFM) and x-ray photoelectron microscopy (XPS) cannot readily be performed on the round enclosed geometry of a capillary.

6.4.1 Adsorption of protein observed during protein A - IgG experiments

As noted in section4.2.2 the signal processing used for the protein A - IgG experiments did not make full use the advanced de-chirping algorithm and the frequency resolution is therfore limited but adequete enough to identify the two frequency components corresponding to the interference patterns identified as AD and CD in figure 5.2. The phase from the AD frequency is very sensitive to the samples bulk refractive index and is the one primarily used, whereas the phase of the CD frequency component does not display significant sensitivity to changes in bulk refractive index. However, clear observations of phase change in the CD component has been observed on multiple occasions during the protein A - IgG binding experiments, which suggests that the CD frequency is sensitive to an adsorbed protein layer. The adsorption of protein A and Immunoglubulin G from water to silicon surfaces (glass is sillicon dioxide) has been studied with

AFM and XPS, showing that protein A formed a primary dense 10 nm thick mono-layer with subsequent secondary and tertiary stacking layers of protein A and the average layer thickness of IgG bound on top of a protein A layer was found to be in the range of 8 nm to 13.5 nm.[114]

Theoretical effect of protein adsorption on frequencies AB and CD

The interference pattern corresponding to the AB and CD frequencies is formed by ray paths reflecting from the air/glass interface (A and D) and the glass/liquid interface (B and C). Since the refractive index of protein (1.4) is very close to that of glass (1.5) the reflection coefficient from a glass/protein interface would be small and the low intensity of light reflected from it would therefore not contribute significantly to the observed fringe pattern. Instead the adsorption of a protein layer can be treated as moving the point of reflection for beam paths B and C from the glass/liquid interface to the protein/liquid interface. Effectively, for the directly backwards reflected fringe pattern, this alters the optical path length of beam paths B and C and the signal for frequencies AB and CD, assuming a 10 nm layer with RI: 1.4, changes according to equation 5.4:

$$\Delta\Phi_{AB,CD} = \frac{2\pi}{632.8\,\text{nm}} 210\,\text{nm}\ 1.4 = 0.278\ \text{rad} \tag{6.2}$$

Theoretical effect of protein adsorption on frequency AD

In case of the AD frequency the added protein layer simply adds to the optical path length of beam path D by an amount equal to four times the thickness of the protein layer, because beam D traverses the protein layer four times, multiplied with the refractive index difference between protein and liquid assumed to be water (RI: 1.33). Thus using equation 5.4 the signal will change:

$$\Delta\Phi_{AD} = \frac{2\pi}{632.8\,\text{nm}} 410\,\text{nm}\ (1.4 - 1.33) = 0.00278\ \text{rad} \tag{6.3}$$

Experimentally observed phase changes for frequencies CD and AD

When increasing amounts of protein A concentrations ($0.17\,\mu\text{g}\,\text{mL}^{-1}$ to $2.5\,\mu\text{g}\,\text{mL}^{-1}$) were injected over a period of 40 minutes (see figure 6.10a) the signal for frequency CD increased accordingly to a plateau of ≈ 0.026 rad that could not be reverted by rinsing with buffer (indicated by arrow), which is in good agreement with the theoretical expected phase change. It is also noticable that the phase change for frequency CD appears to increase initially but then settle at a plateau level well before injection of the maximum concentration of protein A, suggesting that the surface is saturated with protein. A similar change is observed for frequency CD during the end-point measurements of protein A - IgG experiment shown in figure 6.10b. For frequency AD (see figure 6.10) there is no observable change in phase after rinsing with buffer when protein A is

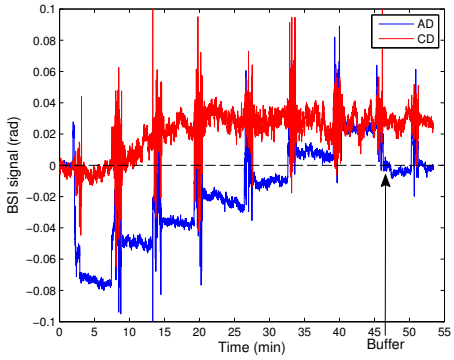

(a) Protein A

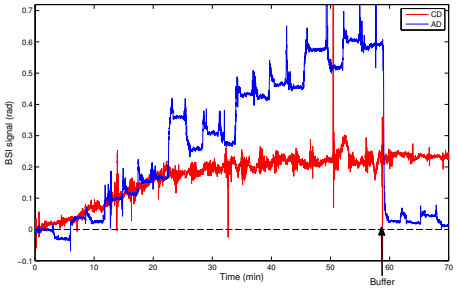

(b) IgG + protein A

Figure 6.10: Unspecific binding signal for frequencies AD and CD observed as baseline signal does not return to zero when the capillary is flushed with buffer. a) Solutions of protein A. b) Solutions of IgG + protein A.

used, however a change of ≈ 0.015 rad is observed when both IgG and protein A is injected, which is in reasonable agreement with the theoretical expected phase change. However it is difficult to conclude precisely on the effect of the AD frequency because long term drift which has been estimated to be ≈ 0.006 rad/hour, may also be a masking factor here.

6.4.2 Discussion

Further and more detailed studies under more controlled conditions would be required to fully disclose the effect of protein adsorption on the measured signal. It is certainly ambiguous that BSI has been advocated as being able to detect both free-solution and surface bound protein binding events and although some of the published BSI studies have taken measures to ensure rigorous cleaning the problem does not seem to be addressed in detail. One publication (Baksh et al., 2011) describes the nonspecific adsorption to the channel walls as not compromising the overall accuracy of the measured values.[15] The most detailed and resent discussion on the difference between BSI free-solution and surface based measurements is given in a paper by Olmsted, Kussrow and Bornhop (2012),[68] but they do not address the issue of non-specific binding as an error source.

Chapter 7

Final discussion and conclusion

In summary the aim of this study was to investigate the potential use of BSI in clinical biochemistry, specifically addressing three applications: immunoassays, protein binding studies and enzymatic assays. BSI is an interferometric refractive index detector which in a most novel manner, has been used to detect a wide range of biomolecular binding events between proteins and various ligands based on observing minute changes in the fringe pattern produced by light reflected from a small channel or capillary. For this purpose an experimental BSI setup was constructed using a large diameter glass capillary as the central optical and sample containing component, as opposed to the smaller microfluidc channels used in previously published studies by other authors. The experimental setup proved to be very sensitive to changes to both ambient and sample temperature and the initial design of the setup was fitted with temperature sensors including one inside the capillary to monitor sample temperature. As a result of temperature data the setup was modified to improve temperature control and ensure pre-heating of sample liquid, which significantly improved long term stability of the signal and reduced signal artifacts caused by temperature variation upon sample injection.

Despite these improvements the initial plans to perform rapid microfluidc mixing of samples and reagents to study protein binding events in real-time was canceled because incomplete mixing created signal artifacts from diffusion of unmixed solutes that could be confused with the actual protein binding signals. The experimental sensitivity and minimum detectability were found to be 27011 rad/RIU and 7.03×10^{-7}RIU respectively (see chapter 4). These numbers were inconsistent with the performance of BSI setups from other studies, which otherwise describe the sensitivity to be independent of the the channel diameter,[68,80] as the sensitivity of the current setup was markedly higher whereas the minimum detectability seemed to be on the same order.

An initial attempt to reproduce the measurement of protein A and immunoglobuling G binding as previously published in literature with BSI failed to detect any binding. Together these findings encouraged a thorough investigation of the optical principles governing BSI and theoretical ray-tracing and wave-based models, which have otherwise previously been used to characterize BSI, were reapplied to demystify the relation between sensitivity and capillary diameter. The results of these models produced were in good agreement with experimental measurements (see chapter 5) revealing that the frequency spectrum of the Fourier transformed fringe pattern consists of six peaks formed by the interference of light reflected from the various air/glass and glass/liquid interfaces of the capillary and that the sensitivity is directly proportional to the capillary diameter.

In light of the initial findings the experimental investigations of BSI as a possible immunoassay and and method for studying protein-binding events were designed as three select binding studies. The three protein binding events studied (trypsin-aminobenzamidine, trypsin-antitrypsin, and antithrombin-heparin) were

chosen because they are known to exhibit either conformational changes and changes in waters of hydration upon binding, which is the current hypothesis of the physical mechanism for refractive index change. In all the three cases presented in chapters 6 BSI failed to detect any binding events. A more positive outcome was found on the study of two enzymatic reactions; the phosphorylation of glucose by hexokinase and the hydrolysis of adenosine phosphates by apyrase. In both cases the enzymatic reactions produced clear changes in refractive index that were observable in real-time and end-point values were linear with respect to substrate concentrations.

7.1 Strengths and limitations of the study

This study was initially set on the assumption that BSI could detect biomolecular binding events and its purpose was therefore not to question the entire paradigm of whether protein binding events are associated with a change in refractive index and the answer to that question falls outside the scope of the original aim of this study. However, to not address this issue would be to ignore the elephant in the living-room. Much effort has therefore been put into addressing and clarifying the optical principles of BSI to ensure that despite small differences in experimental setup, most notably the capillary size, the principle method of measurement was identical to those used in the studies presented by Bornhop et al. Furthermore the continuous monitoring of sample temperature is a novel feature that has not been utilized in other BSI studies and it has most likely provided a better temperature control and ultimately reduced this source of error significantly. The negative results for detection of protein binding events presented in paper II can therefore be viewed as being generally valid for any type of BSI detector and other types of bulk refractive index detectors.

Despite advocating a possible relation between the refractive index of proteins and the specific volume and waters of hydration, this work is not sufficient and further studies would be required to conclude on such a relationship. Similarly, further studies are needed to precisely identify and characterize the effect of respectively bound and free ions on the refractive index as discussed in paper III.

This study has addressed and described sources of error that have not been discussed in detail before in previous BSI studies including; signal artifacts from diffusion of solutes and carryover, degassing and unspecific binding of protein to the capillary surface, however it is difficult to conclude on the presence and impact of such sources of error in studies by other authors due to differences in the types of material used (glass or PDMS) and the geometry of the micro-fluid channel.

7.2 Discussion

7.2.1 Hypothesis I:

Back Scatter Interferometry can be used as a quantitative label-free homegenous antithrombin immunoassay.
No evidence has been found in the experimental investigations that protein-ligand interactions at micro- and nanomolar concentrations produce a change in refractive index that is detectable with BSI and its use as a homogenous (ie. free soluton) immunoassay does not seem possible. This is contrary to the findings of Kussrow, Enders and Castro (2010) who have used BSI to detect picomolar syphilis antibody-antigen reactions in serum samples. The authors use a HeNe laser and a custom made borosilicate microfluidic chip (Micronit, Inc) but do not specify the channel dimensions, however in other published BSI studies by Kussrow the chip dimensions are being described as semicircular with a height of only $40\,\mu m$.[11,15] Kussrow et al. report a signal of 0.09 rad from the binding between $50\,\mu g\,mL^{-1}$ IgG and $100\,\mu g\,mL^{-1}$ treponemal r17 a syphilis antigen, which according to the findings of this work (equation 5.4) would be equivalent to a change of 1.1×10^{-4} RIU, which is by all means too large to be even reasonably explained by changes in protein dn/dc.

BSI is very sensitive to variations in both ambient and sample temperature as well as the amount of dissolved gasses, which would prove challenging to control in a routine laboratory environment. Furthermore, the full effects of carryover and unspecific binding to the capillary surface requires further investigation as it could pose a significant source of error. Taken all these things into consideration BSI does not seem suitable for use as an immunoassay platform and hypothesis I must be rejected.

7.2.2 Hypothesis II:

The binding affinity of antithrombin to thrombin can be characterized in solution, in a label-free manner, with Back Scatter Interferometry
Initial plans to detect antithrombin-thrombin binding was discarded due to the availability and amount of protein needed the experimental investigations of BSI as a possible method for studying antithrombin-thrombin affinity were designed as three select binding studies: trypsin-aminobenzamidine, trypsin-antitrypsin, and antithrombin-heparin. Since there was no a priori knowledge on the magnitude of the refractive index change associated with specific protein-ligand interactions and conformational changes all experiments were performed in relatively high micromolar concentrations which should maximize the total refractive index change. In all the three cases presented in chapter 6 BSI failed

to detect any binding and hypothesis II is therefore rejected.

The combined results of this work does not only reject the singular statements of hypothesis I and II, but furthermore challenges the entire paradigm of how back scatter interferometry functions and whether the refractive index of proteins is actually affected by ligand binding or conformational changes at all.

7.2.3 Hypothesis III:

Back Scatter Interferometry can be used to quantify enzymatic reactions, hereby expanding the possible applications of BSI for in vitro diagnostics.
When the project hypothesis were written the idea of using BSI to study enzymatic reactions was uncharted territory and at the time of conception the confirmation of this hypothesis seemed far more uncertain than using BSI for immunoassays and protein binding studies. As it turned out, enzymatic reactions provided this project with the only examples of BSI actually detecting a biomolecular reaction. Both the enzymatic phosphorylation of glucose by hexokinase and the hydrolysation of adenosine phosphates by apyrase produced changes in bulk refractive index that could be measured in real-time and in the case of hexokinase used to determine the Michaelis-Menten constant. The results are certainly interesting from an academic perspective and a further study on the refractive index of ions in solution or cheated state could provide valuable answers on the exact nature of the refractive index signal. The end-point signal is linear with respect to the substrate concentration and the method could in principle be used to quantify unknown concentrations. Of course, pocket size glucometers have long been on the market, but since refractive index detection does not require the use of labels or coupled indicator reactions it could possibly be used to study a wide range of enzymatic assays without altering the sensor or requiring additional specific reagents. A possible use could also be to implement it in existing or merging optical biosensors such as surface plasmon resonance[29,28] to facilitate measurements of enzyme reactions combined with detection of inhibitor or substrate binding.

7.3 Final conclusion

Overall this study has produced results is directly counter-evident to those published by Bornhop et al. in terms of the performance of BSI and furthermore questions the hypothesis that free solution biomolecular binding events can be detected by refractive index measurements.

Bibliography

[1] Darryl J Bornhop, Joey C Latham, Amanda Kussrow, Dmitry a Markov, Richard D Jones, and Henrik S Sørensen. Free-solution, label-free molecular interactions studied by back-scattering interferometry. *Science (New York, N.Y.)*, 317(5845):1732–6, oct 2007.

[2] D J Bornhop. Microvolume index of refraction determinations by interferometric backscatter. *Applied optics*, 34(18):3234–9, jun 1995.

[3] Hendra J. Tarigan, Paul Neill, Christopher K. Kenmore, and Darryl J. Bornhop. Capillary-Scale Refractive Index Detection by Interferometric Backscatter. *Analytical Chemistry*, 68(10):1762–1770, jan 1996.

[4] Dmitry Markov, Deepak Begari, and Darryl J Bornhop. Breaking the 10(-7) barrier for RI measurements in nanoliter volumes. *Analytical chemistry*, 74(20):5438–41, oct 2002.

[5] Zhanling Wang and Darryl J Bornhop. Dual-capillary backscatter interferometry for high-sensitivity nanoliter-volume refractive index detection with density gradient compensation. *Analytical chemistry*, 77(24):7872–7, dec 2005.

[6] Kelly Swinney, Jana Pennington, and Darryl J. Bornhop. Universal detection in capillary electrophoresis with a micro-interferometric backscatter detector. *The Analyst*, 124(3):221–225, 1999.

[7] Michael P Houlne, Darren S Hubbard, George I Makhataclze, Darryl J Bornhop, George I Makhatadze, and Darryl J Bornhop. Refractive-index-based calorimetric studies of RNAse T1 unfolding in small volumes using microinterferometric backscatter. In *SPIE*, volume 2982, pages 159–167, 1997.

[8] Kelly Swinney, Dmitry Markov, and Darryl J. Bornhop. Chip-scale universal detection based on backscatter interferometry. *Analytical Chemistry*, 72(13):2690–2695, 2000.

[9] Dmitry a Markov, Kelly Swinney, and Darryl J Bornhop. Label-

free molecular interaction determinations with nanoscale interferometry. *Journal of the American Chemical Society*, 126(50):16659–64, dec 2004.

[10] Henrik S. Sørensen, Niels B. Larsen, Joey C. Latham, Darryl J. Bornhop, and Peter E. Andersen. Highly sensitive biosensing based on interference from light scattering in capillary tubes. *Applied Physics Letters*, 89(2006), 2006.

[11] Amanda Kussrow, Eiton Kaltgrad, Mark L Wolfenden, Mary J Cloninger, M G Finn, and Darryl J Bornhop. Measurement of monovalent and polyvalent carbohydrate-lectin binding by back-scattering interferometry. *Analytical chemistry*, 81(12):4889–97, jun 2009.

[12] Joey C. Latham, Richard a. Stein, Darryl J. Bornhop, and Hassane S. Mchaourab. Free-solution label-free detection of apha-crystallin chaperone interactions by back-scattering interferometry. *Analytical Chemistry*, 81(5):1865–1871, 2009.

[13] Ereny F Morcos, Amanda Kussrow, Carolyn Enders, and Darryl Bornhop. Free-solution interaction assay of carbonic anhydrase to its inhibitors using back-scattering interferometry. *Electrophoresis*, 31(22):3691–5, nov 2010.

[14] Pierre Sétif, Nathan Harris, Bernard Lagoutte, Stephen Dotson, and Scot R. Weinberger. Detection of the photosystem I:Ferredoxin complex by backscattering interferometry. *Journal of the American Chemical Society*, 132:10620–10622, 2010.

[15] Michael M Baksh, Amanda K Kussrow, Mauro Mileni, M G Finn, and Darryl J Bornhop. Label-free quantification of membrane-ligand interactions using backscattering interferometry. *Nature biotechnology*, 29(4):357–60, apr 2011.

[16] Ian R Olmsted, Yi Xiao, Minseon Cho, Andrew T Csordas, Jonathan H Sheehan, Jens Meiler, H Tom Soh, and Darryl J Bornhop. Measurement of aptamer-protein interactions with back-scattering interferometry. *Analytical chemistry*, 83(23):8867–70, 2011.

[17] E N Pesciotta, D J Bornhop, and R A Flowers. Backscattering interferometry: an alternative approach for the study of hydrogen bonding interactions in organic solvents. *Org Lett*, 13(10):2654–2657, 2011.

[18] Gabrielle L. Haddad, Sherri C. Young, Ned D. Heindel, Darryl J. Bornhop, and Robert a. Flowers. Back-Scattering Interferometry: An Ultrasensitive Method for the Unperturbed Detection of Acetylcholinesterase-Inhibitor Interactions. *Angewandte Chemie*, 124(44):11288–11292, oct 2012.

[19] Nicholas M Adams, Ian R Olmsted, Frederick R Haselton, Darryl J Bornhop, and David W Wright. The effect of hybridization-induced secondary

structure alterations on RNA detection using backscattering interferometry. *Nucleic acids research*, 41(9):e103, may 2013.

[20] Theresa Tiefenbrunn, Stefano Forli, Michael M Baksh, Max W Chang, Meaghan Happer, Ying-Chuan Lin, Alexander L Perryman, Jin-Kyu Rhee, Bruce E Torbett, Arthur J Olson, John H Elder, M G Finn, and C David Stout. Small Molecule Regulation of Protein Conformation by Binding in the Flap of HIV Protease. *ACS chemical biology*, mar 2013.

[21] Amanda Kussrow, Carolyn S Enders, Arnold R Castro, David L Cox, Ronald C Ballard, and Darryl J Bornhop. The potential of backscattering interferometry as an in vitro clinical diagnostic tool for the serological diagnosis of infectious disease. *The Analyst*, 135(7):1535–7, jul 2010.

[22] Carolyn Sue Enders. *Backscattering interferometry as a diagnostic tool*. PhD thesis, Vanderbilt University, 2009.

[23] Amanda Kussrow. *Interrogation of biomolecular interactions utilizing backscattering interferometry*. PhD thesis, Vanderbilt, 2009.

[24] Je-hyun Baek, Hana Im, Un-beom Kang, K I Moon Seong, Cheolju Lee, Joon Kim, and Myeong-hee Yu. Probing the local conformational change of a 1 -antitrypsin. 5:1842–1850, 2007.

[25] J C Whisstock, R Skinner, R W Carrell, and a M Lesk. Conformational changes in serpins: I. The native and cleaved conformations of alpha(1)-antitrypsin. *Journal of molecular biology*, 296(2):685–699, 2000.

[26] P Björquist and S Boström. Determination of the kinetic constants of tissue factor/factor VII/factor VIIA and antithrombin/heparin using surface plasmon resonance. *Thrombosis research*, 85(3):225–36, feb 1997.

[27] Rakhee Gehlot, Kavita Sharma, and Manoth Mathew. Surface plasmon resonance based biosensor for label free detection of cholesterol. 47(December):1804–1808, 2008.

[28] Kohei Nakamoto, Ryoji Kurita, and Osamu Niwa. One-chip biosensor for simultaneous disease marker/calibration substance measurement in human urine by electrochemical surface plasmon resonance method. *Biosensors & bioelectronics*, 26(4):1536–42, dec 2010.

[29] Hye Jin Lee, Alastair W. Wark, Terry T. Goodrich, Shiping Fang, and Robert M. Corn. Surface enzyme kinetics for biopolymer microarrays: A combination of langmuir and michaelis-men ten concepts. *Langmuir*, 21(9):4050–4057, 2005.

[30] Kelly Swinney and Darryl J Bornhop. D-B-Hydroxybutyrate Reaction Kinetics Studied in Nanoliter Volumes Using a Capillary Polarimeter. *Applied Spectroscopy*, 54(10):2–6, 2000.

[31] H. C. van de Hulst. *Light scattering by small particles*. Dover Publications, Inc., dover edition, 1981.

[32] S A Akhmanov and S Y Nikitin. *Physical Optics*. Clarendon Press, 1997.

[33] EF Casassa and H Eisenberg. PARTIAL SPECIFIC VOLUMES AND REFRACTIVE INDEX INCREMENTS IN MULTICOMPONENT SYSTEMS1. *The Journal of Physical Chemistry*, 1961.

[34] Jose V. Herráez and R. Belda. Refractive Indices, Densities and Excess Molar Volumes of Monoalcohols + Water. *Journal of Solution Chemistry*, 35(9):1315–1328, jul 2006.

[35] S D Deosarkar, V V Pandhare, and P S Kattekar. Densities and Refractive Indices of Potassium Salt Solutions in Binary { Ethanol + Water } Mixture of Different Compositions. 2013, 2013.

[36] Andrea Marchetti, Lorenzo Tassi, and Alessandro Ulrici. Refractive indices of binary mixtures of (1,2-dichloroethane + 2-chloroethanol) at various temperatures. *J. Chem. Thermodyn.*, 31(4):647–660, 1999.

[37] Aleksandar Z. Tasic, Bojan D. Djordjevic, Dusan K. Grozdanic, and Nenad Radojkovic. Use of mixing rules in predicting refractive indexes and specific refractivities for some binary liquid mixtures. *Journal of Chemical & Engineering Data*, 37(16):310–313, 1992.

[38] Ufuk Sancar Vural, V Muradoglu, and Sedat Vural. Excess molar volumes, and refractive index of binary mixtures of glycerol + methanol and glycerol + water at 298.15 K and 303.15 K. *Bulletin of the Chemical Society of Ethiopia*, 25(1):111–118, 2011.

[39] T.M. Aminabhavi. Use of mixing rules in the analysis of data for binary liquid mixtures. *Journal of Chemical Engineering Data*, 55(4):54–55, 1984.

[40] Wilfried Heller. Remarks on Refractive Index Mixture Rules. *The Journal of Physical Chemistry*, 69(4):1123–1129, 1966.

[41] Pilar Brocos, Ángel Piñeiro, Ramón Bravo, and Alfredo Amigo. Refractive indices, molar volumes and molar refractions of binary liquid mixtures: concepts and correlations. *Phys. Chem. Chem. Phys.*, 5(3):550–557, 2003.

[42] Anthony F. Fucaloro. Partial Molar Volumes from Refractive Index Measurements. *Journal of Chemical Education*, 79(7):865, jul 2002.

[43] Tejraj M. Aminabhavi and Petr Munk. Excess Polarizability and Volume of Mixing and Their Effect on the Partial Specific Volume and the Refractive Increment of Polymers in Mixed Solvents. *Macromolecules*, 12(6):1186–1194, 1979.

[44] Tejraj M Aminabhavi. Predicting Refractive Index and Density Increments of Binary Solvent Mixtures. *Journal of Chemical Engineering Data*, 32(4):406–409, 1987.

[45] T M Aminabhavi, R C Patel, E S Jayadevappa, and B R Prasad. Excess volume and excess polarizability during mixing of binary solvents. *J. Chem. Eng. Data*, 27(1):50–53, 1982.

[46] K G Denbigh. The polarisabilities of bonds-I. *Transactions of the Faraday Society*, 36(0):936–948, 1940.

[47] Joyce M Stout and Clifford E Dykstra. Static Dipole Polarizabilities of Organic Molecules. Ab Initio Calculations and a Predictive Model. *Journal of the American Chemical Society*, 117(18):5127–5132, may 1995.

[48] Salvatore Millefiori, Andrea Alparone, Arcangelo Millefiori, and Angelo Vanella. Electronic and vibrational polarizabilities of the twenty naturally occurring amino acids. *Biophysical chemistry*, 132(2-3):139–47, feb 2008.

[49] Thorsten Hansen, Lasse Jensen, Per Olof Åstrand, and Kurt V. Mikkelsen. Frequency-dependent polarizabilities of amino acids as calculated by an electrostatic interaction model. *Journal of Chemical Theory and Computation*, 1(4):626–633, 2005.

[50] Lasse Jensen, Per Olof Åstrand, Anders Osted, Jacob Kongsted, and Kurt V. Mikkelsen. Polarizability of molecular clusters as calculated by a dipole interaction model. *Journal of Chemical Physics*, 116(10):4001–4010, 2002.

[51] Kechen Wu, Jaap G. Snijders, and Chensheng Lin. Reinvestigation of hydrogen bond effects on the polarizability and hyperpolarizability of urea molecular clusters. *Journal of Physical Chemistry B*, 106(35):8954–8958, 2002.

[52] Amanda Kussrow, Carolyn S Enders, and Darryl J Bornhop. Interferometric methods for label-free molecular interaction studies. *Analytical chemistry*, 84(2):779–92, jan 2012.

[53] Kristian O. Sylvester-Hvid, Per-Olof Åstrand, Mark A. Ratner, and Kurt V. Mikkelsen. Frequency-Dependent Molecular Polarizability and Refractive Index: Are Substituent Contributions Additive? *The Journal of Physical Chemistry A*, 103(12):1818–1821, 1999.

[54] Wilfried Heller. Application of dn/dc data for the determination of partial specific volumes of dissolved macromolecules. *Journal of Polymer Science Part A-2: Polymer Physics*, 4(2):209–226, 1966.

[55] Vincent Ball and Jeremy J Ramsden. Buffer dependence of refractive index increments of protein solutions. *Biopolymers*, 46(7):489–492, 1998.

[56] Hajime Noguchi and Jen Tsi Yang. Dilatometric and refractometric studies of the helix–coil transition of poly-L-glutamic acid in aqueous solution. *Biopolymers*, 1:359–370, 1963.

[57] Tigran V Chalikian. Partial Molar Volumes of Proteins in Solution. In E Wilhelm and Trevor M Letcher, editors, *Volume Properties: Liquids, Solutions and Vapours*, chapter 21, pages 542–574. The Royal Society of Chemistry, 2015.

[58] T V Chalikian, M Totrov, R Abagyan, and K J Breslauer. The hydration of globular proteins as derived from volume and compressibility measurements: cross correlating thermodynamic and structural data. *Journal of molecular biology*, 260(4):588–603, jul 1996.

[59] Yehouda Harpaz, Mark Gerstein, and Cyrus Chothia. Volume changes on protein folding. *Structure*, 2(7):641–649, jul 1994.

[60] L R Murphy, N Matubayasi, V a Payne, and R M Levy. Protein hydration and unfolding–insights from experimental partial specific volumes and unfolded protein models. *Folding & design*, 3(2):105–18, jan 1998.

[61] Tigran V Chalikian and Rana Filfil. How large are the volume changes accompanying protein transitions and binding? *Biophysical Chemistry*, 104(2):489–499, jun 2003.

[62] Thomas L. McMeekin, Mildred Wilensky, and Merton L. Groves. Refractive indices of proteins in relation to amino acid composition and specific volume. *Biochemical and Biophysical Research Communications*, 7(2):151–156, 1962.

[63] Huaying Zhao, Patrick H Brown, and Peter Schuck. On the distribution of protein refractive index increments., may 2011.

[64] A Theisen, C Johann, MP Deacon, and SE Harding. *Refractive Increment Data-Book for Polymer and Biomolecular Scientists*. Nottingham University Press, 2000.

[65] www.refractiveindex.info.

[66] http://www.udel.edu/chem/GlassShop/PhysicalProperties.htm.

[67] http://en.wikipedia.org/wiki/Soda-lime glass.

[68] Ian R Olmsted, Amanda Kussrow, and Darryl J Bornhop. Comparison of free-solution and surface-immobilized molecular interactions using a single platform. *Analytical chemistry*, 84(24):10817–22, dec 2012.

[69] Joey C. Latham. *Backscattering Interferometry: From Modeling and Fabrication to Application*. PhD thesis, Vanderbilt University, 2007.

[70] E M Purcell. Life at low Reynolds number, 1977.

[71] Sushanta K. Mitra and Suman Chakraborty. *Microfluidics and Nanofluidics Handbook: Fabrication, Implementation, and Applications*. CRC Press, 2011.

[72] David S Wilkinson. *Mass Transport in Solids and Fluids*. Cambridge University Press, 2000.

[73] Geoffrey Taylor. Dispersion of Soluble Matter in Solvent Flowing Slowly through a Tube. *Proceedings of the Royal Society of London A: Mathematical, Physical and Engineering Sciences*, 219(1137):186–203, aug 1953.

[74] R Aris. On the Dispersion of a Solute in a Fluid Flowing through a Tube. *Proceedings of the Royal Society of London A: Mathematical, Physical and Engineering Sciences*, 235(1200):67–77, apr 1956.

[75] John G Quinn. Evaluation of Taylor dispersion injections: determining kinetic/affinity interaction constants and diffusion coefficients in label-free biosensing. *Analytical biochemistry*, 421(2):401–10, feb 2012.

[76] J Crank. *The Mathematics of Diffusion*. Oxford University Press, 2nd edition, 1975.

[77] A Truskey, George, Fan Yuan, and F Katz, David. *Transport Phenomena in Biological Systems*. Pearson, 2nd edition, 2010.

[78] H. S. Sørensen. *Self Calibrating Interferometric Sensor*. Thesis, Ph.D. Thesis, Technical University of Denmark, 2006.

[79] ASTM. Standard Practice for Refractive Index Detectors Used in Liquid Chromatography E1303. Technical Report Reapproved 2010, 2013.

[80] Kelly Swinney, Dmitry Markov, and Darryl J. Bornhop. Ultrasmall volume refractive index detection using microinterferometry. *Review of Scientific Instruments*, 71(7):2684, 2000.

[81] A Becker, W Köhler, and B Müller. A Scanning Michelson Interferometer for the Measurement of the Concentration and Temperature Derivative of the Refractive Index of Liquids. *A scanning Michelson interferometer for the measurement of the concentration and temperature derivative of the refractive index of liquids*, 99(4):600–608, 1995.

[82] Kelly Swinney, Dmitry Markov, and Darryl J. Bornhop. Chip-scale universal detection based on backscatter interferometry. *Analytical Chemistry*, 72(13):2690–2695, 2000.

[83] S T Jepsen, T M Jørgensen, W Zong, T Trydal, S R Kristensen, and H S Sørensen. Evaluation of back scatter interferometry, a method for detecting protein binding in solution. *The Analyst*, 00:1–7, dec 2014.

[84] Michael G Gore, S Bottomley, A G Popplewell, and Tony Atkinson. The use of tryptophan fluorescence to determine the stability of IgG binding proteins based upon the B domain of protein A from Staphylococcus aureus. *Biochem Soc Trans*, 20(3):288S, 1992.

[85] N L Brown, S P Bottomley, M D Scawen, and M G Gore. A study of the interactions between an IgG-binding domain based on the B domain of staphylococcal protein A and rabbit IgG. *Molecular biotechnology*, 10(1):9–16, 1998.

[86] Loredana Lo Conte, Cyrus Chothia, È Janin, and Joël Janin. The atomic structure of protein-protein recognition sites. *Journal of Molecular Biology*, 285(5):2177–2198, 1999.

[87] Janeway, Travers, and Walport. *Immunobiology: The Immune System in Health and Disease*. New York: Garland Science, 5'th edition, 2001.

[88] B Akerström and L Björck. A physicochemical study of protein G, a molecule with unique immunoglobulin G-binding properties. *The Journal of biological chemistry*, 261(22):10240–7, aug 1986.

[89] K Saha, F Bender, and E Gizeli. Comparative study of IgG binding to proteins G and A: nonequilibrium kinetic and binding constant determination with the acoustic waveguide device. *Analytical chemistry*, 75(4):835–42, feb 2003.

[90] Jo Leanna Wilson, Israel M Scott, and Jonathan L McMurry. Optical biosensing: Kinetics of protein A-IGG binding using biolayer interferometry. *Biochemistry and molecular biology education : a bimonthly publication of the International Union of Biochemistry and Molecular Biology*, 38(6):400–7, nov 2010.

[91] Edward C Hulme and Mike a Trevethick. Ligand binding assays at equilibrium: validation and interpretation. *British journal of pharmacology*, 161(6):1219–37, nov 2010.

[92] Hendra J Tarigan. Simultaneous Modeling of Waveforms Associated With Backscattered HeNe Laser Light from a Fluid Filled Capillary Tube by Use of Geometrical Optics and Wave Theories. In *AIP Conference Proceedings*, volume 1048, pages 541–546, 2008.

[93] S a Evans, S T Olson, and J D Shore. p-Aminobenzamidine as a fluorescent probe for the active site of serine proteases. *The Journal of biological chemistry*, 257(6):3014–7, mar 1982.

[94] J T Vivian and P R Callis. Mechanisms of tryptophan fluorescence shifts in proteins. *Biophysical journal*, 80(5):2093–2109, 2001.

[95] D M Monroe, G B Sherrill, and H R Roberts. Use of p-aminobenzamidine

to monitor activation of trypsin-like serine proteases. *Analytical biochemistry*, 172(2):427–35, 1988.

[96] a Danielsson and I Björk. Mechanism of inactivation of trypsin by antithrombin. *The Biochemical journal*, 207(1):21–8, oct 1982.

[97] R Talhout and J B Engberts. Thermodynamic analysis of binding of p-substituted benzamidines to trypsin. *European journal of biochemistry / FEBS*, 268(6):1554–60, mar 2001.

[98] Olgun Guvench, Daniel J Price, and Charles L Brooks. Receptor rigidity and ligand mobility in trypsin-ligand complexes. *Proteins*, 58(2):407–17, feb 2005.

[99] Ignasi Buch, Toni Giorgino, and Gianni De Fabritiis. Complete reconstruction of an enzyme-inhibitor binding process by molecular dynamics simulations. *Proceedings of the National Academy of Sciences of the United States of America*, 108(25):10184–9, jun 2011.

[100] Ruby H P Law, Qingwei Zhang, Sheena McGowan, Ashley M Buckle, Gary a Silverman, Wilson Wong, Carlos J Rosado, Chris G Langendorf, Rob N Pike, Philip I Bird, and James C Whisstock. An overview of the serpin superfamily. *Genome biology*, 7(5):216, jan 2006.

[101] J Liang and M P McGee. Hydration structure of antithrombin conformers and water transfer during reactive loop insertion. *Biophysical journal*, 75(2):573–82, aug 1998.

[102] J C Whisstock, R N Pike, L Jin, R Skinner, X Y Pei, R W Carrell, and a M Lesk. Conformational changes in serpins: II. The mechanism of activation of antithrombin by heparindagger. *Journal of molecular biology*, 301(5):1287–305, sep 2000.

[103] Maria P McGee, Jie Liang, and James Luba. Hydration effects of heparin on antithrombin probed by osmotic stress. *Biophysical journal*, 82(2):1040–9, feb 2002.

[104] Steven T Olson, K.R. R Srinivasan, Ingemar Bjork, Joseph D. Shore, and I Björk. Binding of high affinity heparin to antithrombin III. Stopped flow kinetic studies of the binding interaction. *The Journal of biological chemistry*, 256(21):11073–9, 1981.

[105] Thomas M. Niemczyk. *Refractive Index Measurement*, volume 2. ACADEMIC PRESS, INC., 1980.

[106] a. Penzkofer, H. Glas, and J. Schamailzl. Optical dispersion and molar refractivities of alkali halide crystals and aqueous solutions. *Chemical Physics*, 70:47–54, 1982.

[107] Patrick Jemmer, Patrick W. Fowler, Mark Wilson, and Paul A. Madden. Environmental Effects on Anion Polarizability: Variation with Lattice

Parameter and Coordination Number. *Journal of Physical Chemistry A*, 102(43):8377–8385, 1998.

[108] P Pacák. Molar refractivity and interactions in solutions. 1. Molar refractivity of some monovalent ions in aqueous and dimethyl sulfoxide solutions. *Chemical Papers*, 43(2):489–500, 1989.

[109] Kelly Swinney, Dmitry Markov, Joseph Hankins, and DJ Bornhop. Micro-interferometric backscatter detection using a diode laser. *Analytica Chimica Acta*, 400(July):265–280, 1999.

[110] Jianqi Shen and Xiaowei Jia. Diffraction of a plane wave by an infinitely long circular cylinder or a sphere: solution from Mie theory. *Appl. Opt.*, 52(23):5707–5712, 2013.

[111] Ambarish Ghosh, Furqan M Fazal, and Peer Fischer. Circular differential double diffraction in chiral media. *Optics Letters*, 32(13):1836 – 1838, 2007.

[112] Joey C. Latham, Dmitry a. Markov, Henrik S. Sørensen, and Darryl J. Bornhop. Photobiotin Surface Chemistry Improves Label-Free Interferometric Sensing of Biochemical Interactions. *Angewandte Chemie*, 118(6):969–972, jan 2006.

[113] Janos Vörös. The density and refractive index of adsorbing protein layers. *Biophysical journal*, 87(1):553–61, jul 2004.

[114] Mc Coen, R Lehmann, P Gröning, M Bielmann, C Galli, and L Schlapbach. Adsorption and Bioactivity of Protein A on Silicon Surfaces Studied by AFM and XPS. *Journal of colloid and interface science*, 233(2):180–189, jan 2001.

ISSN (online): 2246-1302
ISBN (online): 978-87-7112-468-2

AALBORG UNIVERSITY PRESS